UCLA

UCLA Electronic Theses and Dissertations

Title

Investigating the Role of Wild-type and Mutant Copper-Zinc Superoxide Dismutase Amyloid in Amyotrophic Lateral Sclerosis

Permalink

https://escholarship.org/uc/item/7z60q5s1

Author

Chan, Pik Kay

Publication Date

2013

Peer reviewed|Thesis/dissertation

UNIVERSITY OF CALIFORNIA

Los Angeles

Investigating the Role of Wild-type and Mutant Copper-Zinc Superoxide Dismutase

Amyloid in Amyotrophic Lateral Sclerosis

A dissertation submitted in partial satisfaction of the

requirements for the degree Doctor of Philosophy

in Biochemistry and Molecular Biology

by

Pik Kay Chan

2013

ABSTRACT OF THE DISSERTATION

Investigating the Role of Wild-type and Mutant Copper-Zinc Superoxide Dismutase

Amyloid in Amyotrophic Lateral Sclerosis

by

Pik Kay Chan

Doctor of Philosophy in Biochemistry and Molecular Biology

University of California, Los Angeles, 2013

Professor Joan Selverstone Valentine, Chair

Abnormal intracellular protein inclusions are consistently observable in the motor neurons affected by amyotrophic lateral sclerosis (ALS), also commonly referred as Lou Gehrig's disease. This disease was named after the famous Hall of Fame baseball player, Lou Gehrig, who suddenly experienced loss of physical strength and was diagnosed with ALS. The most prevalent hypothesis regarding the mechanism of ALS points to a toxic gain of function resulting from protein misfolding and aggregation. In the SOD1-ALS transgenic mouse model, protein aggregates composed of primarily full length apo SOD1 are consistently found in the spinal cords of mice exhibiting ALS symptoms. Moreover, these aggregates possess a filamentous structure, suggesting the involvement of SOD1 amyloid fibril in ALS pathology.

Research on understanding the formation mechanism of SOD1 fibrils spurred over the past few years. Scientists are now convinced that the demetallated form of SOD1 is the most susceptible to aggregation. In this dissertation, we sought to understand the molecular mechanism by which apo SOD1 rearranges to adopt the fibrillar structure, seek SOD1 amyloid inhibitors as potential therapeutic leads, and use small molecules to modulate and stabilize SOD1 oligomeric intermediates from the amyloid pathway that have never been characterized before. We found that the SOD1 amyloid core is composed of the N-terminal sequence 1-63. The N-terminal tryptic fragment 1-69 is consistently the most trypsin resistant in all the fibrils examined, including WT and six SOD1 mutants. WT fibril displays regular twist pattern along the lateral axis with an average helical pitch distance of 62 nm. While some mutants (L38V, G93A, and G93S) have similar twist pattern as WT, a single point mutation resides within the fibril core can alter the overall amyloid morphology. This is most evident in mutants such as G37R and G41D.

We successfully discovered several SOD1 amyloid inhibitors. Studies from a selection of SOD1 amyloid inhibitors (non-SOD1 synthetic peptides and small molecules) suggest that although peptides exhibiting a beta-strand conformation, such as DpV16 and DpV19, effectively inhibit SOD1 amyloid formation, peptides lacking beta-strand secondary structure, such as AzV31 and colivelin-tat are also effective. Out of all the inhibitors tested, only small molecules such as EGCG (a green tea derived flavonoid) and CLR01 (a molecular tweezer) formed stable oligomers with SOD1. SOD1 oligomers were never observed with peptide inhibitors. DpV16 was able to inhibit the initiation of fibrillation by reduced apo SOD1 but had no effect on the elongation phase, suggesting that it might prevent the formation of amyloid-competent nuclei. For the first time, we characterized SOD1 oligomers isolated from the *in-vitro* fibrillation assay.

These CLR01-stabilized oligomers have an estimated molecular mass of 87,000 and exhibit a significant amount of beta-sheet content.

The dissertation of Pik Kay Chan is approved.

Catherine F. Clarke

Joseph A. Loo

Martina Wiedau-Pazos

Julian P. Whitelegge

Joan Selverstone Valentine, Committee Chair

University of California, Los Angeles

2013

Dedication page

This dissertation is dedicated to:

My Parents

For Their Unconditional Love, Care, and Support

Table of contents

List of Figures

List of Tables

Acknowledgments

VITA

2006   B.S., Biochemical and Biophysical Sciences
University of Houston
Houston, Texas
magna cum laude

2006-2010   University Fellowship
University of California, Los Angeles
Los Angeles, California

2007-2010   National Institutes of Health
Chemistry-Biology Interface Training Grant
University of California, Los Angeles
Los Angeles, California

2013   Janis Okida Hashimoto Endowment Fellowship

Publications

Chan PK, Chattopadhyay M, Sharma S, Souda P, Gralla EB, Borchelt DR, Whitelegge JP, Valentine JS. Structural Similarity of Wild-type and ALS-mutant Superoxide Dismutase-1 Fibrils Using Limited Proteolysis and Atomic Force Microscopy (Submitted to Proc Natl Acad Sci U S A).

Chan PK, Ruchala P, Whitelegge JP, and Valentine JS. Novel inhibitors of Cu, Zn-Superoxide dismutase fibrillation. FASEB Conference. Snowmass, Colorado. (Invited Talk)

Lelie HL, Liba A, Bourassa MW, Chattopadhyay M, **Chan PK**, Gralla EB, Miller LM, Borchelt DR, Valentine JS, Whitelegge JP. Copper and zinc metallation status of copper-zinc superoxide dismutase from amyotrophic lateral sclerosis transgenic mice. *J Biol Chem*. 2011 Jan 28, 286(4):2795-806.

Shaw BF, Lelie HL, Durazo A, Nersissian AM, Xu G, **Chan PK**, Gralla EB, Tiwari A, Hayward LJ, Borchelt DR, Valentine JS, Whitelegge JP. Detergent-insoluble aggregates associated with amyotrophic lateral sclerosis in transgenic mice contain primarily full-length, unmodified superoxide dismutase-1. *J Biol Chem*. 2008 Mar 28; 283(13):8340-50.

Chapter 1

Introduction

1.1 Amyotrophic Lateral Sclerosis and Human Copper-Zinc Superoxide Dismutase

Amyotrophic lateral sclerosis (ALS), also referred as the Lou Gehrig's disease in the United States, is currently an incurable fatal disease characterized by the selective death of motor neurons in the brain stem, cortex, and spinal cord. Progressive denervation of motor neurons leads to atrophy of voluntary muscles causing paralysis and death (1, 2). The majority of patients experience spasticity and muscle weakness in an arm/leg as an early symptom. The cognitive function of the brain is usually unaffected. This progressive motor neuron degeneration eventually spreads to the rest of the body, sparing only muscular functions in the bladder and eye movements. Most patients die of respiratory dysfunction within five years after disease onset.

Most cases of ALS are sporadic, but about ten percent of cases are genetic (familial, fALS). Of the ten percent of cases that are familial, roughly twenty percent are due to dominantly inherited mutations in the *sod1* gene, which encodes a cytoplasmic metalloprotein, Cu, Zn superoxide dismutase (SOD1) (3). The lifetime risk of getting ALS is approximately 2 in 1000. Although the age of disease onset varies, it usually occurs at middle-age, and disease duration ranges from a year to over 17 years (2).

To date, over a hundred different mutations in SOD1 have been found, scattered throughout the entire sequence of SOD1 (http://www.alsod.org). Most mutations are missense mutations leading to a single alteration in the amino acid sequence. Many of the mutations are described as wild-type-like (WTL). These mutations have biophysical properties, such as thermal stability, secondary structure, metal binding affinity, and disulfide status that are nearly indistinguishable from the WT. However, some mutations are highly disruptive structurally, such as the truncated mutants and the mutations at the metal binding sites. Nevertheless, all of the

2

mutations, regardless of the degree of deviation from the WT protein, cause fALS, making it challenging to decipher the common mechanism by which this diverse set of mutations causes ALS pathology.

Clinically, sporadic and familial ALS are indistinguishable, and the SOD1-transgenic mouse model, which closely recapitulates the pathological aspects of SOD1-ALS patients, is the most commonly used model in which to study the underlying abnormalities associated with the disease, in the hope that research from the animal model might provide valuable insights into both sporadic and familial disease mechanism (4-6).

1.2 Copper, Zinc-Superoxide Dismutase (SOD1)

SOD1 is an ubiquitously expressed antioxidant enzyme that catalyzes the disproportionation of two superoxide anions into less reactive dioxygen and hydrogen peroxide in a two-step mechanism through a reduction and subsequent reoxidation of the active site copper (reaction 1.1 and 1.2) (7).

$$(1.1) \quad O_2^- + Cu(II)Zn\text{-}SOD \rightarrow O_2 + Cu(I)Zn\text{-}SOD$$

$$(1.2) \quad O_2^- + 2H^+ + Cu(I)Zn\text{-}SOD \rightarrow Cu(II)ZnSOD + H_2O_2$$

It is located predominately in the cytosol. However, it is also found in the nucleus, peroxisomes, and mitochondrial intermembrane space (8-10). SOD1 is a homo dimer composed of 153 amino acid residue subunits. Fully metallated (holo) mature human SOD1, with one copper, one zinc, and an intra-subunit disulfide in each subunit, is extremely stable with thermal stability higher than 90 ˚C (11, 12). It is highly resistant to denaturants and exists as a dimer at physiological

condition. SOD1 is a highly efficient catalyst for superoxide disproportionation, operating at near diffusion-controlled rates.

Each SOD1 subunit adopts a Greek key beta-barrel fold formed by eight anti-parallel beta-strands interspersed with two functional loops, the electrostatic loop and zinc binding loop (Figure 1) (13, 14). This tertiary beta-barrel fold conformation exists even without bound metals. The electrostatic loop contains a number of positively charged residues that serve to guide superoxide anion to the catalytic copper site. While the copper co-factor is well known for its catalytic function of converting superoxide to dioxygen and hydrogen peroxide, the role of zinc is better understood as a structural stabilizer. (Some recent discoveries suggest that copper may also serve a crucial structural function (15).) Three histidine (His63, His71, and His80) and one aspartate (Asp83) residues form the zinc-binding site. The binding of the zinc metal ion stabilizes the structural integrity in the zinc binding loop region. One of the zinc-binding histidine residues, His63, also coordinates with the copper site by sharing a common imidazolate side chain. This histidine, together with three other histidine residues (His46, His48, and His120), form the copper binding site (2). There are four cysteine residues in each subunit. In addition to the conserved Cys57 and Cys146 forming the intra-subunit disulfide bond holding beta strand 4 and 8 next to each other, Cys6 is buried in the dimer interface, leaving Cys111 the only solvent accessible cysteine in the holo form.
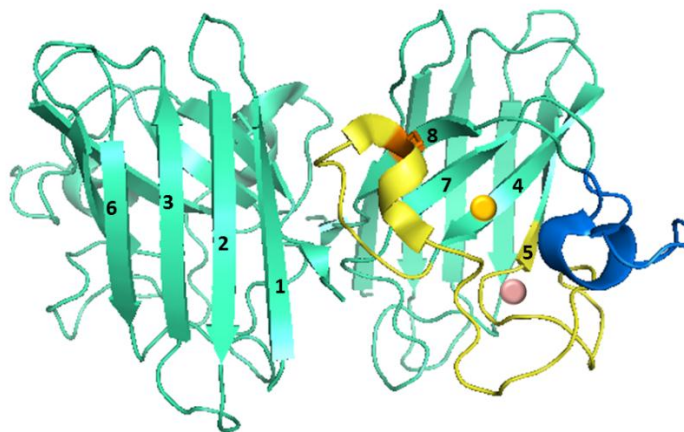
Figure 1.1. Crystal structure of fully metallated disulfide-oxidized SOD1 (PDB 1HL5) (16). Fully mature SOD1 adopts a Greek key beta-barrel fold in each subunit. Copper and zinc ions are shown in yellow and bisque spheres, respectively. The intra-subunit disulfide bond and Cys57 and Cys146 are highlighted in orange. Electrostatic and zinc binding loop are highlighted in yellow and blue, respectively (Features highlighted on the front side only).

1.3 Structure Stability - Metals and Disulfide Bond

Unlike the tertiary structure, formation of the dimeric quaternary structure is highly dependent on cooperative structural stabilization contributed by both metal binding and the formation of intra-subunit disulfide-bond between the highly conserved Cys57 and Cys146 (2). The dimer interface is held together by non-covalent interactions, such as water- and main chain-mediated hydrogen bonds and hydrophobic interaction. The loop containing Cys57 is involved in the dimer interface (Figure 1). The carbonyl oxygen of Cys57 is connected to the copper ligand His48 through a secondary hydrogen bond network with Gly61 and Arg143 (Figure 2). Although disulfide reduction or removal of metal ions alone is insufficient to produce SOD1 monomers, demetallation of SOD1 results in increased susceptibility to disulfide bond reduction and vice versa. Destabilization of the dimer interface shifts the dimer-to-monomer equilibrium toward the

monomeric form. Consequently, disulfide reduction of the apo form results in monomerization. However, either the formation of disulfide-bond or the binding of a copper or zinc ion is enough to shift the equilibrium back to dimer (12).
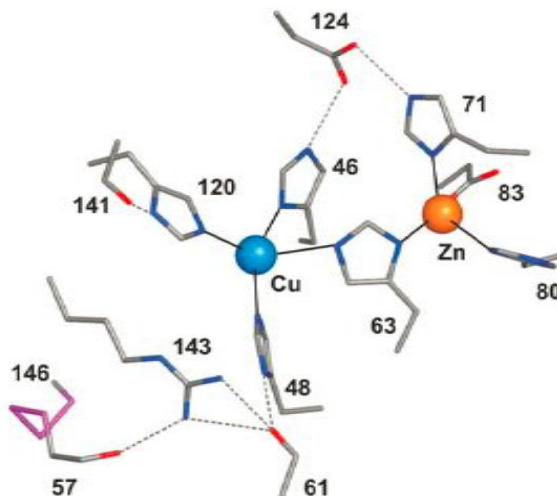
Figure 1.2. Hydrogen bond network connecting the intra-subunit disulfide bond (C57-C146) to copper and zinc binding sites. Hydrogen bonds are shown as dotted lines. Disulfide bond is depicted in pink. Copper and zinc ions are represented by blue and orange spheres, respectively. The carbonyl oxygen is hydrogen bonded to Arg143, which is hydrogen bonded to His48 through Gly61. [Reprinted by permission of Valentine *et al.* (2)].

1.4 ALS Etiology

In SOD1-fALS, the cytotoxicity appears to result from a toxic gain of function by mutant SOD1 rather than a loss of activity. This theory is supported by the following findings: 1) SOD1 knockout mice do not develop ALS (17). 2) Many of the wild-type like mutants retain SOD1 enzymatic activity (2). 3) Expression of functional WT SOD1 cannot ameliorate the toxic effect

of mutant SOD1 (18). When SOD1 was first identified as the causative gene in the familial cases of ALS, it was hypothesized that the disease was caused by abnormal copper-catalyzed oxidative chemistry by SOD1. In the presence of elevated concentration of hydrogen peroxide, hydrogen peroxide can undergo Fenton reaction with copper and generates highly reactive hydroxyl radicals that can either oxidize the active site histidine, thereby causing the release of copper and inactivation of SOD1, or oxidize other substrates leading to cellular damage (reactions 1.3-1.5) (7, 19-21). This aberrant peroxidase activity was once believed to be the cellular toxic origins. However, this hypothesis was disproved when the expression of a histidine-null mutant, which does not bind copper, still caused degeneration in mice (22). Although SOD1 might not be directly causing oxidative damage that leads to cell death, enhanced oxidative stress remains a common feature in ALS pathology. Histopathological studies on postmortem spinal cord and motor cortex of sporadic ALS patients revealed elevated levels of oxidative modifications to proteins, lipids, and DNA (23, 24). Furthermore, enhanced levels of protein carbonyls are commonly observed in transgenic mice tissues (25).

(1.3) $H_2O_2 + Cu(II)Zn\text{-}SOD \rightarrow O_2^- + 2H^+ + Cu(I)Zn\text{-}SOD$

(1.4) $H_2O_2 + Cu(I)Zn\text{-}SOD \rightarrow OH^- + (OH\cdot)Cu(II)Zn\text{-}SOD$

(1.5) $(OH\cdot)Cu(II)Zn\text{-}SOD + substrate \rightarrow oxidized\ substrate + Cu(II)Zn\text{-}SOD$
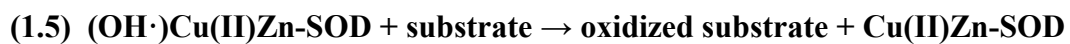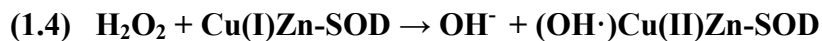
Other proposed pathological mechanisms for mutant SOD1 include mitochondrial dysfunction (26, 27), proteasomal inhibition (28), and metal homeostasis imbalance (29).

However, the most prevalent hypothesis is the formation of cytoplasmic protein aggregates or inclusions. A universal feature of all ALS patients and transgenic mice expressing mutant SOD1 is the appearance of intracellular aggregates in the motor neurons (18, 30). In the transgenic SOD1-ALS mouse model, the predominate protein found in the aggregate is full-length apo SOD1 (31). Although an attractive hypothesis of how these aggregates can cause damage in the motor neurons is by sequestration of other essential proteins by co-aggregation with the aggregates, studies examining the composition of the aggregates from mice show that only SOD1 and ubiquitin are consistently found in the aggregates (31). This suggests that SOD1 is the main component in the aggregation and might carry out the toxic function alone.

1.5 SOD1 Mutation and Toxicity

Most ALS-SOD1 mutations are missense mutations, but some are frameshift mutations leading to small deletions, insertions, or truncations of the SOD1 sequence (32, 33). The ALS-causing point mutations in SOD1 can be classified into two categories based on their location: wild-type-like (WTL) and metal-binding-region (MBR). Point mutations remote from the active sites constitute the wild-type-like (WTL) group. These mutants have biophysical properties such as metal binding, activity, and spectroscopy that are almost indistinguishable from the WT (34-37). Mutations located in the metal binding loops affect the metal binding affinity and thus drastically affect the activity and structural integrity of SOD1. This group of mutants is referred to as the metal-binding-region (MBR) mutants. One of the most disruptive fALS mutations found in patient is L126Z, which is a frameshift mutation resulting in a stop codon at position 126. This results in the truncation of the C-terminal end. As a result of the C-terminal truncation, L126Z does not contain the conserved Cys146 or the catalytically important Arg143. This

mutant does not form disulfide bond and most likely has compromised or no catalytic function. Surprisingly, despite the low level of protein expression in mice due to its instability, L126Z is highly toxic and produces significant aggregation (30, 38). Along this line of observation, it has been reported that in a cell culture system, another C-terminal truncation mutant, G127X, is able to induce misfolding of WT SOD1 (39). These evidence suggest that the C-terminus of SOD1 is not absolutely required in misfolding, aggregation, and toxicity.

1.6 Role of WT SOD1 in sporadic ALS

Although the genetic composition of the SOD1 gene is different between sporadic and SOD1-fALS patients, recent discovery suggests that WT SOD1 might also acquire toxic function by conformational destabilization through deleterious post-translational modifications, suggesting that the involvement of WT SOD1 is possible in some cases of sporadic ALS. Motor neurons in the lumbosacral spinal cords isolated from a subset of sporadic ALS patients (carrying WT SOD1) are immunoreactive with the C4F6 antibody, which is reported to recognize only mutant SOD1 and oxidized WT-SOD1 (40). In support of this harmful role of aberrant WT SOD1 in sporadic cases, van Blitterswijk *et al.* found that sporadic ALS patients with higher levels of anti-SODox antibody, which recognizes the aberrantly oxidized SOD1 (SODox) antigen, had longer survival time, suggesting that the anti-SODox antibodies that sequester oxidized WT SOD1 are beneficial (41). Moreover, astrocytes generated from the post-mortem tissue of sporadic ALS patients are toxic to co-cultured motor neurons in a SOD1-dependent manner (42). When WT SOD1 expression in the astrocytes was reduced, toxicity diminished. The discovery that WT SOD1 can be toxic in transgenic mice, recently reported by Graffmo *et al.* may help to clarify the enigmatic role of WT SOD1. In a transgenic mouse model, over-

expression of WT SOD1 to the same level of a G93A SOD1 expression caused the development of ALS symptoms (43). In the past, the toxic property of WT SOD1 was unnoticed. This is most likely due to the lower expression level of WT SOD1 in those earlier systems.

1.7 Amyloid in Neurodegenerative Disease

The presence of intra- or extra-cellular insoluble protein inclusion in the affected neuronal tissues, formed by their respective polypeptides, is a hallmark of many neurodegenerative diseases, such as Alzheimer's, Parkinson's, and transmissible spongiform encephalopathies (TSEs) (44-46). These deposits have a fibrillar appearance, reminiscent of amyloid fibrils, and can only be dissolved by strong detergents. Amyloid fibrils are well-ordered, unbranched, elongated structures formed by extended cross-beta-sheets, with parallel or anti-parallel beta strands stacking perpendicular to the axis of fibril growth (47-51). Amyloid fibril can be detected by their binding to specific dyes such as Thioflavin-T (ThT), Thioflavin-S (ThS) and Congo Red (CR) (52). One of the proposed models suggests that in the fibril core, side chain residues of the beta-sheets interdigitate to create dry interfaces between sheets (53, 54). Packing of the beta-sheets is sequence-dependent (53). Fibrils made by polypeptides with the same composition but varying order sequence revealed distinct fibril morphologies. Although there is no consensus amino acid sequence among the various fibril forming polypeptides, frequent repetition of hydrophobic and polar residues is prevalent among fibrils. The origin of amyloid-associated toxicity is a highly debated topic and multiple mechanisms, such as impaired mitochondrial function (55), proteasome inhibition (28), inhibition of axonal transport (56), and permeation of the lipid bilayer (57, 58) have been proposed to explain how amyloid fibrils or associated structures can be toxic to a cell. Additionally, studies suggest that toxicity of fibril is

structure-dependent. Fibrils generated from the same polypeptide under different conditions, which lead to structural variations, can exhibit different toxicity in mammalian cells (59).

1.8 SOD1 Amyloid

Similar to other neurodegenerative diseases, SOD1 aggregates found in the spinal cords of G93A transgenic mice have shown to have fibrillar properties, such as filamentous structures visualized using immunogold electron microscopy and the ability to bind thioflavin-S (22, 60, 61). Furthermore, the formation of SOD1 aggregates closely correlates with motor neuron degeneration (62). This evidence suggests that SOD1 is capable of forming amyloid fibrils *in vivo* and that SOD1 amyloid might be the causative agent in the development of fALS.

In vitro, both WT and mutant SOD1 can be converted to amyloid fibrils under various conditions. While other researchers have used stringent conditions to convert soluble SOD1 to insoluble fibrils, such as low pH, heat, and the addition of trifluoroethanol (TFE), each of which drastically disrupts the SOD1 structure (63, 64), our laboratory has developed a relatively mild condition that is more physiologically relevant – simply adding a small amount of reducing agent (15). In the presence of a small amount of reducing agent (a concentration only enough to reduce a minor subpopulation of SOD1), such as glutathione, DTT, or TCEP, fibrils can be made *in vitro* in a 96-well plate with continuous agitation at 37 ˚C. As previously discussed, WT SOD1 can possess toxic function similar to the mutants in patients and animal and cell culture models. This intriguing discovery of the ability of WT SOD1 to convert to amyloid fibrils under the same condition as mutant SOD1 *in vitro* strengthens the evidence suggesting a role for WT SOD1 in sporadic ALS etiology. SOD1 fibrils prepared by DTT as the reducing agent have been shown to

11

be immunoreactive, causing cytokine induction in mononuclear cells and activation of microglial cells (65, 66). Although SOD1 protein inclusions are consistently found in ALS patients and in the transgenic mouse model, it remains unclear whether amyloid fibril or its precursors directly cause the death of motor neurons.

1.9 SOD1 Fibrillation Mechanism
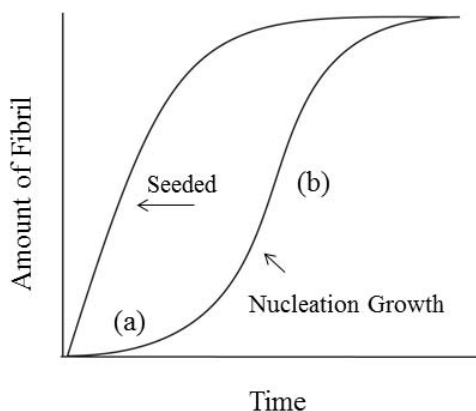
Figure 1.3. Fibril growth kinetics. Amyloid formation is a nucleation-dependent reaction, which is represented by a sigmoidal growth curve consisting of a lag-phase (a) and an elongation phase (b). (a) A nucleation or lag phase is the period within which the thermodynamically unfavorable formation of oligomeric nuclei from misfolded polypeptides occurs. (b) An elongation phase is the period within which the rapid growth of nuclei by addition of monomers (or dimers) occurs. Seeded reaction, which is achieved by adding pre-formed nuclei, significantly reduces lag time.

Amyloid formation is a complex multi-step oligomerization reaction. Similar to protein crystallization and microtubule formation, amyloid formation is generally accepted to be a nucleation-dependent process (67). The general mechanism begins with a thermodynamically unfavorable nucleation step, in which soluble polypeptides at least partially unfold or rearrange

to assemble the nucleus. The nucleus is the minimum number of multi-mer serving as a template that can recruit monomer to elongate and sustain fibril growth. Once the nucleus has formed, the elongation phase is more favorable. The rate-limiting nucleation step constitutes the lag phase, and the elongation phase is represented by an exponential growth. Therefore, the overall nucleation-dependent amyloid formation process is well represented by a sigmoidal curve as monitored by ThT fluorescence (Figure 3). A defining feature of the nucleation-dependent mechanism is the ability to bypass the rate-limiting nucleation step by adding pre-formed fibril nucleus (seed) to the reaction. As a consequence, a seeded/nucleated reaction does not have a lag phase.

Unlike the better characterized Abeta protein and its fibrillation mechanism, the exact molecular mechanism of SOD1 fibrillation is not fully understood, partly because of SOD1's complicated post-translational maturation process (insertion of metal cofactors and formation of disulfide bonds) as discussed above, indicating that various intermediate species can co-exist *in vivo*. Each intermediate species might play a different role in the fibrillation mechanism. Fully mature SOD1 (SS-Cu$_2$Zn$_2$SOD1) is extremely stable and does not form aggregates *in vitro* even after prolonged incubation at 37 °C (15). Since the aggregates isolated from mice are composed of primarily apo unmodified SOD1, studies presented here focus on apo SOD1 proteins.

SOD1 fibrils can be prepared *in vitro* from apo SOD1 under a variety of conditions, such as in the presence of 5 mM DTT or 1 M guanidine hydrochloride (GdmCl) (15). Disulfide reduction of apo SOD1 dimers results in disulfide reduced monomers. On the other hand, the presence of a chaotropic agent, such as 1 M GdmCl, causes SOD1 dimers to dissociate into disulfide-oxidized monomers. Although reduction of the disulfide bond is not an absolute

requirement, structural destabilization of the dimeric apo protein seems to be a prerequisite to initiate aggregation. To our surprise, once initiation (formation of one or more amyloid nuclei) has occurred, elongation can proceed through the recruitment of more structurally stable dimeric apo disulfide-oxidized SOD1 (SS-ApoSOD1) and one zinc per dimer disulfide-oxidized SOD1 (SS-E$_2$EZnSOD1). In experimental settings, the initiation and elongation steps can be assayed separately. A small amount (5% V/V) of disulfide-reduced apo SOD1 (2SH-ApoSOD1) can initiate the fibrillation of SS-ApoSOD1 in the absence of any reducing agent (15). Alternatively, SOD1 can bypass the initiation phase by elongating on SOD1 nuclei prepared by fragmentation of pre-formed fibrils through sonication.

2.0 Current and Future perspectives

Our laboratory focuses on three main goals: 1) Characterize the differences between mutant and WT SOD1 and determine the toxic gain-of-function attributed by mutant SOD1 that causes fALS. 2) Understand the structure and formation mechanism of SOD1 fibril and its precursors and their correlations with both sporadic and familial ALS. 3) Investigate the role of WT SOD1 in sporadic ALS. My work presented in the following chapters will discuss the structural analysis of SOD1 fibrils and the discovery of several SOD1 amyloid inhibitors, their inhibition mechanisms, and the discovery of SOD1 oligomers. Together, these findings provide us new insights into the SOD1 fibrillation mechanism. By following up these findings *in vivo*, it may help us to pinpoint the exact underlying disease-causing entity in both sporadic and familial and their formation mechanisms. Hopefully, our research will lead to the development of effective therapeutic treatment for ALS.

References

1. Bruijn LI, Miller TM, & Cleveland DW (2004) *Annu Rev Neurosci* **27,** 723-749.

2. Valentine JS, Doucette PA, & Zittin Potter S (2005) *Annu Rev Biochem* **74,** 563-593.

3. Rosen DR (1993) *Nature* **364,** 362.

4. Higgins CM, Jung C, & Xu Z (2003) *BMC Neurosci* **4,** 16.

5. Wong PC, Pardo CA, Borchelt DR, Lee MK, Copeland NG, Jenkins NA, Sisodia SS, Cleveland DW, & Price DL (1995) *Neuron* **14,** 1105-1116.

6. Bruijn LI, Becher MW, Lee MK, Anderson KL, Jenkins NA, Copeland NG, Sisodia SS, Rothstein JD, Borchelt DR, Price DL, *et al.* (1997) *Neuron* **18,** 327-338.

7. Goto JJ, Gralla EB, Valentine JS, & Cabelli DE (1998) *J Biol Chem* **273,** 30104-30109.

8. Fridovich I (1997) *J Biol Chem* **272,** 18515-18517.

9. Okado-Matsumoto A & Fridovich I (2001) *J Biol Chem* **276,** 38388-38393.

10. Sturtz LA, Diekert K, Jensen LT, Lill R, & Culotta VC (2001) *J Biol Chem* **276,** 38084-38089.

11. Roe JA, Butler A, Scholler DM, Valentine JS, Marky L, & Breslauer KJ (1988) *Biochemistry* **27,** 950-958.

12. Arnesano F, Banci L, Bertini I, Martinelli M, Furukawa Y, & O'Halloran TV (2004) *J Biol Chem* **279,** 47998-48003.

13. Hart PJ, Liu H, Pellegrini M, Nersissian AM, Gralla EB, Valentine JS, & Eisenberg D (1998) *Protein Sci* **7,** 545-555.

14. Tainer JA, Getzoff ED, Beem KM, Richardson JS, & Richardson DC (1982) *J Mol Biol* **160,** 181-217.

15. Chattopadhyay M, Durazo A, Sohn SH, Strong CD, Gralla EB, Whitelegge JP, & Valentine JS (2008) *Proc Natl Acad Sci U S A* **105,** 18663-18668.

16. Strange RW, Antonyuk S, Hough MA, Doucette PA, Rodriguez JA, Hart PJ, Hayward LJ, Valentine JS, & Hasnain SS (2003) *J Mol Biol* **328,** 877-891.

17. Reaume AG, Elliott JL, Hoffman EK, Kowall NW, Ferrante RJ, Siwek DF, Wilcox HM, Flood DG, Beal MF, Brown RH, Jr.*, et al.* (1996) *Nat Genet* **13,** 43-47.

18. Bruijn LI, Houseweart MK, Kato S, Anderson KL, Anderson SD, Ohama E, Reaume AG, Scott RW, & Cleveland DW (1998) *Science* **281,** 1851-1854.

19. Hodgson EK & Fridovich I (1975) *Biochemistry* **14,** 5299-5303.

20. Hodgson EK & Fridovich I (1975) *Biochemistry* **14,** 5294-5299.

21. Wiedau-Pazos M, Goto JJ, Rabizadeh S, Gralla EB, Roe JA, Lee MK, Valentine JS, & Bredesen DE (1996) *Science* **271,** 515-518.

22. Wang J, Slunt H, Gonzales V, Fromholt D, Coonfield M, Copeland NG, Jenkins NA, & Borchelt DR (2003) *Hum Mol Genet* **12,** 2753-2764.

23. Shibata N, Nagai R, Uchida K, Horiuchi S, Yamada S, Hirano A, Kawaguchi M, Yamamoto T, Sasaki S, & Kobayashi M (2001) *Brain Res* **917,** 97-104.

24. Fitzmaurice PS, Shaw IC, Kleiner HE, Miller RT, Monks TJ, Lau SS, Mitchell JD, & Lynch PG (1996) *Muscle Nerve* **19,** 797-798.

25. Andrus PK, Fleck TJ, Gurney ME, & Hall ED (1998) *J Neurochem* **71,** 2041-2048.

26. Dal Canto MC & Gurney ME (1994) *Am J Pathol* **145,** 1271-1279.

27. Jaarsma D, Rognoni F, van Duijn W, Verspaget HW, Haasdijk ED, & Holstege JC (2001) *Acta Neuropathol* **102,** 293-305.

28. Urushitani M, Kurisu J, Tsukita K, & Takahashi R (2002) *J Neurochem* **83,** 1030-1042.

29. Nagano S, Satoh M, Sumi H, Fujimura H, Tohyama C, Yanagihara T, & Sakoda S (2001) *Eur J Neurosci* **13,** 1363-1370.

30. Jonsson PA, Ernhill K, Andersen PM, Bergemalm D, Brannstrom T, Gredal O, Nilsson P, & Marklund SL (2004) *Brain* **127,** 73-88.

31. Shaw BF, Lelie HL, Durazo A, Nersissian AM, Xu G, Chan PK, Gralla EB, Tiwari A, Hayward LJ, Borchelt DR*, et al.* (2008) *J Biol Chem* **283,** 8340-8350.

32. Cleveland DW & Rothstein JD (2001) *Nat Rev Neurosci* **2,** 806-819.

33. Andersen PM, Sims KB, Xin WW, Kiely R, O'Neill G, Ravits J, Pioro E, Harati Y, Brower RD, Levine JS*, et al.* (2003) *Amyotroph Lateral Scler Other Motor Neuron Disord* **4,** 62-73.

34. Valentine JS & Hart PJ (2003) *Proc Natl Acad Sci U S A* **100,** 3617-3622.

35. Hayward LJ, Rodriguez JA, Kim JW, Tiwari A, Goto JJ, Cabelli DE, Valentine JS, & Brown RH, Jr. (2002) *J Biol Chem* **277,** 15923-15931.

36. Rodriguez JA, Valentine JS, Eggers DK, Roe JA, Tiwari A, Brown RH, Jr., & Hayward LJ (2002) *J Biol Chem* **277,** 15932-15937.

37. Tiwari A & Hayward LJ (2003) *J Biol Chem* **278,** 5984-5992.

38. Zu JS, Deng HX, Lo TP, Mitsumoto H, Ahmed MS, Hung WY, Cai ZJ, Tainer JA, & Siddique T (1997) *Neurogenetics* **1,** 65-71.

39. Grad LI, Guest WC, Yanai A, Pokrishevsky E, O'Neill MA, Gibbs E, Semenchenko V, Yousefi M, Wishart DS, Plotkin SS*, et al.* (2011) *Proc Natl Acad Sci U S A* **108,** 16398-16403.

40. Bosco DA, Morfini G, Karabacak NM, Song Y, Gros-Louis F, Pasinelli P, Goolsby H, Fontaine BA, Lemay N, McKenna-Yasek D*, et al.* (2010) *Nat Neurosci* **13,** 1396-1403.

41. van Blitterswijk M, Gulati S, Smoot E, Jaffa M, Maher N, Hyman BT, Ivinson AJ, Scherzer CR, Schoenfeld DA, Cudkowicz ME*, et al.* (2011) *Amyotroph Lateral Scler* **12,** 430-438.

42. Haidet-Phillips AM, Hester ME, Miranda CJ, Meyer K, Braun L, Frakes A, Song S, Likhite S, Murtha MJ, Foust KD*, et al.* (2011) *Nat Biotechnol* **29,** 824-828.

43. Graffmo KS, Forsberg K, Bergh J, Birve A, Zetterstrom P, Andersen PM, Marklund SL, Brannstrom T (2013) *Hum Mol Genet* **22,** 51-60.

44. Honjo K, Black SE, Verhoeff NP (2012) *Can J Neurol Sci* **39,** 712-728.

45. Aarsland D, Londos E, & Ballard C (2009) *Int Psychogeriatr* **21,** 216-219.

46. Hope J, Reekie LJ, Hunter N, Multhaup G, Beyreuther K, White H, Scott AC, Stack MJ, Dawson M, Wells GA (1988) *Nature* **336,** 390-392.

47. Cohen AS & Calkins E (1959) *Nature* **183,** 1202-1203.

48. Geddes AJ, Parker KD, Atkins ED, & Beighton E (1968) *J Mol Biol* **32,** 343-358.

49. Sunde M & Blake C (1997) *Adv Protein Chem* **50,** 123-159.

50.   Sunde M, Serpell LC, Bartlam M, Fraser PE, Pepys MB, & Blake CC (1997) *J Mol Biol* **273,** 729-739.

51.   Eanes ED & Glenner GG (1968) *J Histochem Cytochem* **16,** 673-677.

52.   Nilsson MR (2004) *Methods* **34,** 151-160.

53.   Makin OS, Atkins E, Sikorski P, Johansson J, & Serpell LC (2005) *Proc Natl Acad Sci U S A* **102,** 315-320.

54.   Thompson MJ, Sievers SA, Karanicolas J, Ivanova MI, Baker D, & Eisenberg D (2006) *Proc Natl Acad Sci U S A* **103,** 4074-4078.

55.   Eckert A, Hauptmann S, Scherping I, Meinhardt J, Rhein V, Drose S, Brandt U, Fandrich M, Muller WE, Gotz J (2008) *J Mol Med (Berl)* **86,** 1255-1267.

56.   Strom AL, Shi P, Zhang F, Gal J, Kilty R, Hayward LJ, & Zhu H (2008) *J Biol Chem* **283,** 22795-22805.

57.   Williams TL, Day IJ, & Serpell LC (2010) *Langmuir* **26,** 17260-17268.

58.   Shaw BF & Valentine JS (2007) *Trends Biochem Sci* **32,** 78-85.

59.   Nekooki-Machida Y, Kurosawa M, Nukina N, Ito K, Oda T, & Tanaka M (2009) *Proc Natl Acad Sci U S A* **106,** 9679-9684.

60.   Basso M, Massignan T, Samengo G, Cheroni C, De Biasi S, Salmona M, Bendotti C, & Bonetto V (2006) *J Biol Chem* **281,** 33325-33335.

61.   Jaarsma D, Teuling E, Haasdijk ED, De Zeeuw CI, & Hoogenraad CC (2008) *J Neurosci* **28,** 2075-2088.

62.   Prudencio M, Hart PJ, Borchelt DR, & Andersen PM (2009) *Hum Mol Genet* **18,** 3217-3226.

63.   DiDonato M, Craig L, Huff ME, Thayer MM, Cardoso RM, Kassmann CJ, Lo TP, Bruns CK, Powers ET, Kelly JW, *et al.* (2003) *J Mol Biol* **332,** 601-615.

64.   Doucette PA, Whitson LJ, Cao X, Schirf V, Demeler B, Valentine JS, Hansen JC, & Hart PJ (2004) *J Biol Chem* **279,** 54558-54566.

65.   Fiala M, Chattopadhay M, La Cava A, Tse E, Liu G, Lourenco E, Eskin A, Liu PT, Magpantay L, Tse S, *et al.* (2010) *J Neuroinflammation* **7,** 76.

66.   Roberts K, Zeineddine R, Corcoran L, Li W, Campbell IL, Yerbury JJ (2013) *Glia* **61,** 409-419.

67.   Jarrett JT & Lansbury PT, Jr. (1993) *Cell* **73,** 1055-1058.

Chapter 2

Structural Analysis of Superoxide Dismutase-1 Fibrils Using Limited Proteolysis

and Atomic Force Microscopy

(Submitted to *Proceedings of the National Academy of Sciences U.S.A*)

Abstract

Abnormal assemblies formed by misfolded superoxide dismutase-1 (SOD1) proteins are the likely cause of SOD1-linked familial amyotrophic lateral sclerosis (fALS) and may be involved in some cases of sporadic ALS. To analyze the structure of the insoluble SOD1 amyloid fibrils, we first used limited proteolysis followed by mass spectrometric analysis. Digestion of amyloid fibrils formed from full-length N-acetylated wild-type (WT) SOD1 with trypsin, chymotrypsin, or Pronase revealed that the first 63 residues of the amino-terminal were protected from protease digestion by fibril formation. Furthermore, every tested ALS-mutant SOD1 protein (G37R, L38V, G41D, G93A, G93S, and D101N SOD1) showed a similar protected fragment after trypsin digestion. Our second approach to structural characterization used atomic force microscopy to image the SOD1 fibrils and revealed that WT and mutants showed similar twisted morphologies. WT fibrils had a consistent average helical pitch distance of 62.1 nm. The ALS-mutant SOD1 proteins L38V, G93A, and G93S formed fibrils with helical twist patterns very similar to those of WT, while small but significant structural deviations were observed for the mutant proteins G37R, G41D, and D101N. Overall, our studies suggest that all the WT and mutants tested have an intrinsic propensity to fibrillate through the N-terminus and that single amino-acid substitutions can lead to changes in helical twist pattern.

Introduction

Amyotrophic lateral sclerosis (ALS) or Lou Gehrig's disease is a devastating motor neuron disease characterized by the formation of abnormal protein aggregates in neuronal cells. Over one hundred different mutations in sod1 have been identified and linked to familial ALS (fALS). While the precise mechanism(s) by which this diverse group of mutations causes fALS

remains unclear, it is generally agreed that the ALS mutant SOD1 proteins are prone to misfold and that they acquire toxic properties as a consequence (1-3). Abnormal protein deposits are frequently seen in protein misfolding diseases, and SOD1-containing aggregates have consistently been found in the spinal cords of ALS transgenic mice and fALS patients (4, 5). Moreover, in ALS transgenic mice, these proteinaeous deposits have frequently been shown to have amyloid-like properties such as filamentous structures and the ability to bind thioflavin-S (6-8). A number of other proteins that have been linked to neurodegenerative diseases form amyloid fibrils. Such fibrils are elongated, unbranched, and highly ordered protein aggregates composed mainly of cross-beta sheets, with parallel or anti-parallel beta strands stacking perpendicular to the axis of fibril growth (9-13).

Detergent-resistant aggregates isolated from the spinal cords of ALS transgenic mice contain full length and metal-free hSOD1 proteins, suggesting that it is full-length apo hSOD1 that acquires toxic properties in the disease mechanism (14). Moreover, as established earlier in our laboratory, full-length, soluble apo hSOD1 can readily be converted in vitro to a morphologically homogeneous preparation of amyloid fibrils by incubation with a small amount of reducing agent (15). SOD1 fibrils made under these conditions have recently been shown to induce cytokine expression in mononuclear cells, thus causing inflammation (16), and to activate microglial cells (17), suggesting that fibrils made under these mild physiologically relevant conditions have toxic properties that may be related to ALS. However, due to the insolubility and non-crystalline nature of these materials, the molecular structure(s) of such materials have not yet been determined by methods such as NMR and X-ray crystallography.

The goals of the present study were to determine which regions of the WT and ALS mutant SOD1 proteins form the amyloid core of the SOD1 fibrils prepared using the conditions developed in our laboratory (15, 18) and to compare the structural morphologies of these WT and ALS mutant SOD1 fibrils.

We used limited proteolysis coupled to LC-MS and MS/MS, which has been widely used to probe the structure of amyloid fibrils (19-24), and we also studied the fibrils using atomic force microscopy. We find that the core regions of both WT and mutant fibrils are consistently composed of the N-terminus of the SOD1 protein, but that the twist patterns of mutant SOD1 fibrils may differ from those of the WT protein.

Results

The Most Protease-Resistant Region of Wild-Type SOD1 is Formed by the Amino-Terminal Region of SOD1. To determine the region of WT hSOD1 that is most resistant to protease digestion in the fibrils, soluble WT SOD1 was induced to form fibrils in the presence of 5 mM dithiothreitol (DTT), following the protocol previously published (15). The formation of fibrils was monitored by the fluorescence emission of Thioflavin-T (ThT). Mature fibrils, as indicated by reaching the plateau of Thioflavin-T binding, were retrieved from the plate, collected by ultra-centrifugation, and subjected to partial trypsin proteolysis. After digestion, the protease was quenched with 1 mM PMSF and re-centrifuged to separate the digested soluble peptides (S2) from the proteolytically resistant region of SOD1 that remained insoluble (P2). P2 was then solubilized by 7.2 M guanidine hydrochloride (GdnHCl) and 0.5 M DTT overnight at 37 ˚C. One major advantage of using trypsin is that peptides released in S2 are not digested to

single amino acids and can thus be identified by mass spectrometry. The compositions of P2 and S2 were then analyzed by HPLC-MS.

When soluble WT SOD1 was digested by trypsin under the same condition, twelve peptides spanning the full-length sequence of SOD1 were recovered and identified by HPLC-MS (Table S1) demonstrating that soluble apo WT disulfide-oxidized SOD1 can be completely digested by this trypsin digestion condition. However, when WT SOD1 fibrils were digested, one polypeptide with a retention time of 30.49 min was found to be the primary product in P2, as shown by the total ion count (TIC) chromatograph (Fig. 1). This peptide has a measured average molecular mass of 7,285 Da, corresponding to the mass of the N-terminal acetylated tryptic peptide 1-69 in the sequence of WT SOD1 (numbered from the mature N-terminus with the initiating Met residue removed). Note that five tryptic cleavage sites (K3, K9, K23, K30, and K36) in this region that were accessible in soluble WT protein became protected in the fibrillar configuration. In contrast, C-terminal peptides were cut and released to S2. The most abundant species from S2 were from the carboxyl-terminal end of the SOD1 sequence. Peptide bonds at residues R115, K122, R143 were cleaved, resulting in the release of peptides 80-115, 116-122, and 144-153 to S2. These results suggest that the regions surrounding these corresponding cleavage sites were neither sterically nor conformationally hindered. Small amounts of tryptic peptides from the N-terminal region of SOD1 were also found in the soluble S2 fraction, possibly due to a small degree of heterogeneity of fibrils (subsets of fibrils with different conformations), over-digestion, or dissociation of SOD1 from the fibril due to the dynamic nature of amyloid fibrils (25).

To confirm our findings, Pronase and chymotrypsin, proteases with broader specificity, were used. In both cases, the protease-resistant region found in P2 was shortened to residues 1-63. The identity of the peptide was confirmed by MS/MS (Fig. S4, S5, and Table S4). Sixteen chymotryptic cleavage sites (L8, D11, N19, F20, E21, E24, N26, W32, L38, E40, L42, F45, E49, F50, D52, and N53) from the N-terminus became protected in the fibrils. Since Pronase is a mixture of proteases that is capable of digesting the solvent-accessible region completely to single amino acid residues, the fact that 1-63 remained undigested strongly suggests that these residues comprise the minimal protease-resistant core region in WT SOD1 fibrils under these digestion conditions.

WT and Mutant Fibrils Share the Same Amino-terminal Core. Single point mutations in the SOD1 gene are responsible for causing SOD1-linked fALS. Most of these mutations result in SOD1 proteins with single amino-acid substitutions and with biophysical properties very similar to the WT, making it difficult to postulate the disease-causing property conferred by these mutations. Moreover, it has recently been reported that not only mutant hSOD1 but also WT hSOD1 protein expressed at high levels in transgenic mice can lead to ALS (26). Large amounts of aggregated WT hSOD1 protein were found in spinal cords and brains of these mice suggesting that WT hSOD1 protein may also become toxic in some forms. Thus, we aimed to determine whether ALS-mutant SOD1 protein fibrils prepared using our protocol have structures distinct from that of the WT SOD1 fibrils.

To minimize heterogeneity among different samples attributable to sample handling or ambient conditions, fibrils were made from the mutant proteins and WT SOD1 simultaneously and were also trypsin digested simultaneously. Three amino-terminal mutants (G37R, L38V, and

G41D) and three carboxyl-terminal mutants (G93A, G93S, and D101N) were tested. P2 of each contained primarily one peak with LC-MS retention time of around 30 min (Fig. S2). Peptide molecular mass deconvolution of each entire chromatogram revealed predominantly one species, the N-terminal residues 1-69 of each mutant, as in WT, with altered mass for the N-terminal mutations but unchanged mass for the C-terminal mutants (Fig. 2). Occasionally, a small amount of the C-terminal peptide 143-153 was also found in P2 (Table S3), though it was always more abundant in S2. These observations strongly suggest a unifying fibrillation mechanism in which the N-terminal end of SOD1 embedded in the core acquires protease resistance and forms the most inaccessible region of these fibrils.

Atomic Force Microscopy (AFM) Analysis on WT and Mutant SOD1 Fibrils. AFM in tapping mode was employed to analyze the morphology of the SOD1 fibrils. It has been reported that fibril structures can evolve over time (27). Therefore, to achieve maximum consistency, fibril samples were taken from the plate after 45 hours of incubation and placed on the mica immediately. As has been observed in other amyloid fibrils, periodic twists that give the fibrils "bead-like" morphology were observed on the SOD1 fibrils (27-29). Since the width measurement of the fibril is subjected to variation of the AFM tip, height measurement was used as an indication of fibril diameter. The typical heights of the peaks of the fibrils were about 5-7 nm and the heights of the trough were around 3.5-4.0 nm. The lengths of the fibrils vary from 200 nm to 3 μm. These measurements fall into the range reported for other amyloid fibrils.

We were able to measure the pitch distances on the SOD1 fibrils to nanometer resolution (Fig. 3). By sectioning along the fibril using SPIPTM, more than 200 helical twists on at least 30 fibrils for each WT and mutant were counted. Fibrils that were thinner than 4 nm or shorter than

500 nm were excluded from measurement since they might be protofibrils that had yet to adopt the final conformation. Histograms were constructed based on each individual peak distance measurement, and Gaussian curve fits on the histograms were constructed using OriginPro 8.1 (Fig. 4). The helical pitch distances along the WT fibrils are mostly consistent despite a small degree of variation. Nevertheless, general twist patterns are observed. The average twist distance for WT is ~ 62.14 nm with a standard deviation of +/- 15.10 nm (Fig. S3). The average helical pitch distances for L38V, G93A, and G93S are not significantly different from WT. In contrast, G37R and G41D showed a substantial decrease in average helical pitch distance, to 35.80 nm (G37R) and 35.07 nm (G41D) compared with 62.14 nm (WT). The distribution of helical twists for D101N was more irregular, as is evident in the wider distribution in the histogram and the larger standard deviation.

Discussion

The studies presented here provide two major new observations. First, in our partial proteolysis experiments, we show that the most protease-resistant region of the WT and of each of the SOD1 mutant fibrils tested here is remarkably similar, being largely composed of the acetylated amino-terminus of the SOD1 polypeptide. Five trypsin cleavage sites within residues 1-69 became inaccessible when the proteins were in the fibrillar form, consistently for WT and across all the mutants we tested. When the fibrils were digested with Pronase, the minimal core region further shortened to residues 1-63. Since a flexible region of about ten residues is required on the substrate for proteolysis to occur (30), the actual SOD1 sequence participated in the core might be shorter than 63 residues even though position 63-64 is the last peptide bond susceptible

to digestion. Our results are thus consistent with the findings reported by Lang et al. that loops IV and VII are not required for fibril formation (31).

The N-terminal 1-63 residues form beta strands 1-4 in the native SOD1 structure (Fig 5), with beta strands 1-3 and 6 forming one beta sheet and beta strand 4 crossing over to the other side to form a second beta sheet with strands 5, 7, and 8; together forming the Greek-key beta barrel fold. Since strand 4, which is natively present in the second sheet, associates with strands 1-3 in the fibrillar state, our data demonstrate that the beta strand connectivity must undergo a major change in the process of fibril formation. In this respect, it is interesting to note that apo WT and ALS-mutant proteins (A4V, G93R, H48Q) are known to exist at physiological temperature as partially unfolded beta barrels, in which residues 21-53, which includes strands 3 & 4, undergo rapid exchange of the backbone protons with deuterons (H/D exchange) (32). Increased H/D exchange in strands 3 and 4 implies a loosening of the hydrogen-bond networks with strands 2 & 6 and strands 5 & 7, respectively (Fig. 5). This increased flexibility might render hydrogen bond donors and acceptors on strands 3 and 4 more available, possibly creating unprotected beta-sheet edges that might drive the non-native intermolecular interaction of the N-terminus with other SOD1 subunits to form amyloid fibrils (residues 53-104 were not recovered from the reported H/D exchange experiment, and thus it is not known whether disruption of the hydrogen-bond network extends to this region). It should also be noted that strands 3 and 4 contain the segment 33-38, which has been predicted to be amyloidogenic based on the steric zipper model (33). In addition, aromatic residues are frequently found within amyloid-forming proteins, and it is postulated that they play a role in fibril stability (34). Interestingly, one

trytophan and three phenylalanines are present in the N-terminus while there are no aromatic residues in the C-terminus.

The protected N-terminal core region we observe in our experiments is remarkably consistent between WT SOD1 and each of the six mutant SOD1 proteins we examined, in contrast to the wide assortment of protected regions reported by Furukawa *et al*. for fibrils prepared by their method (35). This discrepancy is likely explained by their use of a non-native N-terminal sequence and/or the different fibrillation conditions. The recombinant SOD1 used in the Furukawa study contained a four amino-acid residue extension at the N-terminus and lacked the native N-terminal acetyl group (The peptide Gly-Ser-His-Met was the remnant of a cleaved His$_6$ tag.). Post-translational modifications, such as N-terminal acetylation (36, 37) and C-terminal amidation (38, 39), have been reported in some instances to have profound effects on the structure and amyloidogenicity of peptides. In addition, since it is known that A4V is an ALS-causing mutation in SOD1, we felt it wise to ensure the complete fidelity of our SOD1 preparations by retaining the native N-acetyl Ala SOD1 N-terminus.

Our fibrillation conditions were also different from those reported by Furukawa *et al*. (35), potentially contributing to differences in degrees of structural homogeneity of the fibril structures. Another possible explanation for the differences could be different fibrillation conditions. Fibril structure can be strongly influenced by multiple factors such as buffer, pH, temperature, mode and intensity of agitation (40-42). Our fibrils have a consistent gross fibrillar morphology as seen in both AFM (Fig. 3) and EM (Fig. S6). By contrast, the EM images of the fibrils reported by Furakawa et al. show a wide assortment of widths and shapes, suggesting to us that these fibrils have diverse morphologies.

While we found the C-terminal peptide 143-153 to be present in relatively high abundance in the S2 fraction, we also occasionally found a small amount of this peptide in the P2 residual fibril. Its presence in sub-stoichiometric amounts in P2 suggests that this region is not part of the amyloid core of the major fibrillar species, but rather that it arises from a small fraction of the total fibrils, since a small degree of fibril polymorphism cannot be ruled out from our data. Another possibility is an attachment of this peptide to the N-terminal peptide present in the pellet through the native disulfide bond (C57-C146). As previously reported, disulfide-intact apo SOD1 can be recruited to the fibril by disulfide-reduced apo SOD1(15). However, since this peptide (containing C146) is found mostly in S2, it suggests that the native disulfide bond in most proteins in the fibrils is not intact.

Our second set of findings concerns the morphology of the fibrils as visualized by our AFM experiments. Both mutants and WT protein form amyloid fibrils with a twisted morphology. For three of the mutant protein fibrils, L38V, G93A, and G93S, the morphology was strikingly similar to that of WT, but the other three showed significant differences in pitch length. Intriguingly, these latter mutations, G37R, G41D, and D101N, cause a net change in charge. While the extended beta-sheet of fibrils is largely stabilized by the hydrogen bonding network of the polypeptide backbone, side chain residues can also form hydrogen bonds and contribute to the fibril stability (29, 43). Additionally, the packing of the beta-sheet is sequence-dependent (44). In the steric zipper model developed from the crystal structures of micro-crystals of amyloidogenic short polypeptides, the side-chains of two beta-sheets interdigitate to create a "dry zipper" in the core (44, 45). Inside the fibrils, beta-sheets can be zipped together and stabilized by the noncovalent interactions (hydrophobic, π-π stacking or salt-bridge) of the side

chains. Therefore, mutations within the core beta-sheets have a higher potential of altering the alignment and arrangement of beta sheet packing and the extent of the hydrogen-bond network, which dictate the twist and rigidity of a single strand of protofilament. Since the packing of protofilaments within the fibril is stabilized by many weak long range electrostatic (or hydrophobic) interactions along the protofilaments, all of which must accommodate the twist and rigidity of the protofilaments, changes in the beta-sheet packing pattern and the stability of the beta-sheet induced by a single mutation are likely to propagate to the supermolecular packing and the final twist of the fibrils (46-48). This result is demonstrated for mutations such as G37R and G41D, both of which occur within the N-terminal region that forms the fibril core and constitute significant changes in size as well as in charge. Interestingly, D101N, a substitution with a change in charge that is outside of the core region also changes the amyloid helical pitch. This result may be explained by the changes in electrostatic interactions on the surface of the protofilaments. On the other hand, L38V, another substitution within the core region that does not change the overall charge, does not cause a change in helical twist pattern, indicating that mutations within the core do not necessarily perturb the fibril superstructure.

Morphological differences such as those we have observed might be related to differences in toxic properties of the fibrils. The origin of amyloid-associated toxicity is a highly debated topic and multiple mechanisms, such as impaired mitochondrial function (49), proteasome inhibition (50), and permeation of the lipid bilayer (51, 52) have been proposed to explain how amyloid fibrils or associated structures can be toxic to a cell. These effects may be dependent on the structure of the fibrils or their fibrillar precursors. The toxicity of amyloid fibrils from huntingtin exon1 toward cultured cells, was different for fibrils generated under

various growth conditions that lead to structural differences (53). Furthermore, seeding specificity in prion has been shown to be dependent on fibril structure (54). Although formation of in vivo aggregates seeded by in-vitro SOD1 fibrils has not been reported, SOD1 fibrils or associated species might act as a template for the formation of the toxic species. It has been noted for SOD1-associated fALS patients that SOD1 mutations resulting in a change of net charge tend to correlate with longer survival times (> 5 years) (55). It is possible that these changes in survival times are related to the significantly changed fibril structures in mutants with a change in net charge.

Relevance of the N-terminus of SOD1 in aggregation and toxicity in vivo has also been highlighted in several papers. A recent paper from Prudencio *et al.* showed that an antibody raised against residues 24-36 could not recognize aggregated mutant SOD1 formed in cell culture model, while antibody targeting the C-terminal residues 143-151 recognized both soluble and aggregated SOD1(56). Second, Cashman et al., reported that G127X and G85R induced misfolding of WT SOD1 in a Trp32-dependent manner (57); when Trp32 was altered to Ser, this ability was demolished. In addition, a Trp to Phe substitution (W32F) in G93A decreased motor neuron death due to the G93A alteration (58). On the other hand, the C-terminus appears to be non-essential in amyloid/aggregation formation and toxicity related to ALS (59-61).

In summary, we provide evidence that WT and ALS-mutant SOD1 proteins, despite their different structural properties, have a strong tendency to form amyloid fibrils with the amino-terminus as the core. Fibrils formed from ALS-mutant SOD1 proteins with an overall net charge different from that of WT appear to deviate more in overall fibril morphology than mutant proteins with the same overall net charge. It is important to note here also that, although the C-

terminus is not a major part of the core of the amyloid fibril structure, it is likely to play a secondary role in the amyloid packing pattern and in the mechanism of amyloid propagation. Our work here also provides information that could be used for structure-based drug design, either to destabilize the fibril conformations or to stabilize them, depending upon the relative toxicities of the SOD1 fibrils and their associated precursors. In any case, preventing the amino-terminus from self-associating may be a goal for drug design, in order to prevent the formation of toxic fibrils or soluble intermediates formed during the amyloid formation cascade. We also show that substitutions at position 37 or 41 to charged residues significantly lowers the twist distances within the fibrils. Since different fibril morphology might have different interacting partners and seeding ability in vivo, experiments designed to test the toxicity of different conformations of fibrils may be important in understanding of the role of SOD1 fibrils in ALS.

Materials and Methods

SOD1 Expression and Purification

WT and site-directed mutagenesis of WT were performed as described in (62, 63). WT and fALS SOD1 were purified from the EG118 strain of Saccharomyces cerevisiae following the procedures from (64), yielding SOD1 with the initial Met1 removed and Ala2 N-acetylated covalently identical to SOD1 from human sources. To convert to apo, purified SOD1 was dialyzed three times against 50 mM EDTA and 100 mM sodium acetate at pH 3.8. The protein was then dialyzed three times in 100 mM NaCl and 100 mM sodium acetate, pH 3.8, to remove SOD1-bound EDTA. After demetallation, SOD1 was dialyzed in 10 mM potassium phosphate, pH 7.0, filter-sterilized, and flash-frozen in liquid nitrogen and kept at − 20 °C until use.

Inductively coupled plasma (ICP)-MS was used to quantify metal status (14). All apo-proteins contain less than 0.10 equivalents of copper and zinc per dimer.

In Vitro Fibril Formation

To make fibrils, 50 μM of apo SOD1 was prepared in 10 mM potassium phosphate, pH 7.0, with 5 mM DTT and 40 μM of thioflavin-T (ThT) as described (15). After mixing, the solution was placed in a 96-well plate with a 1/8-in teflon ball and incubated at 37 °C with continuously shaking at 300 rpm for forty-five hours. Assembly of fibril was monitored by fluorescence measurement at λem = 485 nm (λex =444 nm) using a Fluoroskan plate-reader (Thermo Fisher). All solutions were made with chelexed metal-free distilled deionized water (ddH2O) and filtered through a 0.22 μm filter.

Proteolysis of Fibrillar and Soluble SOD1

Soluble and purified SOD1 fibrils were subjected to trypsin (Promega, porcine) proteolysis in 50 mM NH_4HCO_3 at 37 °C for 30 min at 1:30 (W/W) E:S ratio. Separation of SOD1 fibrils from other soluble contaminants was performed by ultracentrifugation in an airfuge (Beckman Coulter) at 125,000 X g for 30 minutes and the pellet was washed with 50 mM NH_4HCO_3. Quantity of SOD1 in the fibril was determined by subtracting soluble SOD1 in the supernatant from the starting amount. The amount of SOD1 in the supernatant was measured using A_{280} nm in a RP-HPLC-MS system. Soluble apo SOD1 was diluted to the same concentration as the fibril with 50mM NH_4HCO_3 and digested similarly.

After partial proteolysis, the reaction was quenched by adding 1 mM PMSF and the fibrils were spun down at 125,000 X g for 30 min to collect the protease-resistant pellet and the

protease-digestible supernatant. The pellet was further dissolved in 7.2 M GdnHCl and 0.5 M DTT at 37 °C overnight. Supernatant was subjected to reduction by 250 mM DTT at 37°C for one hour. Both pellet and supernatant were subsequently analyzed by RP-HPLC-MS.

Proteolysis with chymotrypsin (Promega, bovine) was the same as above except in 100 mM Tris-HCl, 10 mM $CaCl_2$, pH 8.0. Digestion with Pronase (Calbiochem) was at an 2:9 (w/w) E:S ratio for 30 min at 37 °C in 50 mM Tris, 100 mM NaCl, 5 mM $CaCl_2$, pH 8.0

HPLC-ESI-MS and MS/MS

After solubilization, P2 was desalted using a C18 Zip-Tip (Millipore) with final elution in 70% acetonitrile (ACN) containing 0.1% formic acid (FA). After elution, samples were diluted to 7% ACN with ddH2O, 0.1% FA prior to reversed-phase chromatography (PLRP-S, 2.1 x 150 mm, 300Å, 5 μm, Agilent). S2 was concentrated (SpeedVac) to the same volume as P2 before injecting to the column. A linear gradient, was used to elute the column (5% B, 0 - 10 min; 21% B at 14 min; 46% B at 39 min; 95% B from 39.1 - 49 min. B is ACN, 0.1% FA). Column eluent was directed to the electrospray ionization source (Ionmax) of a linear ion trap mass spectrometer (LTQ, Thermo Scientific) operated in positive-ion mode. Protein/peptide molecular mass deconvolution used Promass software (Novatia). Only peptides with intensity at least ten percent of the most dominant peptide are reported. High-resolution MS/MS was performed on a static nanospray 7T LTQ-FT system (Thermo Scientific) as previously reported (15). MS/MS data analysis was done both manually and using Prosight PC (Thermo Scientific).

Atomic Force Microscopy

Purified SOD1 fibrils were suspended and diluted to a final concentration of 25 µM with 10 mM potassium phosphate, pH 7.0. 15 µl of fibril solution was added to the cleaved mica surface and allowed to adhere. After incubation at room temperature for one min, the mica was washed three times with 50 µl ddH2Oto remove unbound material and allowed to air dry overnight. Dimension 5000 (Bruker) Scanning Probe Microscope was used to image SOD1 fibrils using an APPNANO ACT tip under tapping mode. Height images were collected at 1024 X 1024 pixels at a scan rate of 1.5 Hz. Image processing was performed using a scanning probe image processor SPIP^{TM}.
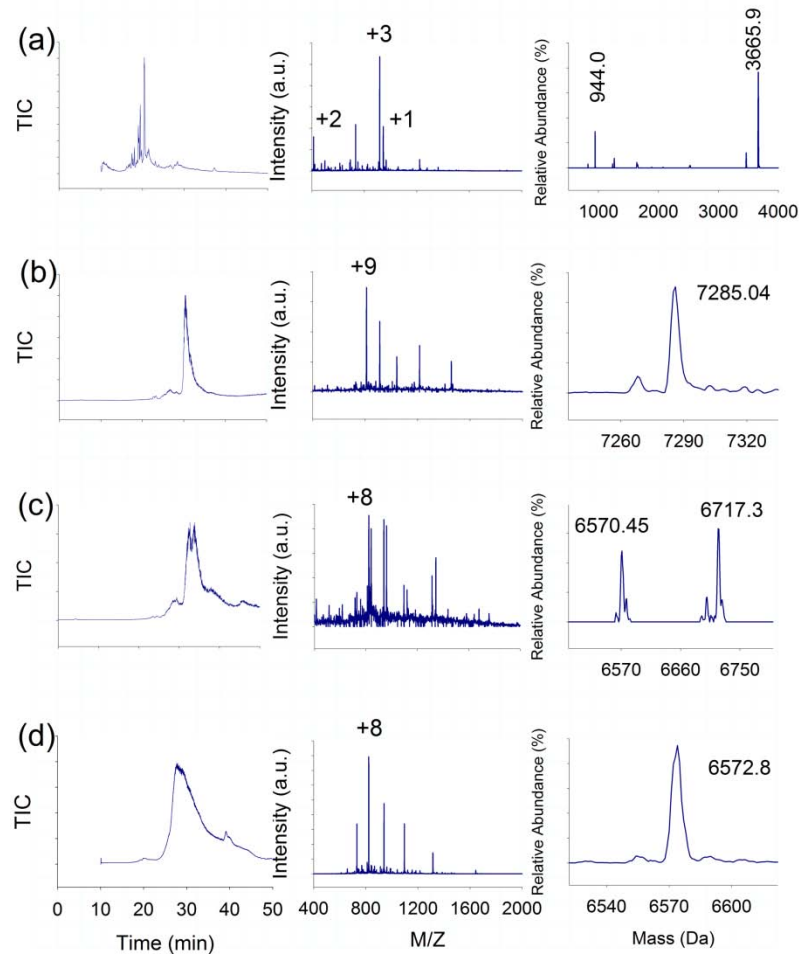
Figure 2.1. Liquid chromatography mass spectrometry of hWT SOD1 fibrils partially digested by trypsin, chymotrypsin, and Pronase. (Left) Total ion chromatogram (TIC) from reverse-phase LC-MS (Middle) Electrospray-ionization mass spectrum integrated across the entire chromatogram and (Right) measured average masses resulting from deconvolution. (a) Soluble peptides released from the partially trypsin-digested fibrils (S2) are predominantly from the C-terminal half of the protein. (b,c,d) Peptides from the insoluble fibril core after partial digestion (P2). In each case a major peptide product composed of at least sixty-three continuous residues from the N-terminus of SOD1 is consistently recovered from protease-resistant core fibrils after partial digestion with (b) trypsin, (c) chymotrypsin, and (d) Pronase. Theoretical average masses of the WT SOD1 peptides are as follows: 1-63 (6571.36 Da), 1-64 (6719.60 Da), 1-69 (7287.05 Da), 80-115 (3666.04 Da), 116-122 (825.99), and 144-153 (945.18 Da). See Table S2 for a complete list of peptides found in S2 and P2

37
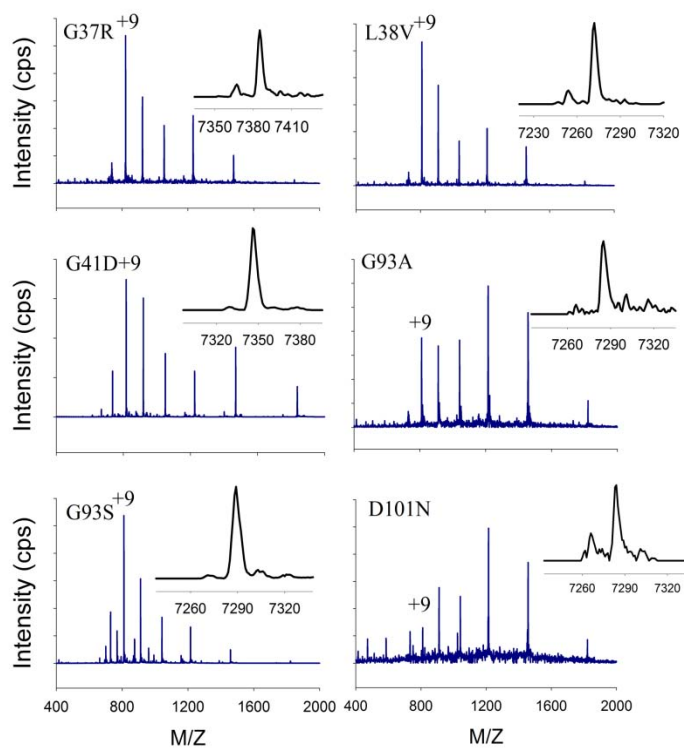
Figure 2.2. Mass spectrum of P2 peptide from mutant fibrils (G37R, L38V, G41D, G93A, G93S, and D101N) partially digested by tryspin. Mass spectrum integrated from the entire chromatogram and measured average mass (inset). Theoretical average masses of the N-acetylated 1-69 SOD1 peptides are 7287.5 Da (WT, G93A, G93S, and D101N), 7386.39 Da (G37R), 7273.23 Da (L38V), and 7345.29 Da (G41D). See Table S3 for complete list of peptides detected.
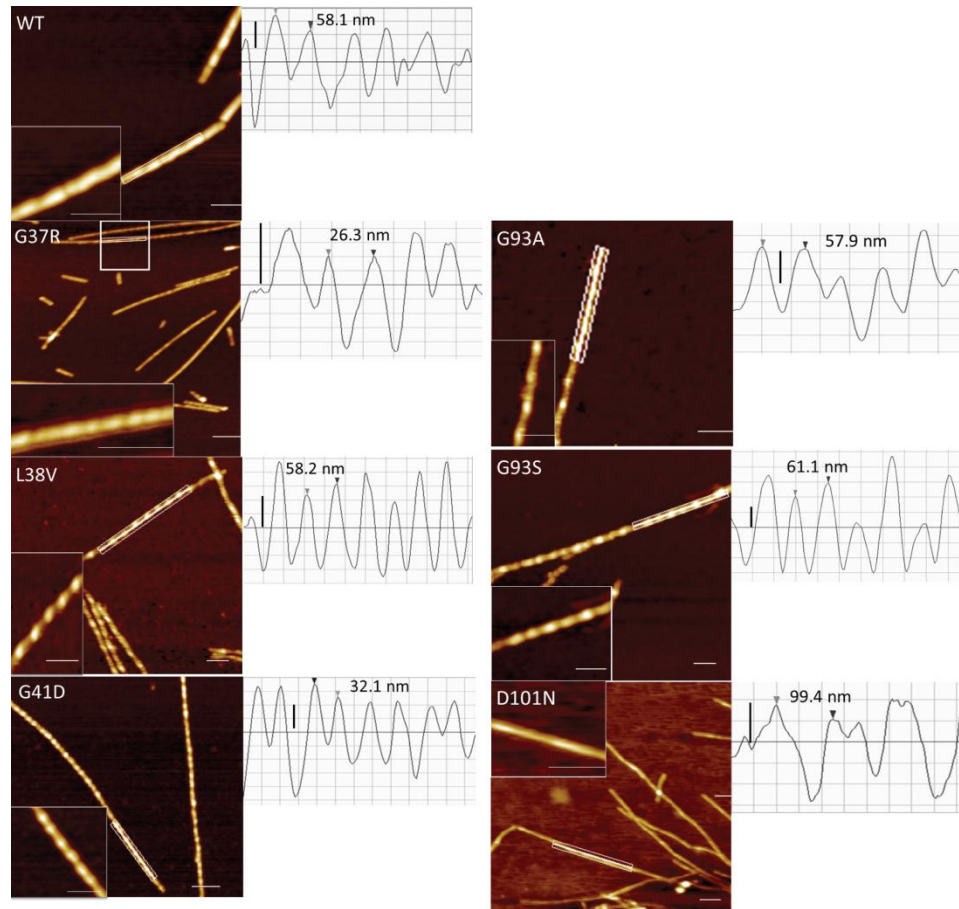
Figure 2.3. Atomic force microscopy of WT and mutant SOD1 fibrils. Figures with insets show the magnified helical twist of the fibrils. WT, L38V, G93A, and G93S have average pitch length around 55 nm to 65 nm. Scale bar = 100 nm. Periodicity profile along the fibril axis is shown on the right of each AFM image (vertical bar = 0.4 nm). Distance between two peaks (pitch distance) is marked by the arrows.
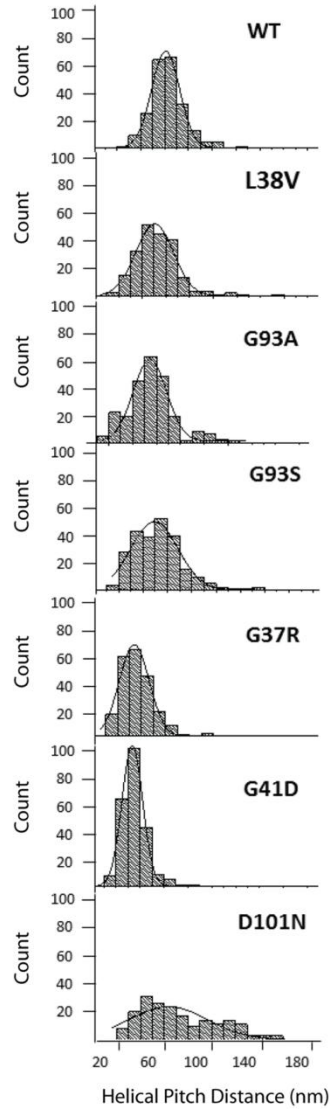
Figure 2.4. Helical pitch distances for WT and mutant SOD1 fibrils. Histogram (bin size = 10 nm) of helical pitch distances for WT and mutants with Gaussian fit peak curve (black line), n > 200 counts. WT, L38V, G93A, and G93S have peaks center at 60.9 nm, 50.5 nm, 54.5 nm, and 49.3 nm respectively. Peak centers for G37R and G41D are left shifted to shorter length, 33.9 nm and 33.6 nm. The distribution of helical pitch distances for D101N is more diverse and the peak centers at 63.3 nm.
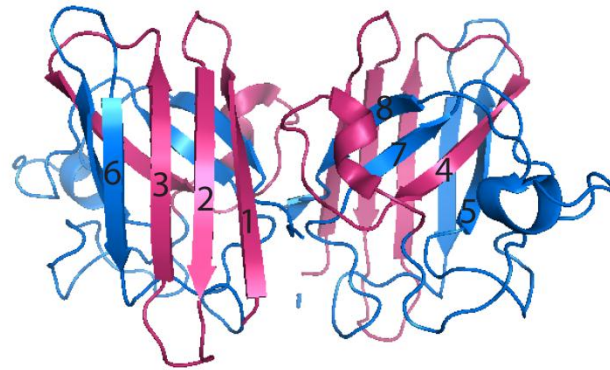
Figure 2.5. Schematic representation of apo WT SOD1 structure (PDB 1HL4) (65) and the hypothetical structural change leading to fibril formation. Residues that are protected from protease digestion in the fibrils are colored in magenta (strands 1-4). Significant rearrangement of the structure must accompany fibril formation such that strands 1-4 become tightly packed in the protease-resistant core.
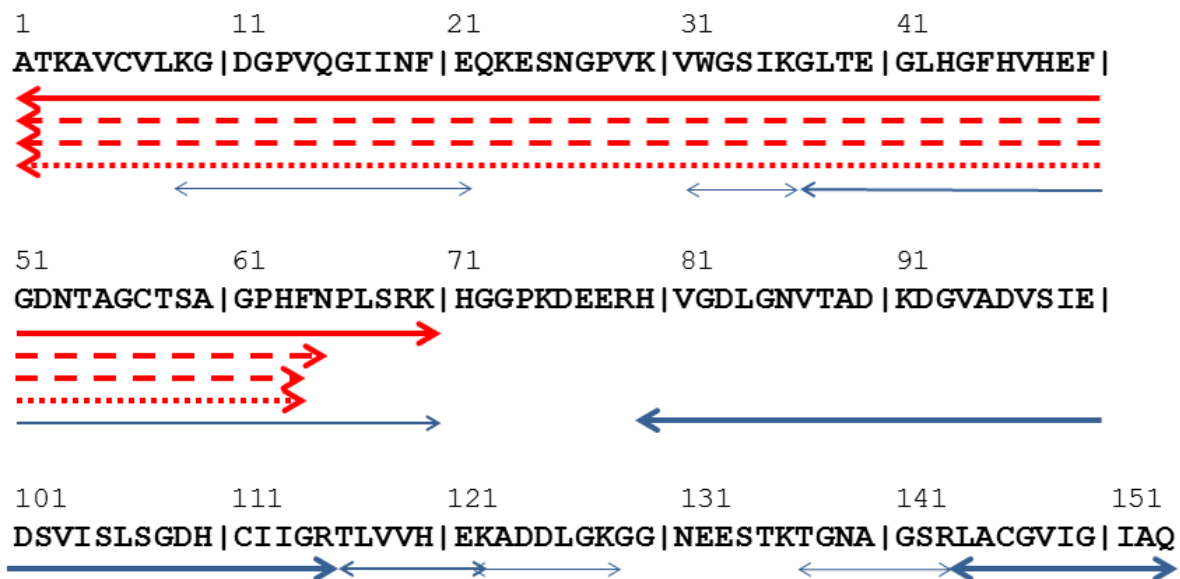
Figure S2.1. Peptide mapping after partial proteolysis of SOD1 fibrils. Soluble peptides (S2; blue) and insoluble core peptides (P2; red) are mapped to the SOD1 sequence (after removal of initiating Met). The N-terminus is more protease-resistant than the C-terminus with five sites consistently resisting cleavage. Major species identified from the protease resistant pellet (P2), digested with three different proteases, are from the amino-terminus spanning at least sixty-three residues. Peptides 80-115 and 144-153 are the most abundant in the S2. Solid arrow indicates peptides from trypsin digestion. Dashed arrow indicates peptides from chymotrypsin digestion. Dotted arrow represents fragments from Pronase digestion.

Table S1. Tryptic peptides of soluble apo WT SOD1 from LC-MS

| Retention Time (min) | Average Molecular Mass (Da) | | SOD1 sequence |
	Theoretical	Experimental	
11.0	825.99	825.50	116-122
11.2	662.68	662.50	137-143
11.6	361.42	361.50	1-3 acetyl
11.6	2991.28	2990.10	123-153
11.7	730.80	730.42	24-30
11.9	618.67	618.42	123-128
13.9	632.85	632.50	4-9
18.5	689.83	689.42	31-36
18.9	3464.78	3463.60	37-69
19.1	1502.68	1501.42	10-23
19.8	945.18	944.58	144-153
22.4	3666.04	3665.90	80-115

Table S2. Proteolytic peptides identified in P2 and S2 from partially digested WT SOD1 Fibrils

SOD1 Fibril - Partially Digested	Retention Time (min)	Average Molecular Mass (Da)		SOD1 Sequence
		Theoretical	Experimental	
P2 – Trypsin	30.5	7287.25	7285.04	1-69 acetyl
P2 – Chymotrypsin	32.3	6571.36	6570.45	1-63 acetyl
	33.9	6719.60	6717.30	1-64 acetyl
P2 – Pronase	28.5	6571.36	6572.8	1-63 acetyl
S2 – Trypsin	10.7	825.99	824.8	116-122
	11.5	622.68	661.42	137-143
	11.9	618.67	617.42	123-128
	18.1	689.83	688.6	31-36
	19.0	3464.78	3464.6	37-69
	19.2	1502.68	1501.2	10-23
	19.5	945.18	944.0	144-153
	20.4	3666.04	3665.9	80-115

Table S3. Tryptic peptides identified in P2 from partially digested WT and mutant SOD1 Fibrils

SOD1 Fibril – Partially Digested	Retention Time (min)	Average Molecular Mass (Da)		SOD1 sequence
		Theoretical	Experimental	
P2 WT	30.5	7287.25	7285.04	1-69 acetyl
P2 G37R	26.2	3666.04	3665.90	80-115
	30.1	7386.39	7384.56	1-69 acetyl
P2 L38V	20.5	1588.84	1587.60	137-153
	20.5	944.52	944.75	144-153
	26.9	7273.23	7271.46	1-69 acetyl
P2 G41D	23.3	2458.90	2457.90	1-23 acetyl
	29.2	7345.29	7346.60	1-69 acetyl
P2 G93A	26.7	2458.90	2456.90	1-23 acetyl
	29.4	7287.25	7284.66	1-69 acetyl
P2 G93S	25.1	3841.59	3841.30	1-36 acetyl
	28.5	7287.25	7288.30	1-69 acetyl
P2 D101N	29.1	7287.25	7283.40	1-69 acetyl
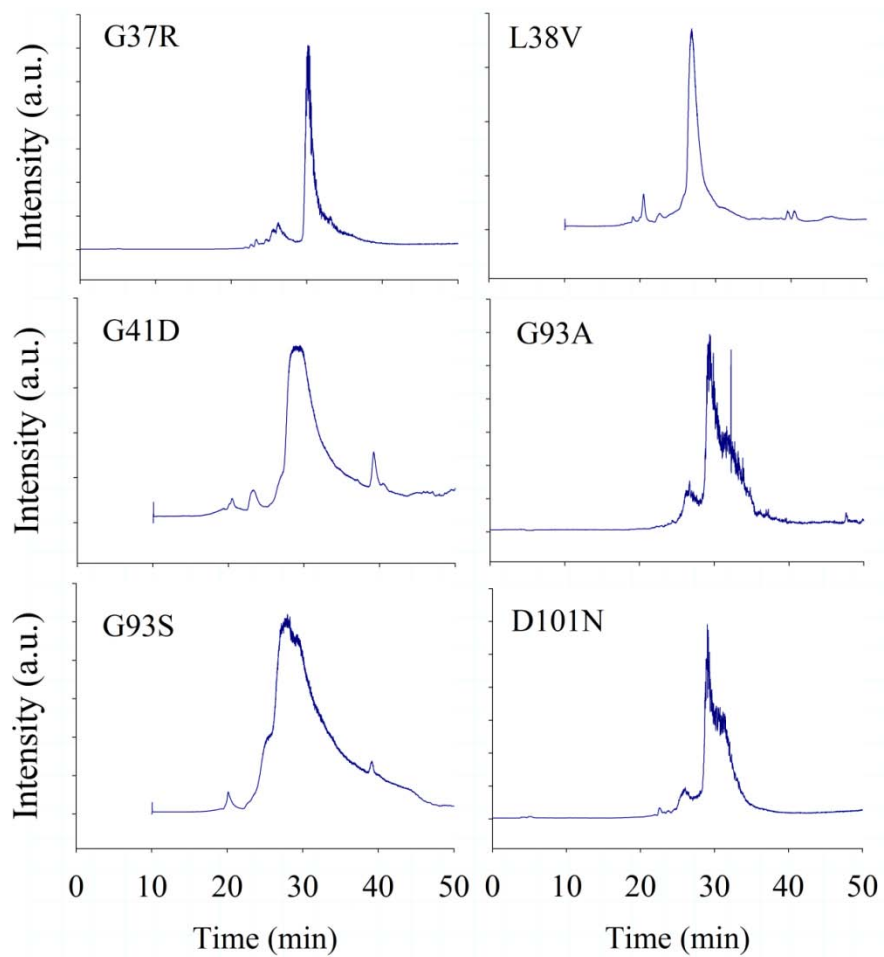
Figure S2.2. LC-MS chromatograph (TIC) of trypsin-resistant pellet from partially digested mutant fibrils. A polypeptide composed of residues acetyl 1-69 is consistently detected all mutant fibrils.
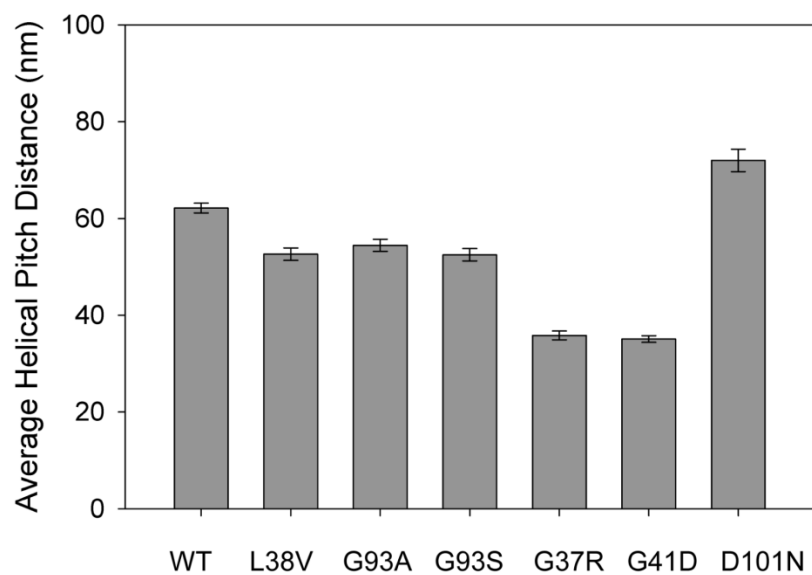
Figure S2.3. Average helical pitch distances of WT and mutant SOD1 fibrils. Means, with standard error of the mean (s.e.m.) values (n>200 helical pitch distance measurements) are shown.
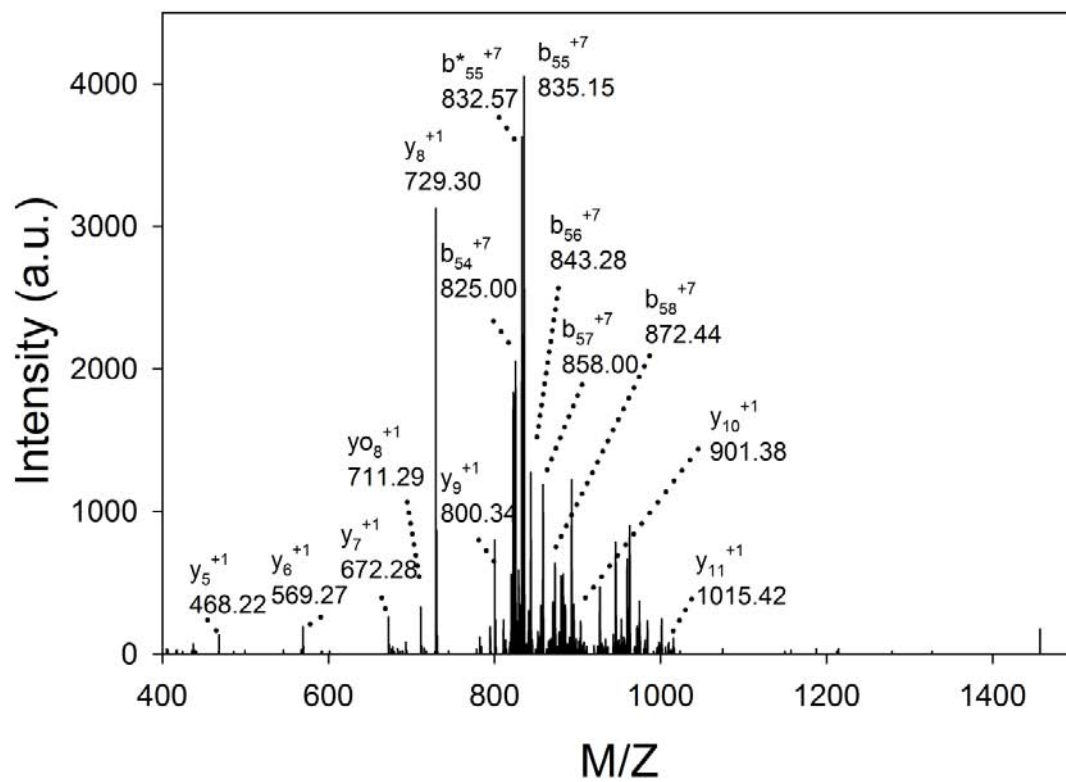
Figure S2.4. MS/MS spectrum of WT P2-Pronase containing N-acetylated residues 1-63 of the SOD1 sequence with a monoisotopic mass of 6567.2603 Da. Daughter ions (y and b) are labeled in the spectrum ("bo" or "yo" and "b*" or "y*" indicate daughter ions that have undergone the loss of H_2O and NH_3, respectively).

Table S4. MSMS *b*- and *y*-ions matching to the N-acetylated residues 1-63 of WT SOD1 with mass accuracy better than 10 ppm.

Fragment Ion	m/z Monoisotopic	Mass Monoisotopic	Theoretical Mass	Error (Da)	Error (ppm)
B8	828.469	827.462	827.458	0.004	4.75
B16	783.922	1565.829	1565.820	0.006	3.55
B40	845.050	4220.216	4220.23	-0.015	-3.51
B48	851.781	5104.641	5104.67	-0.031	-6.03
B49	873.288	5233.686	5233.71	-0.028	-5.29
B50	897.808	5380.806	5380.78	0.024	4.41
B51	907.310	5437.814	5437.8	0.010	1.91
B52	926.477	5552.820	5552.83	-0.011	-1.90
B52	794.269	5552.831	5552.83	0.000	0.04
B53	945.478	5666.824	5666.87	-0.050	-8.88
B54	962.335	5767.967	5767.92	0.046	7.94
B55	974.163	5838.935	5838.96	-0.023	-4.00
B55	835.147	5838.975	5838.96	0.016	2.78
B56	843.284	5895.936	5895.98	-0.044	-7.50
B56	983.667	5895.961	5895.98	-0.019	-3.26
B57	857.999	5998.940	5998.99	-0.049	-8.20
B57	1000.831	5998.941	5998.99	-0.048	-8.06
B58	872.436	6100.000	6100.04	-0.037	-6.13
B59	884.874	6187.064	6187.07	-0.005	-0.73
B60	895.018	6258.077	6258.11	-0.029	-4.71
B61	903.172	6315.152	6315.13	0.024	3.86
Y6	569.273	568.266	568.263	0.004	6.18
Y7	672.279	671.272	671.272	0.000	0.26
Y8	729.303	728.295	728.293	0.002	3.10
Y9	800.343	799.335	799.33	0.005	6.45
Y10	901.383	900.376	900.378	-0.002	-2.09
Y11	1015.431	1014.424	1014.42	0.003	3.08
Y57	851.292	5951.995	5951.95	0.049	8.19

b1   -A-T-K-A-V-C{V-L}K-G-D-G-P-V-Q-G}I-I-N-F-E-Q-K-E-S- y39

b26 -N-G-P-V-K-V-W-G-S-I-K-G-L-T-E}G-L-H-G-F-H-V-H}E}F} y14

b51 -G}D{N}T}A}G{C}T}S}A}G}P-H-   y1

Figure S2.5. MSMS b- and y-ions from a precursor ion with monoisotopic mass of 6567.2603 Da, matching to the N-acetylated 1-63 sequence of WT SOD1.
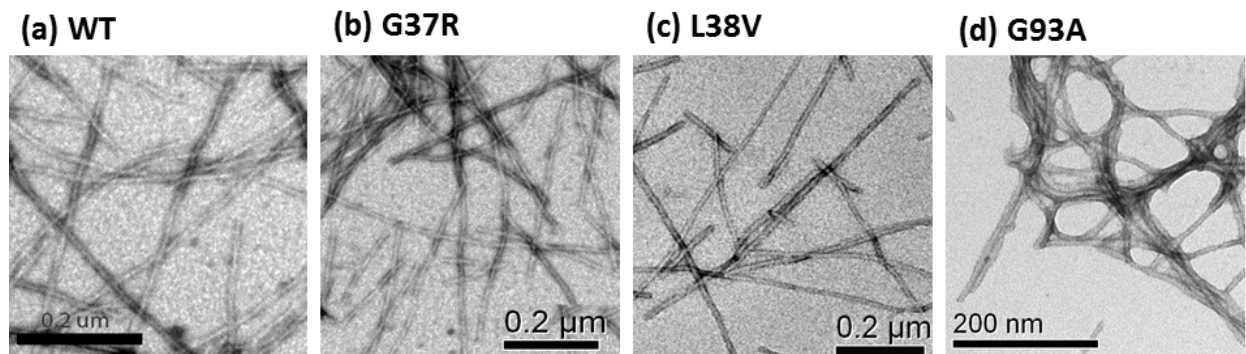
Figure S2.6. Electron micrographs of WT and mutant hSOD1 fibrils show elongated fibrillar morphology.

SI Materials and Methods

Electron Microscopy (EM)

10 μl of samples were deposited on the glow-discharged formvar-coated copper grid (Ted Pella, Inc) and allowed to absorb for one minute before blotted dry with filter paper. Samples were then washed twice with 10 μl ddH2O for twenty seconds. To achieve negative staining, samples were stained with 1% uranyl acetate for six seconds (2X) then forty-five seconds (1X) and blotted dry. Stained grids were kept in a grid box inside a desiccator before imaging.

References

1.   Valentine JS, Doucette PA, & Zittin Potter S (2005) Annu Rev Biochem 74, 563-593.

2.   Valentine JS & Hart PJ (2003) Proc Natl Acad Sci U S A 100, 3617-3622.

3.   Sheng Y, Chattopadhyay M, Whitelegge J, & Valentine JS Curr Top Med Chem.

4.   Kato S, Hayashi H, Nakashima K, Nanba E, Kato M, Hirano A, Nakano I, Asayama K, & Ohama E (1997) Am J Pathol 151, 611-620.

5.   Shibata N, Hirano A, Kobayashi M, Sasaki S, Kato T, Matsumoto S, Shiozawa Z, Komori T, Ikemoto A, Umahara T, et al. (1994) Neurosci Lett 179, 149-152.

6.   Wang J, Slunt H, Gonzales V, Fromholt D, Coonfield M, Copeland NG, Jenkins NA, & Borchelt DR (2003) Hum Mol Genet 12, 2753-2764.

7.   Basso M, Massignan T, Samengo G, Cheroni C, De Biasi S, Salmona M, Bendotti C, & Bonetto V (2006) J Biol Chem 281, 33325-33335.

8.   Jaarsma D, Teuling E, Haasdijk ED, De Zeeuw CI, & Hoogenraad CC (2008) J Neurosci 28, 2075-2088.

9.   Cohen AS & Calkins E (1959) Nature 183, 1202-1203.

10.   Geddes AJ, Parker KD, Atkins ED, & Beighton E (1968) J Mol Biol 32, 343-358.

11.   Sunde M & Blake C (1997) Adv Protein Chem 50, 123-159.

12.   Sunde M, Serpell LC, Bartlam M, Fraser PE, Pepys MB, & Blake CC (1997) J Mol Biol 273, 729-739.

13.   Eanes ED & Glenner GG (1968) J Histochem Cytochem 16, 673-677.

14.   Shaw BF, Lelie HL, Durazo A, Nersissian AM, Xu G, Chan PK, Gralla EB, Tiwari A, Hayward LJ, Borchelt DR, et al. (2008) J Biol Chem 283, 8340-8350.

15.   Chattopadhyay M, Durazo A, Sohn SH, Strong CD, Gralla EB, Whitelegge JP, & Valentine JS (2008) Proc Natl Acad Sci U S A 105, 18663-18668.

16.   Fiala M, Chattopadhay M, La Cava A, Tse E, Liu G, Lourenco E, Eskin A, Liu PT, Magpantay L, Tse S, et al. (2010) J Neuroinflammation 7, 76.

17.   Roberts K, Zeineddine R, Corcoran L, Li W, Campbell IL, & Yerbury JJ (2013) Glia 61, 409-419.

18.   Chattopadhyay M & Valentine JS (2009) Antioxid Redox Signal 11, 1603-1614.

19. Miake H, Mizusawa H, Iwatsubo T, & Hasegawa M (2002) J Biol Chem 277, 19213-19219.

20. Kheterpal I, Williams A, Murphy C, Bledsoe B, & Wetzel R (2001) Biochemistry 40, 11757-11767.

21. Sajnani G, Pastrana MA, Dynin I, Onisko B, & Requena JR (2008) J Mol Biol 382, 88-98.

22. Frare E, Mossuto MF, Polverino de Laureto P, Dumoulin M, Dobson CM, & Fontana A (2006) J Mol Biol 361, 551-561.

23. Baxa U, Taylor KL, Wall JS, Simon MN, Cheng N, Wickner RB, & Steven AC (2003) J Biol Chem 278, 43717-43727.

24. Polverino de Laureto P, Taddei N, Frare E, Capanni C, Costantini S, Zurdo J, Chiti F, Dobson CM, & Fontana A (2003) J Mol Biol 334, 129-141.

25. Carulla N, Caddy GL, Hall DR, Zurdo J, Gairi M, Feliz M, Giralt E, Robinson CV, & Dobson CM (2005) Nature 436, 554-558.

26. Graffmo KS, Forsberg K, Bergh J, Birve A, Zetterstrom P, Andersen PM, Marklund SL, Brannstrom T (2013) Hum Mol Genet 22, 51-60.

27. Chiti F, Webster P, Taddei N, Clark A, Stefani M, Ramponi G, & Dobson CM (1999) Proc Natl Acad Sci U S A 96, 3590-3594.

28. Tycko R Annu Rev (2011) Phys Chem 62, 279-299.

29. Knowles TP, Fitzpatrick AW, Meehan S, Mott HR, Vendruscolo M, Dobson CM, & Welland ME (2007) Science 318, 1900-1903.

30. Hubbard SJ, Campbell SF, & Thornton JM (1991) J Mol Biol 220, 507-530.

31. Lang L, Kurnik M, Danielsson J, & Oliveberg M (2012) Proc Natl Acad Sci U S A 109, 17868-17873.

32. Durazo A, Shaw BF, Chattopadhyay M, Faull KF, Nersissian AM, Valentine JS, & Whitelegge JP (2009) J Biol Chem284, 34382-34389.

33. Goldschmidt L, Teng PK, Riek R, & Eisenberg D (2010) Proc Natl Acad Sci U S A 107, 3487-3492.

34. Gazit E (2002) FASEB J 16, 77-83.

35. Furukawa Y, Kaneko K, Yamanaka K, & Nukina N (2010) J Biol Chem 285, 22221-22231.

36. Trexler AJ & Rhoades E (2012) Protein Sci 21, 601-605.

37. Maltsev AS, Ying J, & Bax A (2012) Biochemistry 51, 5004-5013.

38. Yonemoto IT, Kroon GJ, Dyson HJ, Balch WE, & Kelly JW (2008) Biochemistry 47, 9900-9910.

39. Padrick SB & Miranker AD (2001) J Mol Biol 308, 783-794.

40. Petkova AT, Leapman RD, Guo Z, Yau WM, Mattson MP, & Tycko R (2005) Science 307, 262-265.

41. Dzwolak W, Smirnovas V, Jansen R, & Winter R (2004) Protein Sci 13, 1927-1932.

42. Relini A, Torrassa S, Ferrando R, Rolandi R, Campioni S, Chiti F, & Gliozzi A (2010) Biophys J 98, 1277-1284.

43. Wiltzius JJ, Sievers SA, Sawaya MR, Cascio D, Popov D, Riekel C, & Eisenberg D (2008) Protein Sci 17, 1467-1474.

44. Makin OS, Atkins E, Sikorski P, Johansson J, & Serpell LC (2005) Proc Natl Acad Sci U S A 102, 315-320.

45. Thompson MJ, Sievers SA, Karanicolas J, Ivanova MI, Baker D, & Eisenberg D (2006) Proc Natl Acad Sci U S A 103, 4074-4078.

46. Jimenez JL, Nettleton EJ, Bouchard M, Robinson CV, Dobson CM, & Saibil HR (2002) Proc Natl Acad Sci U S A 99, 9196-9201.

47. Shammas SL, Knowles TP, Baldwin AJ, Macphee CE, Welland ME, Dobson CM, & Devlin GL (2011) Biophys J 100, 2783-2791.

48. Adamcik J & Mezzenga R (2011) Soft Matter 7, 5437-5443.

49. Eckert A, Hauptmann S, Scherping I, Meinhardt J, Rhein V, Drose S, Brandt U, Fandrich M, Muller WE, & Gotz J (2008) J Mol Med (Berl) 86, 1255-1267.

50. Urushitani M, Kurisu J, Tsukita K, & Takahashi R (2002) J Neurochem 83, 1030-1042.

51. Williams TL, Day IJ, & Serpell LC (2010) Langmuir 26, 17260-17268.

52. Shaw BF & Valentine JS (2007) Trends Biochem Sci 32, 78-85.

53. Nekooki-Machida Y, Kurosawa M, Nukina N, Ito K, Oda T, & Tanaka M (2009) Proc Natl Acad Sci U S A 106, 9679-9684.

54. Jones EM & Surewicz WK (2005) Cell 121, 63-72.

55. Bystrom R, Andersen PM, Grobner G, & Oliveberg M J (2010) Biol Chem 285, 19544-19552.

56. Prudencio M & Borchelt DR (2011) Mol Neurodegener 6, 77.

57. Grad LI, Guest WC, Yanai A, Pokrishevsky E, O'Neill MA, Gibbs E, Semenchenko V, Yousefi M, Wishart DS, Plotkin SS, et al. (2011) Proc Natl Acad Sci U S A 108, 16398-16403.

58. Taylor DM, Gibbs BF, Kabashi E, Minotti S, Durham HD, & Agar JN (2007) J Biol Chem 282, 16329-16335.

59. Ghadge GD, Wang L, Sharma K, Monti AL, Bindokas V, Stevens FJ, & Roos RP (2006) Neurobiol Dis 21, 194-205.

60. Wang J, Xu G, Li H, Gonzales V, Fromholt D, Karch C, Copeland NG, Jenkins NA, & Borchelt DR (2005) Hum Mol Genet 14, 2335-2347.

61. Zu JS, Deng HX, Lo TP, Mitsumoto H, Ahmed MS, Hung WY, Cai ZJ, Tainer JA, & Siddique T (1997) Neurogenetics 1, 65-71.

62. Hough MA, Grossmann JG, Antonyuk SV, Strange RW, Doucette PA, Rodriguez JA, Whitson LJ, Hart PJ, Hayward LJ, Valentine JS, et al. (2004) Proc Natl Acad Sci U S A 101, 5976-5981.

63. Wiedau-Pazos M, Goto JJ, Rabizadeh S, Gralla EB, Roe JA, Lee MK, Valentine JS, & Bredesen DE (1996) Science 271, 515-518.

64. Doucette PA, Whitson LJ, Cao X, Schirf V, Demeler B, Valentine JS, Hansen JC, & Hart PJ (2004) J Biol Chem 279, 54558-54566.

65. Strange RW, Antonyuk S, Hough MA, Doucette PA, Rodriguez JA, Hart PJ, Hayward LJ, Valentine JS, & Hasnain SS (2003) J Mol Biol 328, 877-891.

Chapter 3

Novel Inhibitors of *In-vitro* SOD1 Fibrillation and the Inhibition Mechanism

Introduction

Amyloid fibrils, with its characteristic cross-beta elongated conformation with extended beta strands stacking perpendicular to the fibril lateral axis, are commonly found in protein misfolding diseases, including neurodegenerative diseases such as Alzheimer's, Parkinson's, and prion diseases. Studies suggest that the toxic species associated with the amyloid fibril formation pathway are the causes of degeneration in these diseases (1, 2). Similarly, formation of abnormal fibrillar protein aggregates has been discovered in both SOD1-linked familial amyotrophic lateral sclerosis (SOD1-fALS) patients and transgenic mice over-expressing mutant SOD1 (3, 4). In the spinal cords of transgenic mice carrying SOD1 mutation, the protein aggregates found in the spinal cords are composed of mainly full-length, unmodified apo SOD1 (5). Although whether the exact disease-causing culprit originates from soluble or insoluble intermediates or mature fibrillar species is a matter of debate, finding inhibitors of the SOD1 fibrillation process is indisputably important. First, it could lead to the development of potential therapeutics. Secondly their study will provide invaluable insights into the SOD1 fibrillation mechanism by which the soluble, globular antioxidant protein, SOD1, rearranges and self assembles into well-ordered insoluble amyloid fibril, and thus enhance our understandings of SOD1-fALS etiology.

Unlike that of other well-studied amyloids, the SOD1 fibrillation mechanism has remained elusive, and inhibiting it remains a relatively uncharted territory. There are several approaches in therapeutic intervention for other protein-misfolding diseases. Most of them focus on reducing the level of amyloid forming proteins in the cell. Such approaches target increasing clearance of the misfolding protein or polypeptide, stabilizing the native state, and/or inhibiting

the self-assembly pathway. To date, there are several known inhibitors of amyloidogenesis formed by polypeptides such as Abeta (6), α-synuclein (7), and transthyretin (8, 9). Although the toxicity of mature amyloid fibrils is uncertain, these inhibitors were able to reduce cytotoxicity associated with the corresponding amyloid forming proteins or polypeptides, suggesting that the inhibitors were not only able to inhibit amyloid formation, but also inhibiting the formation of the toxic species that are associated with the fibrils. Some of the better studied inhibitors are polyphenols (such as flavanols) (10-13), aminopyrazole (14), and the molecular tweezer (15, 16).

Most of the established inhibitors are small molecules, but in this chapter, small peptides in addition to the conventional small molecules drug candidates are explored. These peptides were selected based on their structural correlations with beta-sheet structure, their hydrophobicity, or their demonstrated inhibitory effect on other amyloid systems. While most small molecule inhibitors have been found by large scale screening, peptide inhibitors are usually discovered based on rational designs. Although small molecules are easier to optimize for stability and pharmokinetics by medicinal chemistry, they tend to be relatively promiscuous and have multiple binding sites. On the other hand, while peptide inhibitors are designed to be more specific, they are more susceptible to degradation in vivo.

In spite of the fact that there is no consensus in the primary amino acid sequence among all the amyloid forming peptides, it is believed that all amyloid assemblies share similar super-structure and physical properties. The fact that most of the amyloid inhibitors discovered can bind to multiple amyloidogenic polypeptides suggests that it is binding to a common amyloidogenic conformation instead of binding to specific primary amino acid sequences. Most of the peptide inhibitors presented here either have beta strand secondary structures or have

strong binding affinity to beta-sheet structures as previously established. They are referred as the beta blocker inhibitors. Many are mimics of the amyloidogenic segment with modifications that would allow the inhibitor to incorporate into the internal amyloidogenic region but prevent further binding with another peptide/protein to inhibit self-assembly. Such modifications include but are not limited to amino acid substitution of the amyloidogenic region (17, 18), modification of amino acid residues (such as N-methylation and acetylation) (19), insertion of a proline residue (20, 21), and D-amino acids (22, 23). Since amyloid-associated oligomers been have found to be able to interpolate to the cell plasma membrane (24-27), peptide inhibitors composed of or contain the cell permeating sequence were also tested.

The goal of this study is to screen for inhibitors of SOD1 fibrillation and to employ these newly discovered inhibitors to decipher the SOD1 fibrillation and inhibition mechanism. Several published inhibitors were described to be able to induce or re-direct the soluble polypeptide to form thermodynamically stable oligomers (13, 28). Although these reported oligomers can be toxic or non-toxic depending on the individual polypeptide and the state of the oligomers, the discovery and identification of any oligomers associated with the SOD1 fibrillation pathway would be an essential piece of information to understand the SOD1 fibrillation mechanism since on-pathway SOD1 oligomeric intermediates exist too transiently to allow further examination. These inhibitors might bind such oligomers and trap them in a form that can be isolated for further study. Use of these inhibitors would help us discover intermediate SOD1 species associated with the fibrillation pathway and identify the toxic gain-of-function species that are unambiguously linked to ALS pathology.

In this chapter, we describe our testing of the inhibitory effect of five peptide and one small molecule inhibitors using the SOD1 in-vitro fibrillation assay. We show that EGCG, colivelin-tat, DpV16, and AzV31 are each able to inhibit SOD1 fibrillation in submolar ratios. DpV19, a more hydrophilic derivative of DpV16 also exhibits inhibitory effects, although it requires a higher concentration. Data presented here indicate that, while hydrophobicity might influence the efficacy of an amyloid inhibitor, it is not an absolute requirement. Furthermore, peptide lacking predominant secondary structure, such as AzV31, could effectively inhibit SOD1 fibrillation, suggesting that unstructured peptides can also be used as amyloid inhibitors. On the other hand, PL170 did not show any inhibitory effect even in molar excess quantities. Out of the six inhibitors tested, only SOD1 treated with EGCG formed stable oligomer instead of fibrils in the fibrillation assay, as observed in a native gel.

To investigate further the inhibition mechanism, inhibitors were tested in the initiation and elongation steps of fibrillation. Data show that the two inhibitors tested, Colivelin-Tat and DpV16, were able to inhibit or attenuate initiation but have no effect on the elongation phase, suggesting that these inhibitors inhibit fibrillation by interfering with the initiation step. Interestingly, EGCG preferentially inhibit WT more efficiently than L38V and G93A. L38V and G93A are located in close proximity in the native structure (strand 3 and 6), suggesting that this region is important for EGCG binding and that this region might be directly or indirectly involved in the fibril formation process.

Results

Selection of Inhibitors

To minimize potential problems with cellular toxicity inflicted by the inhibitor alone, all of the inhibitors selected for the fibrillation assays have been previously tested in vivo, either in cell cultures and/or animal models. Hence, we assume that all of the inhibitors tested here are relatively non-toxic. To understand the biophysical criteria needed to inhibit SOD1 amyloid formation, six inhibitors with varying degrees of hydrophobicities and secondary structures were selected – DpV16, DpV19, colivelin-tat, AzV31, PL170, and (-)-epi-gallocatechine gallate (EGCG) (see Methods for details of inhibitors). DpV16, also referred as PP-Leu, is a thirteen-amino acid peptide with a D-Pro-L-Pro dyad at positions 7 and 8. Together with the stabilizing internal disulfide bond, this hairpin motif is very resistant to protease digestion. It is an analogue based on the sequence of a broad-spectrum antiviral peptide named θ-defensins. It is reported as a potent inhibitor for Abeta fibrillogenesis (29). A derivative of DpV16, DpV19, was also selected. However, in this peptide, each of the hydrophobic leucine residues is replaced by D-His. The amino acid substitutions altered the hydrophobicity of the peptide, changing it from hydrophobic to hydrophilic, with a mean hydrophobicity score changed from 3.06 to -1.08. (HydroMCalc) (30). Two other peptides containing a membrane permeable domain, colivelin-tat and AzV31, were also selected. Colivelin-tat is a hydrophobic fusion peptide of humanin (HN) and activity-dependent neurotrophic factor (ADNF) conjugated with a membrane transduction domain, Tat. Although the peptide sequence of colivelin by itself has no direct evidence linking it to the amyloid structure, colivelin has been reported to suppress neuronal cell death induced by mutant SOD1 in fM concentration and improved motor function of G93A-SOD1 transgenic mice

(31, 32). However, the role of colivelin in SOD1 aggregation has not been investigated before. With the tat domain, colivelin-tat was designed to have enhanced affinity for amyloid and/or amyloid associated species. AzV31 is a peptide derivative from azurin. Azurin is a cupredoxin that has antiproliferative activity against a number of tumor cell lines (33). Unlike the DpV peptide family, AzV31 has no secondary structure as determined by CD (data not shown). Since aromatic residues have been postulated to play a role in fibril stability, (-)-epi-gallocatechine gallate (EGCG) and PL170 were also selected. EGCG is a green tea derived flavonoid, and was reported to inhibit fibrillogenesis of α-synuclein (34) and Abeta (12, 35) by redirecting soluble species into amorphous oligomers. It is an aromatic compound with multiple hydroxyl groups (36). Its inhibitory action is believed to be interacting with the aromatic amino acids in the amyloid fibril; and the hydroxyl groups on EGCG seem essential (11). EGCG was also demonstrated to have neuroprotective and anticancerogenic effects in cell culture models (37, 38). Lastly, PL170 is composed of non-native amino acids. The alpha carboxylic positions of glutamate are replaced with proper amines giving benzylamides and isobutylamides. These bulky hydrophobic moieties are placed in alternating positions along the peptide sequence.

In-vitro Fibrillation Assay

Monomerization of SOD1 has been postulated to be the initiating step in SOD1 fibrillation (39). In the in-vitro fibrillation assay, apo SOD1 was induced to fibrillate by the addition of 5 mM DTT. This condition allows at least partial dimer dissociation and initiates fibrillation (40). This DTT-treated reaction served as a positive fibrillation control. Inhibitors at different molar ratios were added at the beginning of the fibrillation in parallel with the positive control. After 45 hours of incubation at 37° C with continuous agitation, when the thioflavin-T

(ThT) signal of the positive control has reached plateau indicating the completion of fibril formation, reactions were stopped. The ThT intensity of the inhibitor treated samples was normalized to the ThT intensity of the positive control as an indication of the relative amount of fibrils; hence indicating the inhibition efficiency (Figure 1).

DpV16. After 45 hours incubation and agitation, SOD1 samples with 1:10, 1:5, and 1:1 molar ratios (DpV:SOD1) yielded only 2 % , 3.5 %, and 6 % of the total ThT fluorescence intensity of SOD1 positive control (with DTT only).

DpV19. At 1:1 molar ratio, DpV19 has no inhibitory effect on SOD1 fibrillation. However, when DpV19 was added in excess of SOD1, 2:1 and 5:1 (DpV19:SOD1), fibrillations were suppressed to 72% and 21% of the positive control.

Colivelin-tat. At 1:1 molar ratio, the ThT intensity of colivelin-tat treated sample was suppressed to 20% of the positive control. Surprisingly, the levels of inhibition decreased to 26% and 33.9% as the concentrations of Colivelin-tat to SOD1 increased to 2:1 and 5:1.

AzV31 (DC-SIGN 31). At 1:1 ratio, fibrillation was suppressed to 3%. At submolar ratios at 1:10 and 1:5, AzV31 was able to suppress fibrillation to 4.1% and 3.4%, respectively, showing potent concentration-dependent effect.

PL170. This peptide is ineffective at 1:1 molar ratio. The amount of fibrils formed in the presence of 1:1 PL170 was very comparable to the untreated positive control, giving a ThT intensity of 95 % of the positive control. More surprisingly, this peptide promoted SOD1 fibrillation at molar excess ratios, showing 184%, and 188% intensities of the positive control at 2:1, and 5:1, respectively.

(-)-epi-gallocatechine gallate (EGCG). EGCG was able to suppress SOD1 fibrillation to 4 % and 1.8% of the untreated sample at 1:1 and 5:1 molar ratio (EGCG:SOD1), respectively. In submolar ratio, 1:5, EGCG was able to inhibit SOD1 fibrillation to 10 %.
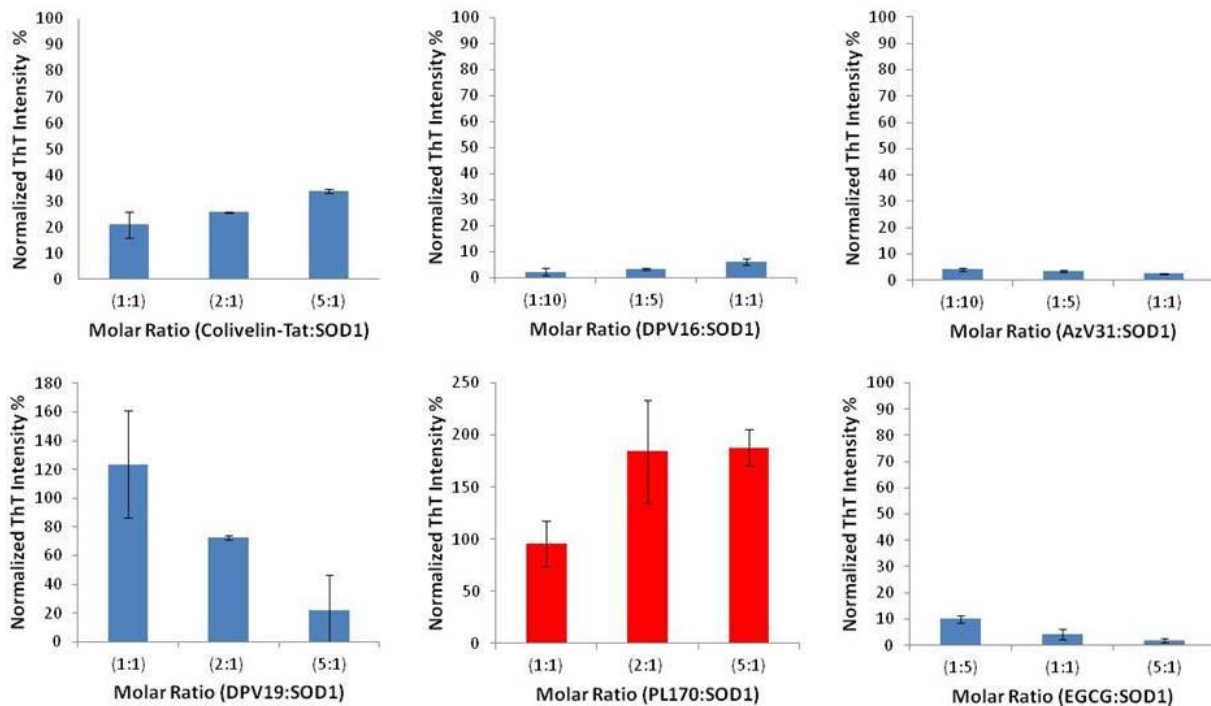
Figure 3.1. Inhibition of WT SOD1 fibril formation by small peptides and EGCG. Formation of fibril was monitored by thioflavin-T (Th-T) binding. Th-T intensity of each sample after 45 hours of incubation was normalized to the positive control (DTT only, no inhibitor). Data are the average of three experiments with calculated standard deviations. Four of the six inhibitors show significant inhibition at 1:1 molar ratio (Colivelin-Tat, DpV16, AzV31, and EGCG). DpV19 shows concentration-dependent inhibitory effect at molar excess. PL170 has no inhibitory effect.

Formation of Oligomers

Intermediate oligomers (either on- or off-pathways) have been reported and extensively studied for Abeta, α-synuclein, and other amyloid forming proteins and peptides (13, 35, 41, 42). However, intermediate oligomeric SOD1 species associated with the fibrillation pathway have not been reported probably because they are too unstable and quickly convert to more (or less) aggregated forms. To investigate whether the inhibitors can stabilize SOD1 oligomers and prevent their forming amyloid fibrils, samples were retrieved from the 96-well plate after 45 hours of incubation. They were then subjected to centrifugation at 16,000 X g for 15 min to separate the soluble protein from insoluble aggregates. Soluble proteins were then separated on a 10% native gel and visualized by an alpha imager with Coomassie blue staining. Note in panel A that metallated as-isolated WT (AI WT) migrates slightly slower than apo WT SOD1. This is most likely a structural effect due to the different conformations adopted by metallated and apo WT SOD1. A smear migrating faster than dimeric SOD1 is apparent for the S1 of apo WT negative control (lane 3, no DTT and inhibitor), suggesting a basal level of protein degradation as a consequence of prolonged agitation at 37° C. No oligomers were observed for DpV16, DpV19, Colivelin-Tat, and AzV31 inhibited samples. Out of the five inhibitors tested, only the sample treated with EGCG had bands/smear with migration slower than dimeric SOD1, suggesting the presence of higher molecular weight species (Figure 2).

A

AI WT SOD1	+					
Apo WT SOD1		+				
Apo WT SOD1			+	+	+	+	+
+ 5 mM DTT			+	+	+	+
+ DpV16				+		
+ AzV31					+	
+ DpV19						+

S1

B

146 kDa —

Apo WT
32 kDa —

20 kDa —

Colivelin-Tat   1:1   1:2   1:5

C

Apo WT —

EGCG   1:1   1:5
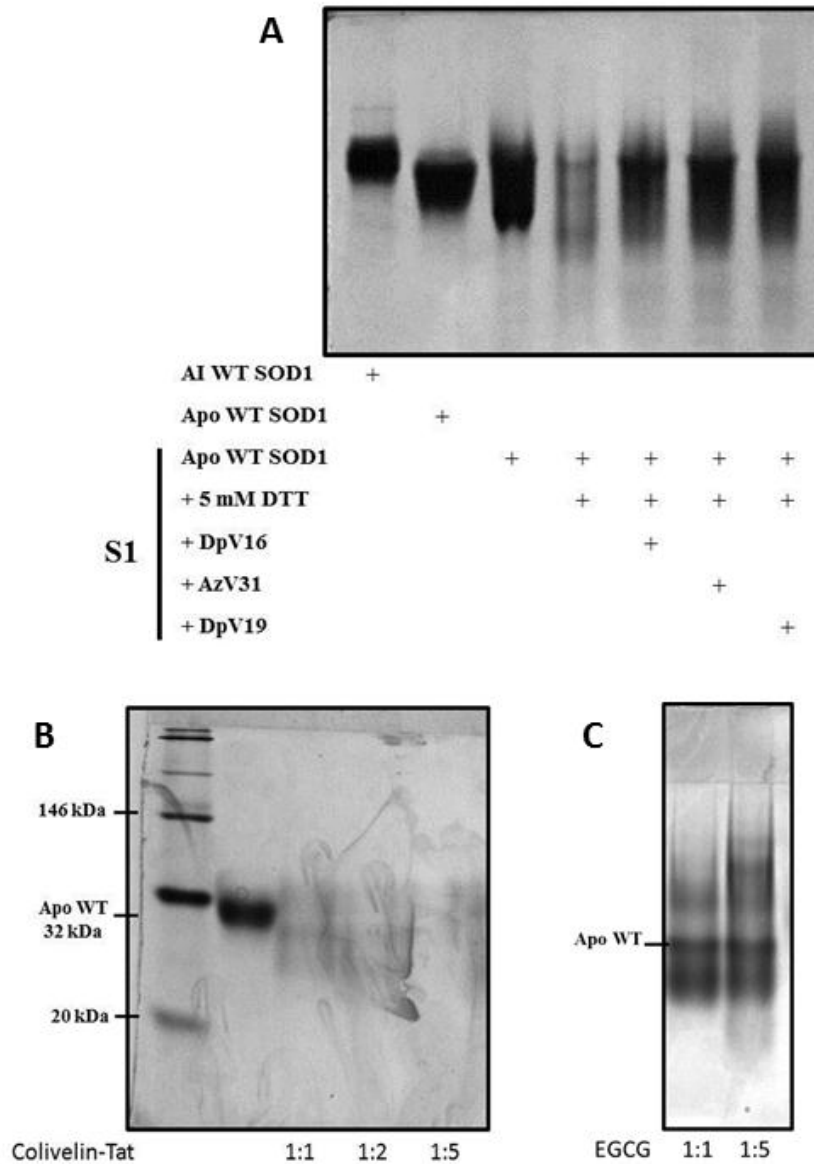
Figure 3.2. EGCG stabilized the formation of WT SOD1 oligomers. Native PAGE analysis of SOD1 fibrillation samples harvested after 45 hours incubation with DTT ± inhibitor. Fibrillation samples were retrieved from the plate after 45 hours incubation and subjected to ultracentrifugation. Soluble supernatants (S1) were loaded onto the native gel. *A*. As-isolated WT (lane 1) and apo WT (lane 2) were loaded as sizing standards. No oligomers were observed for DpV16, DpV19, and AzV31 inhibited samples (1:1 molar ratio). *B*. S1 of WT fibrillation with 1:1, 1:2, and 1:5 molar ratios (SOD1: Inhibitor) of Colivelin-Tat. *C*. S1 of WT fibrillation with 1:1 and 1:5 molar ratios of EGCG. Bands migrating significantly slower than dimeric SOD1 are apparent, suggesting the presence of high molecular weight oligomers.

Initiation and Elongation

To investigate further the inhibition mechanism, selected inhibitors were tested in different stages of the fibrillation process. Fibrillation is a very complex multi-step phenomenon. The general mechanism consists of a nucleation step that requires a high activation energy barrier followed by a rapid elongation phase that recruits soluble polypeptide to the existing nuclei (43). To investigate the mechanism by which the inhibitors attenuate fibrillation, inhibitors were tested separately in initiation and elongation experiments.

Apo SOD1 with the native disulfide bond intact (SS-ApoSOD1) is very robust and does not form amyloid even after prolonged agitation (40). However, Chattopadhyay et al. showed that apo disulfide-reduced SOD1 (2SH-ApoSOD1) initiates the fibrillation of SS-ApoSOD1. Hence, the initiation ability of a protein preparation can be tested by co-incubating it with SS-ApoSOD1 and following the fibrillation process (see Method for details). When 50% (V/V) of WT 2SH-ApoSOD1 was mixed with 50% WT SS-ApoSOD1, fibrils were formed with a lag time of around 10 hours. When Colivelin-tat was added in 1:1 molar ratio with WT 2SH-ApoSOD1, the lag time was unchanged, suggesting that colivelin-tat has no effect on the initiation of WT fibrillation (Figure 3).

SOD1 mutants are more susceptible to reduction of the native disulfide bond than WT (44), and it is believed that this vulnerability makes mutant SOD1 more prone to exist in the apo, disulfide-reduced state in vivo, which is the most aggregation-prone. Intriguingly, in cell culture model, co-expression of WT with mutant SOD1 accelerated aggregation rate compared to the expression of mutant alone (45, 46), suggesting that the co-existence of WT and mutant SOD1 is more toxic than WT and mutant SOD1 individually. To test the effect of colivelin-tat on the

initiation of WT SS-ApoSOD1 by mutant 2SH-ApoSOD1, 1:1 molar ratio of coliveline-tat to mutant 2SH-ApoSOD1 was added. The lag time for the initiation of WT by G93A was unchanged compared to the initiation without colivelin-tat (Figure 3). On the other hand, the lag time of D101N initiation was increased from 10 hours to around 30 hours. More significantly, colivelin-tat almost completely inhibited the initiations of G37R and L38V. DpV16 was also tested in the initiation assays. Unlike colivelin-tat, DpV16 was able to significantly inhibit initiations by WT and all mutants tested (G37R, L38V, and D101N) (Figure 4).

The elongation phase is defined as a process in which fibrils were fragmented and act as seeds (nuclei) with sticking ends to rapidly recruit soluble proteins. Because the nuclei have already formed, the elongation phase bypasses the rate-limiting step of initiation; hence it has a much lower kinetic barrier and faster kinetic compares to the initiation phase. To test whether the inhibitor can inhibit the elongation phase, seeds prepared from WT SOD1 (see Method for details), were added to soluble WT and mutant SS-ApoSOD1. When 20% (V/V) seed was added, fibrils were formed with a much shorter lag time of ~ 5 hours (Figure 5). When colivelin-tat was added to the reaction in 1:1 molar ratio with the seed, a concentration sufficient to inhibit fibrillation assay, the lag time was unchanged, indicating the lack of inhibitory effect in WT elongation. To compare the inhibitory effect of colivelin-tat in the elongation of mutant SOD1, WT seeds were added to soluble mutant SS-ApoSOD1. Similar to the WT, colivelin-tat has no effect on the elongation of mutant SOD1 (Figure 5).
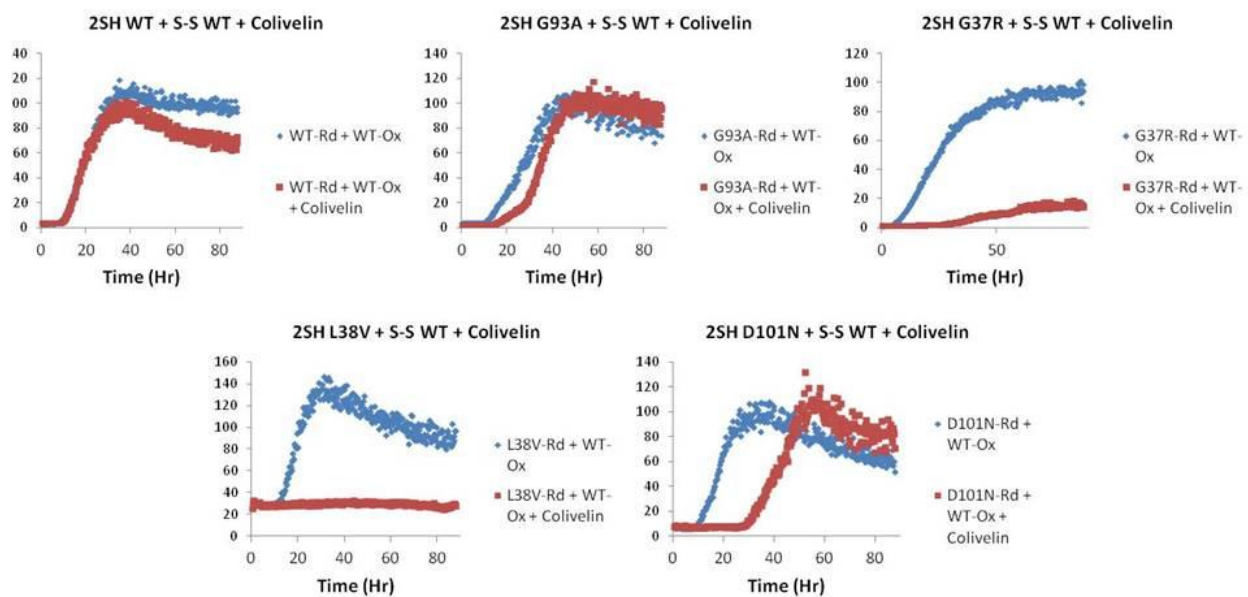
Figure 3.3. Colivelin-tat attenuated fibrillations of disulfide-oxidized apo WT initiated by disulfide-reduced G37R, L38V, and D101N, but had no effect on initiation by reduced WT and G93A. Raw Th-T intensity of disulfide-oxided WT initiated by disulfide-reduced WT, G93A, G37R, L38V, and D101N (from left to right and top to bottom). Plotted values are average of triplicates.
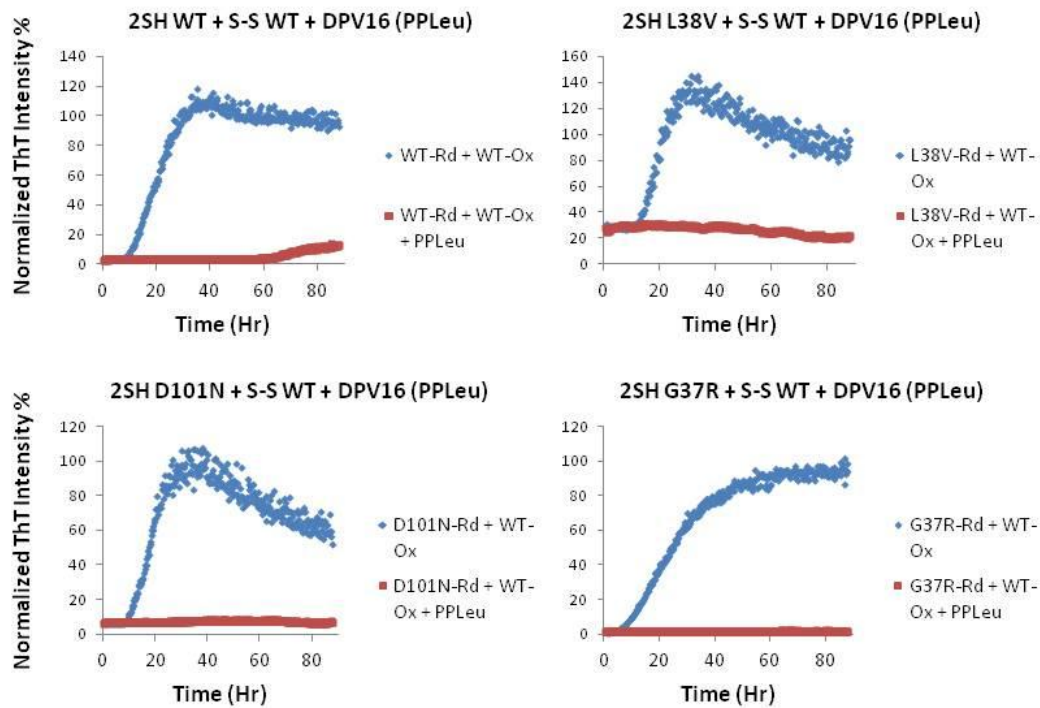
Figure 3.4. DpV16 inhibited initiations of disulfide-oxidized WT by disulfide-reduced WT, L38V, D101N, and G37R (from left to right and top to bottom). Plotted values are average of triplicates.
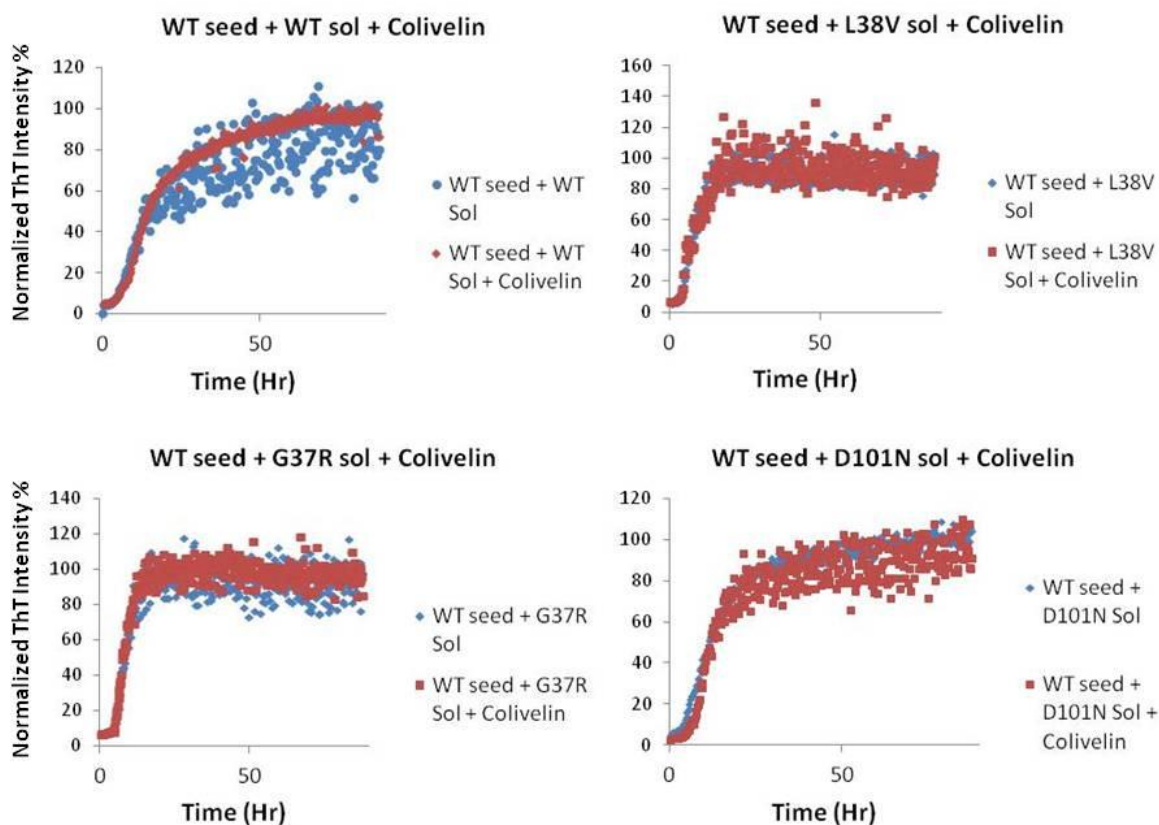
Figure 3.5. Colivelin-tat had no effect on elongation by WT fibrils. Fibrillation of soluble apo SOD1 seeded by 20 % (V/V) WT fibril seeds in the presence (red) and absence (blue) of colivelin-tat. From left to right and top to bottom: soluble WT, L38V, G37R, and D101N. The lag times of colivelin-treated samples were unchanged compare to the untreated samples. Plotted values are average of triplicates.

Inhibiting the formation of denaturant-resistant dimer

Aberrant formation of denaturant- and reductant-resistant SOD1 dimers and oligomers has been detected in both in-vitro fibrillation assay and in symptomatic ALS transgenic mice and cell cultures expressing mutant SOD1. When SOD1 fibrils made in reactions using 5 mM DTT were denatured in the presence of 6.5 M Gdm-HCl and tris (2-carboxyethyl) phosphine (TCEP) and subjected to SDS PAGE analysis, SOD1 dimers, trimers, and oligomers were apparent in the gel (40). In vivo, SDS- and heat-resistant SOD1 oligomers were also found in the homogenates of mouse spinal cords carrying SOD1 mutations (G37R and G85R), but not in homogenates from unaffected tissues (47). Similarly, high molecular weight SOD1 oligomers were detected in human embryonic kidney (HEK) cells expressing mutant SOD1 (48). Together, these observations suggest that abnormal denaturant-resistant SOD1 dimer and oligomers might be involved in the toxic mechanism associated with the SOD1 aggregation pathway. To test whether the inhibitor can prevent the formation of abnormal dimers and oligomers, apo SOD1 was incubated with 5 mM TCEP, in the presence and absence of inhibitor, at 37 ^{0}C without agitation. Aliquots were taken out at 0, 2, 4, 6, and 24 hours. Samples were then heat denatured and separated by 12% SDS PAGE, a condition in which native SOD1 dimer would monomerize. To account for all the denaturant-resistant dimer, soluble and possibly insoluble oligomers (which would not enter the gel), the amount of monomer was measured instead. The band corresponding to SOD1 monomer was quantified by counting pixels with ImageJ. The amount of monomer remaining over time was normalized to the amount of monomer present at t=0 and compared with the negative control (TCEP, without inhibitor) (Figure 6). After six hours of incubation, the amounts of monomers remaining were comparable among inhibitor-treated and control samples,

ranging from 75 %-92 %, suggesting that most SOD1 were still in the native form. However, after 24 hours of incubation, the amount of monomeric SOD1 remained in the negative control was about 6 %, suggesting that most of the SOD1 have formed denaturant-resistant dimer and oligomers. When AzV31, colivelin-tat, and DpV16 were added in 1:1 molar ratio with SOD1, the amount of monomeric SOD1 remained increased to 19 %, 46 %, and 56 %, respectively, suggesting that these inhibitors were able to prevent the formation of denaturant-resistant dimer induced by disulfide bond reduction.
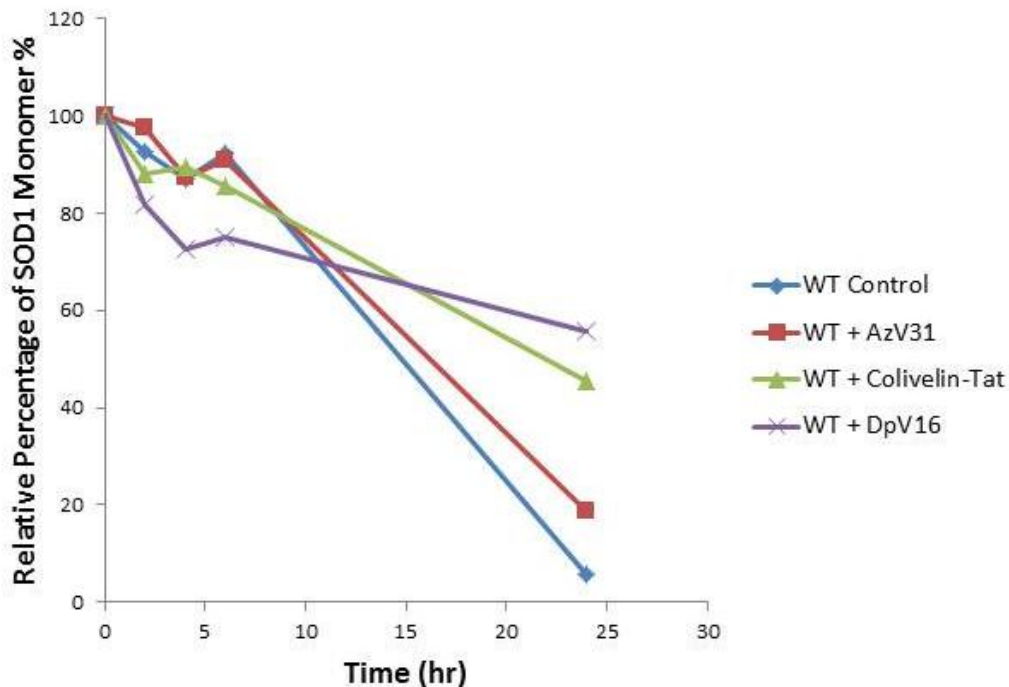
Figure 3.6. AzV31, colivelin-tat, DpV16 reduced the formation of SDS-resistant WT dimers induced by TCEP reduction. Apo WT SOD1 was incubated with 5 mM TCEP in 10 mM KPi at 37° C water bath for 0, 2, 4, 6, and 24 hours. At each time point, aliquot was taken out and flash frozen immediately with liquid nitrogen. Samples were then mixed with 1 part of SDS-PAGE loading dye without reducing agent and heat denatured for 5 minutes before loading onto a 12% SDS gel. Analysis of SDS PAGE was done by staining with Coomassie Brilliant Blue, visualized by AlphaImager, and the relative monomer band intensity was measured by counting pixels with ImageJ.

Selective Inhibition by EGCG

FALS-linked mutations occur throughout the entire SOD1 sequence and appear in different regions of the native SOD1 structure, making it challenging to postulate the pathological mechanism by which mutations cause fALS. Given the complexity of the fibrillation mechanism, it is reasonable to believe that there is more than one SOD1 aggregation interface along the different stages of fibrillation. In contrast to peptide inhibitors, small molecule inhibitors in general have more than one binding sites. To investigate whether mutations in different regions of SOD1 would affect the inhibitory effect of EGCG, EGCG was tested in fibrillation assays of L38V-SOD1 and G93A-SOD1. At 1:1 and 1:5 molar ratio (SOD1: inhibitor), EGCG was able to suppress fibrillation to 4% and 2% in WT, respectively (Figure 7). In contrast, when EGCG was added to G93A, fibrillation was only suppressed to 32% and 7% at 1:1 and 1:5 molar excess, respectively. The effect of EGCG on L38V was significantly less than in WT. At 1:1 and 1:5 molar ratios, L38V retained 56% and 26% of the fibril formation, respectively.
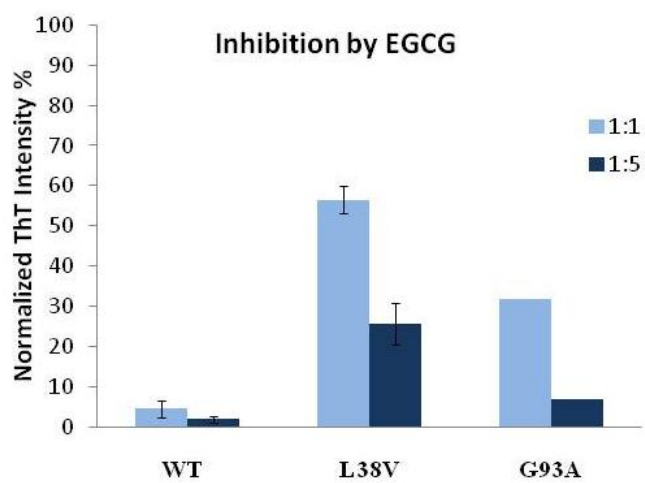
Figure 3.7. EGCG inhibits SOD1 WT fibrillation more efficiently than L38V and G93A. ThT intensity of EGCG treated samples were measured after 45 hours of incubation and normalized to the untreated control (DTT alone).

Discussion

Of the six inhibitors tested, five of them exhibited inhibitory effects to varying extent. The inactive exception was PL170. DpV19 and EGCG demonstrated a concentration dependent effect on SOD1 fibrillation, while the degree of inhibition remains the same level throughout the different concentrations tested for AzV31 (1:10-1:1, inhibitor:SOD1). On the contrary, colivelin-tat and DpV16 inhibit fibrillation most effectively at lower molar ratios than in higher molar ratios, confirming that some inhibitors can have both amyloid inhibitory and stimulating properties. Although more detailed experiments will be needed to determine the exact sequence that is responsible for the inhibition, both peptides containing the membrane transduction domain (colivelin-tat and AzV31) were able to inhibit SOD1 fibrillation at 1:1 molar ratio, suggesting that transmembrane sequences might be a good candidate for amyloid inhibition. When all the leucine residues were replaced with histidine, consequently creating a hydrophilic peptide, DpV19 was still able to inhibit SOD1 fibrillation although it required a higher concentration than DpV16. Since both DpV19 and DpV16 could inhibit SOD1 fibrillation, it indicates that hydrophobicity is not an indispensable property of an amyloid inhibitor. In addition, AzV31, which is unstructured as determined by CD spectroscopy, was also able to inhibit fibrillation. This result suggests that having the beta-strand or beta-hairpin configuration is not a requirement to prevent fibrillation. Unstructured peptide could also exert an inhibitory effect on SOD1 fibrillation.

While most molecular chaperones seem to have the stabilizing effect that prevent protein aggregation (49), some chaperones, such as Hsp104, have been shown to enhance fibrillation by

stabilizing the "nucleation-competent" seed (50). One of the peptides tested here, PL170, seems to fall in that category. Fibrillation was enhanced when PL170 concentration increased. Other small molecules have also been shown to enhance fibrillation, such as trimethylamine N-oxide. One possible fibrillation enhancing effect might be to alter the hydration of the polypeptide to generate a less folded state that leads to the enhanced structural rearrangement and formation of extended beta sheets (51).

There are several possible pathways by which the inhibitors could prevent formation of SOD1 fibrils. An inhibitor could stabilize the SOD1 dimer interface, thus preventing monomerization and making it more resistant to disulfide bond reduction. Alternatively, it could directly or indirectly interact with the initiation sites, preventing the formation of amyloid nuclei. Another approach is to inhibit elongation by binding to the aggregation sites that are essential in elongation, either in the nucleus or in soluble SOD1. From the initiation and elongation assays, we found that colivelin-tat and DpV16 were more effective in inhibiting the initiation step than the elongation step. In support of this notion, colivelin-tat and DpV16 were both able to attenuate the formation of denaturant-resistant dimer induced by incubation with reductant, possibly by stabilizing the native dimer interface, and thereby preventing reduction of the native disulfide bond and the subsequent structural rearrangement that allows the formation of denaturant-resistant dimer. This hypothesis is particularly evident for colivelin-tat. At 1:1 molar ratio, colivelin-tat was able to inhibit in-vitro SOD1 fibrillation to 20% of the positive control. However, when SOD1 was pre-treated with reductant and thus monomerized, as in the initiation assay, colivelin-tat was not as effective. In agreement with this notion, colivelin-tat was also ineffective when it was added in the elongation phase. Together, these observations suggest that

79

colivelin-tat suppresses the early stage of fibrillation, possibly by preventing monomerization and thus the formation of aberrant nuclei.

Some of these inhibitors might interfere with the early stage of the fibrillation by redirecting the polypeptide into an alternative pathway before they become destined to amyloidogenic. Among other known amyloid inhibitors, several of them bind to the native state of the peptide and promote self-assembly that is distinct from the amyloid formation cascade. Ehrnhoefer et al. reported the formation of highly stabled unstructured oligomers of Abeta and α-synuclein induced by EGCG. These oligiomers are non-toxic to PC12 cells (13). Another inhibitor, TRiC, a modulator of huntingtin fibrillogenesis, in combination with Hsp70 and Hsp40 promoted the formation of soluble oligomers instead of fibrils (52). These oligomers are non-toxic, suggesting that it might be formed by an alternative pathway other than the toxic aggregation. Out of all the inhibitors tested, only EGCG promoted the formation of oligomeric SOD1. Since EGCG also inhibited the fibrillation of Abeta and α-synuclein, forming oligomers as a consequence, it is reasonable to speculate that EGCG binds to a consensus amyloidenic conformation among the different polypeptides that is not amino acid sequence specific. The oligomeric SOD1 formed by EGCG might be non-toxic as in the case for oligomers formed in EGCG-treated Abeta and α-synuclein.

While EGCG effectively suppressed WT SOD1 fibrillation to less than 4 %, its inhibitory effect is less potent in mutants such as L38V and G93A, 56 % and 32 %, respectively. Since L38V and G93A are geographically adjacent to each other in the native structure (on strand 3 and strand 6, which are connected through the hydrogen bond network as part of the beta barrel), it is possible that mutation at this location lowers the binding affinity of EGCG to this region of

SOD1. This evidence suggests that this region might play an important role in the mechanism by which apo SOD1 rearranges and self-assembles to amyloid fibril.

Future experiments will aim to address in more detail the inhibition mechanisms of these inhibitors, such as to determine all the inhibitor binding sites and the seeding potential of the oligomer formed by EGCG. In vivo experiments will also be done to validate the efficacy of these inhibitors in cell culture and animal models. Although many caveats remain and there are numerous hurdles toward developing potential therapeutic agents based on these inhibitors, these inhibitors provide us valuable information on the SOD1 fibrillation inhibition mechanism and give us the rationale for developing the next generation of inhibitors.

Materials and Methods

SOD1 Expression and Purification

WT and site-directed mutagenesis of WT were performed as described in (53, 54). WT and fALS SOD1 were purified from the EG118 strain of Saccharomyces cerevisiae following the procedures from (55), yielding SOD1 with the initial Met1 removed and Ala2 N-acetylated covalently identical to SOD1 from human sources. To convert to apo, purified SOD1 was dialyzed three times against 50 mM EDTA and 100 mM sodium acetate at pH 3.8. The protein was then dialyzed three times in 100 mM NaCl and 100 mM sodium acetate, pH 3.8, to remove SOD1-bound EDTA. After demetallation, SOD1 was dialyzed in 10 mM potassium phosphate, pH 7.0, filter-sterilized, and flash-frozen in liquid nitrogen and kept at − 20 °C until use. Inductively coupled plasma (ICP)-MS was used to quantify metal status (5). All apo-proteins contain less than 0.10 equivalents of copper and zinc per dimer.

In Vitro Fibril Formation

To make fibrils, 50 μM of apo SOD1 was prepared in 10 mM potassium phosphate, pH 7.0, with 5 mM DTT and 40 μM of thioflavin-T (ThT) as described (40). After mixing, the solution was placed in a 96-well plate with a 1/8-in teflon ball and incubated at 37 °C with continuously shaking at 300 rpm for forty-five hours. Assembly of fibril was monitored by Thioflavin-T fluorescence measurement at λem = 485 nm (λex =444 nm) using a Fluoroskan plate-reader (Thermo Fisher). All solutions were made with chelexed metal-free distilled deionized water (ddH2O) and filtered through a 0.22 μm filter.

Fibril Initiation and Elongation Assays

For the initiation experiment, 50% (V/V) of disulfide-reduced monomeric SOD1, collected by size-exclusion chromatography-HPLC (SEC-HPLC), was mixed with disulfide-oxidized dimeric SOD1 and subjected to continuous agitation in a 96-well plate at 37° C as described above. Fibril seeds were prepared from mature fibrils formed in fibrillation reactions catalyzed by 5 mM DTT as described above. DTT Fibrils were subjected to ultra-centrifugation at 16,800 X g for 15 minutes to remove the soluble contaminants. Purified fibrils were then incubated with 2 M guanidinium hydrochloride, 10 mM potassium phosphate, pH 7 at 37° C for 90 min, then sonicated in a water bath for 20 minutes. 20% (V/V) of freshly prepared fibril seeds were added to soluble disulfide-oxidized SOD1 to begin elongation. The molar ratio of inhibitor to the initiating or elongation agent was 1:1.

SEC-HPLC

Disulfide-oxidized and disulfide-reduced apo SOD1, which are dimeric and monomeric, respectively, in non-denaturing condition, were separated and collected from a 7.5 mm X 30 cm TSK G2000 SW column (Toyosoda, Japan) equipped with a guard column using an Agilent 1200 HPLC with a mobile phase containing 50 mM sodium chloride, 50 mM potassium phosphate, and 5 mM DTT at pH 6.7. Retention time of the dimeric and monomeric SOD1 was monitored by absorbance at A280nm. A mixture of molecular weight markers ranging from 1,350 to 670,000 daltons was used as sizing standards (Bio-Rad).

TCEP Reduction and SDS PAGE

50 uM of apo WT SOD1 was incubated with 5 mM TCEP in 10 mM potassium phosphate at pH 7.0 at 37° C water bath for 0, 2, 4, 6, and 24 hours. At each time point, an aliquot was taken out and flash frozen immediately with liquid nitrogen. Samples were then mixed with 1 part of SDS-PAGE loading dye without reducing agent and heat denatured for 5 minutes at 95 ˚C before loading onto a 12% SDS gel. Analysis of SDS PAGE was done by staining with Coomassie Brilliant Blue, visualized by AlphaImager, and the relative band intensity was measured by ImageJ densitometry.
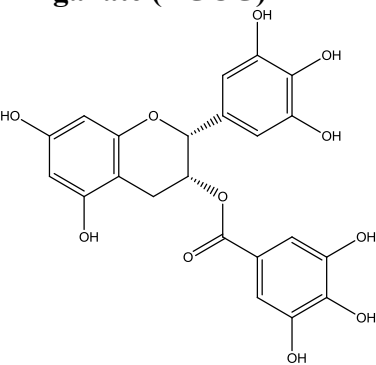
Native Page

Samples were mixed in 1:1 by volume with the native sample buffer (Bio-Rad). Samples were then separated on a 10% resolving acrylamide gel (as described) (40), followed by staining with Coomassie Brilliant Blue, visualized by AlphaImager, and analyzed by ImageJ.

Inhibitor Preparation

Synthetic peptides were synthesized and provided by Dr. Piotr Ruchala from the UCLA Peptide Synthesis Core Facility. Peptides were synthesized via Fmoc chemistry on the solid phase and purified by RP-HPLC. EGCG was purchased from Sigma-Aldrich. Lyophilized powders of EGCG, PL170, and Colivelin-tat were re-suspended in ddH2O to make a 10 mM stock. DpV16, DpV19, and AzV31 were re-suspended in DMSO.

Table 1. Inhibitor sequence and structure

Inhibitor (Amino Acid Sequence)	Molecular Weight (Da)
DpV16 (PP-Leu) - ICRLIL-(D)Pro-Pro-LRLIC-Amide	1520.04
DpV19 - ICR-(D)His-I-(D)His-(D)Pro-Pro-(D)His-R-(D)His-IC-Amide	1615.96
Colivelin-tat - SALLRSIPAPAGASRLLLLTGEIDLP-PEG$_3$-GRKKRRQRRRPPQ-Amide	4534.42
AzV31 (DCSIGN-L31) - YK-Cha-Cha-Cys-Tle-Cha-Oic-GHRT-Cha-Cys-K-Amide	1969.57
PL170* - E$^{(aBzA)}$-H-E$^{(aIsBut)}$-H-E$^{(aBzA)}$-H-E$^{(aBzA)}$-CONH$_2$	1267.42
(-) Epigallocatechin gallate (EGCG) [(2R,3R)-5,7-dihydroxy-2-(3,4,5-trihydroxyphenyl)chroman-3-yl] 3,4,5-trihydroxybenzoate	458.37

PEG$_3$ = 11-Amino-3,6,9-Trioxaundecanoic Acid, Cha-(L) = Cyclohexyl-Alanine, Oic-(L) = Octahydroindole-2-carboxylic acid, Tle-(L) = tert-Leucine, GRKKRRQRRR = Tat

* peptide is assembled via side chains of Glu. Alpha carboxylic positions of Glu are substituted with proper amines giving amides (BzA = benzylamide, IsBut=isobutylamide)

References

1. Thompson AJ & Barrow CJ (2002) Curr Med Chem 9, 1751-1762.

2. Chiti F & Dobson CM (2006) Annu Rev Biochem 75, 333-366.

3. Kato S, Hayashi H, Nakashima K, Nanba E, Kato M, Hirano A, Nakano I, Asayama K, & Ohama E (1997) Am J Pathol 151, 611-620.

4. Shibata N, Hirano A, Kobayashi M, Sasaki S, Kato T, Matsumoto S, Shiozawa Z, Komori T, Ikemoto A, Umahara T, et al. (1994) Neurosci Lett 179, 149-152.

5. Shaw BF, Lelie HL, Durazo A, Nersissian AM, Xu G, Chan PK, Gralla EB, Tiwari A, Hayward LJ, Borchelt DR, et al. (2008) J Biol Chem 283, 8340-8350.

6. Hawkes CA, Deng LH, Shaw JE, Nitz M, McLaurin J (2010) Eur J Neurosci 31, 203-213.

7. Yoshida W, Kobayashi N, Sasaki Y, Ikebukuro K, Sode K (2013) Int J Mol Sci 14, 2590-2600.

8. Palaninathan SK, Mohamedmohaideen NN, Orlandini E, Ortore G, Nencetti S, Lapucci A, Rossello A, Freundlich JS, & Sacchettini JC (2009) PLoS One 4, e6290.

9. Bulawa CE, Connelly S, Devit M, Wang L, Weigel C, Fleming JA, Packman J, Powers ET, Wiseman RL, Foss TR, et al. (2012) Proc Natl Acad Sci U S A 109, 9629-9634.

10. Suzuki Y, Brender JR, Hartman K, Ramamoorthy A, & Marsh EN (2012) Biochemistry 51, 8154-8162.

11. Cao P & Raleigh DP (2012) Biochemistry 51, 2670-2683.

12. Bieschke J, Russ J, Friedrich RP, Ehrnhoefer DE, Wobst H, Neugebauer K, & Wanker EE (2010) Proc Natl Acad Sci U S A 107, 7710-7715.

13. Ehrnhoefer DE, Bieschke J, Boeddrich A, Herbst M, Masino L, Lurz R, Engemann S, Pastore A, & Wanker EE (2008) Nat Struct Mol Biol 15, 558-566.

14. Kroth H, Ansaloni A, Varisco Y, Jan A, Sreenivasachary N, Rezaei-Ghaleh N, Giriens V, Lohmann S, Lopez-Deber MP, Adolfsson O, et al. (2012) Biol Chem 287, 34786-34800.

15. Prabhudesai S, Sinha S, Attar A, Kotagiri A, Fitzmaurice AG, Lakshmanan R, Ivanova MI, Loo JA, Klarner FG, Schrader T, et al. (2012) Neurotherapeutics 9, 464-476.

16. Sinha S, Du Z, Maiti P, Klarner FG, Schrader T, Wang C, & Bitan G (2012) ACS Chem Neurosci 3, 451-458.

17. Hughes SR, Goyal S, Sun JE, Gonzalez-DeWhitt P, Fortes MA, Riedel NG, & Sahasrabudhe SR (1996) Proc Natl Acad Sci U S A 93, 2065-2070.

18.	Porat Y, Mazor Y, Efrat S, & Gazit E (2004) Biochemistry 43, 14454-14462.

19.	Kokkoni N, Stott K, Amijee H, Mason JM, & Doig AJ (2006) Biochemistry 45, 9906-9918.

20.	Wood SJ, Wetzel R, Martin JD, & Hurle MR (1995) Biochemistry 34, 724-730.

21.	Moriarty DF & Raleigh DP (1999) Biochemistry 38, 1811-1818.

22.	Tjernberg LO, Lilliehook C, Callaway DJ, Naslund J, Hahne S, Thyberg J, Terenius L, & Nordstedt C (1997) J Biol Chem 272, 12601-12605.

23.	Chalifour RJ, McLaughlin RW, Lavoie L, Morissette C, Tremblay N, Boule M, Sarazin P, Stea D, Lacombe D, Tremblay P, et al. (2003) J Biol Chem 278, 34874-34881.

24.	Anguiano M, Nowak RJ, & Lansbury PT, Jr. (2002) Biochemistry 41, 11338-11343.

25.	Arispe N (2004) J Membr Biol 197, 33-48.

26.	Demuro A, Mina E, Kayed R, Milton SC, Parker I, & Glabe CG (2005) J Biol Chem 280, 17294-17300.

27.	Green JD, Kreplak L, Goldsbury C, Li Blatter X, Stolz M, Cooper GS, Seelig A, Kistler J, & Aebi U (2004) J Mol Biol 342, 877-887.

28.	Williams AD, Sega M, Chen M, Kheterpal I, Geva M, Berthelier V, Kaleta DT, Cook KD, & Wetzel R (2005) Proc Natl Acad Sci U S A 102, 7115-7120.

29.	Yamin G, Ruchala P, & Teplow DB (2009) Biochemistry 48, 11329-11331.

30.	Fauchere JL, Charton M, Kier LB, Verloop A, & Pliska V (1988) Int J Pept Protein Res 32, 269-278.

31.	Chiba T, Yamada M, Hashimoto Y, Sato M, Sasabe J, Kita Y, Terashita K, Aiso S, Nishimoto I, & Matsuoka M (2005) J Neurosci 25, 10252-10261.

32.	Chiba T, Yamada M, Sasabe J, Terashita K, Aiso S, Matsuoka M, & Nishimoto I (2006) Biochem Biophys Res Commun 343, 793-798.

33.	Mehta RR, Yamada T, Taylor BN, Christov K, King ML, Majumdar D, Lekmine F, Tiruppathi C, Shilkaitis A, Bratescu L, et al. (2011) Angiogenesis 14, 355-369.

34.	Masuda M, Suzuki N, Taniguchi S, Oikawa T, Nonaka T, Iwatsubo T, Hisanaga S, Goedert M, & Hasegawa M (2006) Biochemistry 45, 6085-6094.

35.	Ehrnhoefer DE, Duennwald M, Markovic P, Wacker JL, Engemann S, Roark M, Legleiter J, Marsh JL, Thompson LM, Lindquist S, et al. (2006) Hum Mol Genet 15, 2743-2751.

36.	Porat Y, Abramowitz A, & Gazit E (2006) Chem Biol Drug Des 67, 27-37.

37. Mandel SA, Avramovich-Tirosh Y, Reznichenko L, Zheng H, Weinreb O, Amit T, & Youdim MB (2005) Neurosignals 14, 46-60.

38. Khan N, Afaq F, Saleem M, Ahmad N, & Mukhtar H (2006) Cancer Res 66, 2500-2505.

39. Rakhit R, Crow JP, Lepock JR, Kondejewski LH, Cashman NR, & Chakrabartty A (2004) J Biol Chem 279, 15499-15504.

40. Chattopadhyay M, Durazo A, Sohn SH, Strong CD, Gralla EB, Whitelegge JP, & Valentine JS (2008) Proc Natl Acad Sci U S A 105, 18663-18668.

41. Muchowski PJ & Wacker JL (2005) Nat Rev Neurosci 6, 11-22.

42. Rochet JC & Lansbury PT, Jr. (2000) Curr Opin Struct Biol 10, 60-68.

43. Jarrett JT & Lansbury PT, Jr. (1993) Cell 73, 1055-1058.

44. Tiwari A & Hayward LJ (2005) Neurodegener Dis 2, 115-127.

45. Prudencio M, Durazo A, Whitelegge JP, & Borchelt DR (2010) Hum Mol Genet 19, 4774-4789.

46. Prudencio M, Durazo A, Whitelegge JP, & Borchelt DR (2009) J Neurochem 108, 1009-1018.

47. Wang J, Xu G, & Borchelt DR (2002) Neurobiol Dis 9, 139-148.

48. Johnston JA, Dalton MJ, Gurney ME, & Kopito RR (2000) Proc Natl Acad Sci U S A 97, 12571-12576.

49. Muchowski PJ, Schaffar G, Sittler A, Wanker EE, Hayer-Hartl MK, & Hartl FU (2000) Proc Natl Acad Sci U S A 97, 7841-7846.

50. Shorter J & Lindquist S (2006) Mol Cell 23, 425-438.

51. Yang DS, Yip CM, Huang TH, Chakrabartty A, & Fraser PE (1999) J Biol Chem 274, 32970-32974.

52. Behrends C, Langer CA, Boteva R, Bottcher UM, Stemp MJ, Schaffar G, Rao BV, Giese A, Kretzschmar H, Siegers K, et al. (2006) Mol Cell 23, 887-897.

53. Hough MA, Grossmann JG, Antonyuk SV, Strange RW, Doucette PA, Rodriguez JA, Whitson LJ, Hart PJ, Hayward LJ, Valentine JS, et al. (2004) Proc Natl Acad Sci U S A 101, 5976-5981.

54. Wiedau-Pazos M, Goto JJ, Rabizadeh S, Gralla EB, Roe JA, Lee MK, Valentine JS, & Bredesen DE (1996) Science 271, 515-518.

55. Doucette PA, Whitson LJ, Cao X, Schirf V, Demeler B, Valentine JS, Hansen JC, & Hart PJ (2004) J Biol Chem 279, 54558-54566.

Chapter 4

Discovery of SOD1 Oligomers by Stabilization with Molecular Tweezer

Introduction

Amyloid fibril formation and its associated oligomeric species are implicated in many misfolding diseases, such as Alzheimer's, Parkinson's, transmissible spongiform encephalopathies (TSEs), and systematic amyloidosis (1-4). Although the end stage product, insoluble amyloid fibrils with the characteristic cross-beta conformation, are consistently found in the affected organs of many neurodegenerative patients, emerging evidence suggests that the real pathological culprit responsible for disease etiology is the more soluble, diffuse form of oligomer associated with the amyloid formation pathway (5-7). Most studies suggest that soluble oligomers correlate better with disease severity than insoluble fibrils (8-10). Consequently, these soluble oligomers, either formed in the early stage of aggregation or released from disaggregated fibrils, have become the focus of recent amyloid research.

Unlike the mature SOD1 amyloid fibril, little is known about the building blocks that precede its formation. Although the exact mechanism of fibril formation varies from protein to protein, the most accepted mechanism of fibrillation begins with a rate-limiting, thermodynamically unfavorable nucleation step in which monomers change their conformations to form a fibril-competent nucleus (the smallest multi-mer capable to initiate fibrillation). The nucleus then further recruits monomers to elongate favorably to form and sustain growth of mature amyloid fibril. However, more recently this model has been expanded, and three more detailed models have been proposed to explain the earliest event in fibril formation, the transition from monomers to nucleus.

In the native-like aggregation model, the monomers slightly rearrange to expose aggregation-prone regions but retain most of their native structure. Once these aggregation-prone

90

regions are exposed, the monomers can then self-assemble to form native-like oligomers. These oligomers can then convert to amyloid fibril. Proteins that have been reported to follow this aggregation pathway include β2-microglobulin (11) and transthyretin (12, 13). These proteins have the intrinsic property to aggregate.

In the nucleated conformation conversion model, monomers readily unfold to form oligomers lacking significant secondary structure. These oligomers slowly convert to amyloid-like oligomers, which then form fibrils. In this model, the rate-limiting step is the conversion of unstructured oligomers to the amyloid-like oligomers. This model was demonstrated in Aβ (14, 15), IAPP (16), and huntingtin (17).

In the nucleation growth model, monomers directly convert to the amyloid-competent form. In this case, the nucleus can be as small as a monomer. The pathway chosen toward amyloid formation depends on the protein, and the same protein can follow different pathways, even simultaneously, depending on the individual protein and parameters such as buffer composition, pH, and protein concentration (18, 19). Due to the various pathways that a polypeptide can undertake, the oligomers observed and reported in the literature vary vastly. The term "soluble oligomer" simply broadly embraces all species that remain soluble after ultra-centrifugation. Other amyloid-associated intermediates reported other than soluble oligomers include insoluble oligomer and spherical or linear protofibrils.

Soluble oligomers present polymorphism in terms of their size (20), secondary structure, morphology (21), and stability (22). Such oligomer polymorphism exists even within the same pathway formed by the same polypeptide. For instance, the sizes of the Abeta oligomers reported in the literature range from 40 kDa to 250 kDa (5, 23-25). Most of these oligomers are toxic to

cell cultures. Moreover, oligomeric species of tau, Abeta, huntingtin and α-synuclein have been found in their respective neurodegenerative patients (26). These oligomeric species induced toxic responses when administered to animal models after isolation from diseased specimens (27, 28). Interestingly, there seems to be a general negative correlation between the size of an oligomer and their toxicity in cell culture (7). However, since Chiti et al. found that oligomers formed by the same polypeptide that are similar in size can also have different levels of toxicity (29), this correlation is at best a trend, not a rule. The observation that oligomers formed by dissimilar primary amino acid sequences exhibit similar toxic properties suggests that toxicity is an inherent property of amyloid oligomer independent of the sequence of the amino acid residues. Hence, to unveil the presence of any oligomers associated with the SOD1 fibrillation pathway would be a crucial discovery, and detailed investigation on the different species might allow us to pinpoint the exact toxic entity directly linked to ALS etiology.

In vivo, SOD1 oligomers have been discovered in the detergent-insoluble aggregates isolated from the spinal cords of affected transgenic mice expressing mutant SOD1 and fALS patients harboring an A4V mutation, which is the most common and severe form of mutation in the United States, with an average survival time less than 2 years (30-32). Although it has been shown that aggregates (mostly amorphous) isolated from the spinal cord of tgSOD1G93A mice can seed amyloid formation in vitro (33), it is not known whether the oligomers found in the aggregates from the transgenic mice and fALS patients were indeed intermediates of the amyloid fibril pathway. In vitro, SOD1 oligomers have been observed from in-vitro fibrillation experiments (not published), but the transient nature of these oligomers has made it difficult to investigate their structural properties, assembly pathways, and their relationship to the final

fibrils. One successful approach has been the use of small molecule to stabilize the intermediate oligomeric species (34-37). The outcome of such studies of these small molecule amyloid inhibitors was the consensus that small molecules cannot completely inhibit all possible self-assembly pathway of the amyloidogenic polypeptides. Since protein aggregates have a relatively large buried area compares to the small size of a molecule, a small molecule cannot prevent the interaction of all possible inter-molecular interfaces. However, a small molecule can stabilize the formation of oligomers, either on or off the amyloid cascade, making it an ideal means to capture amyloid intermediates (38).

CLR01, a molecular tweezer, is composed of nine annulated six-membered rings forming a hydrophobic cavity with two rotatable peripheral anionic phosphonate groups (Figure 1) (39, 40). With the high electron density on its inner surface, it has high binding affinity for basic amino acid residues such as lysine and arginine, with the strongest affinity for lysine. CLR01 inhibits the aggregation and toxicity of a broad range of amyloidogenic proteins such as α-synuclein, amyloid β-protein (Aβ), tau, and islet amyloid polypeptide (41). Furthermore, it can disaggregate mature α-synuclein, Abeta and insulin amyloid fibrils (40, 41). In this chapter, we show that SOD1 fibrillation was inhibited and that pre-formed mature SOD1 fibrils were disaggregated by CLR01. Upon inhibition of SOD1 fibrillogenesis and disaggregation of SOD1 fibrils, SOD1 oligomers were formed. Such oligomeric species were present in both WT and mutant SOD1 samples. The size, property, and the role of disulfide bond in the formation of these oligomers were investigated in this chapter. The goal of the chapter is to identify and characterize the newly discovered oligomers associated with the amyloid pathway, which is a

critical step to advance our understanding of the aggregation mechanism of SOD1 and to define

the role of SOD1 oligomers in ALS.
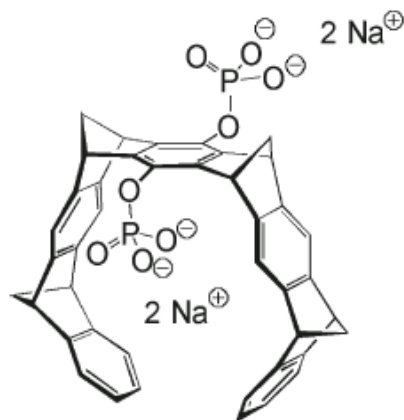
Figure 4.1. Molecular structure of the molecular tweezer, CLR01 (40). CLR01 is composed of nine annulated six-membered rings forming a hydrophobic pocket, which gives its high affinity for the aliphatic carbon side chain of lysine and arginine. The positively charged guanidinium and amino group of arginine and lysine, respectively, stabilizes the binding with CLR01 through electrostatic attraction with the phosphate anions [Reprinted from Prabhudesai *et al*. (40)]

Results

In-vitro Fibrillation Assay

To test whether CLR01 can be used as a SOD1 amyloid inhibitor, an in-vitro fibrillation assay (as discussed in chapter 4) was performed. As a positive control, apo SOD1 was induced to fibrillate by reducing the intra-subunit disulfide bond of a subpopulation of SOD1 protein molecules by the addition of 5 mM DTT. Inhibitors at different molar ratios were added at the beginning of the fibrillation in parallel with the positive control. After forty-five hours of incubation at 37 °C with continuous agitation in a 96-well plate, when the thioflavin-T (ThT) signal of the positive control has reached plateau indicating the completion of fibril formation, reactions were stopped, and aliquots were flash frozen if not studied immediately. ThT intensity of the CLR01 reaction was normalized to the positive control reaction. At 10:1 and 5:1 (CLR01:SOD1) molar ratios, CLR01 completely inhibited WT fibrillation with DTT (Figure 2). At equivalent molar ratio, CLR01 was only marginally effective. At submolar ratio, 1:2, CLR01 failed to inhibit SOD1 fibrillation. To test whether CLR01 is also effective in inhibiting the fibrillation of mutant SOD1, CLR01 was also tested with the G93A and D101N mutants. Similar to WT, CLR01 completely inhibited fibrillation at 10:1 and 5:1 molar excess, but the effects at 1:1 and 1:2 molar ratios were insignificant.
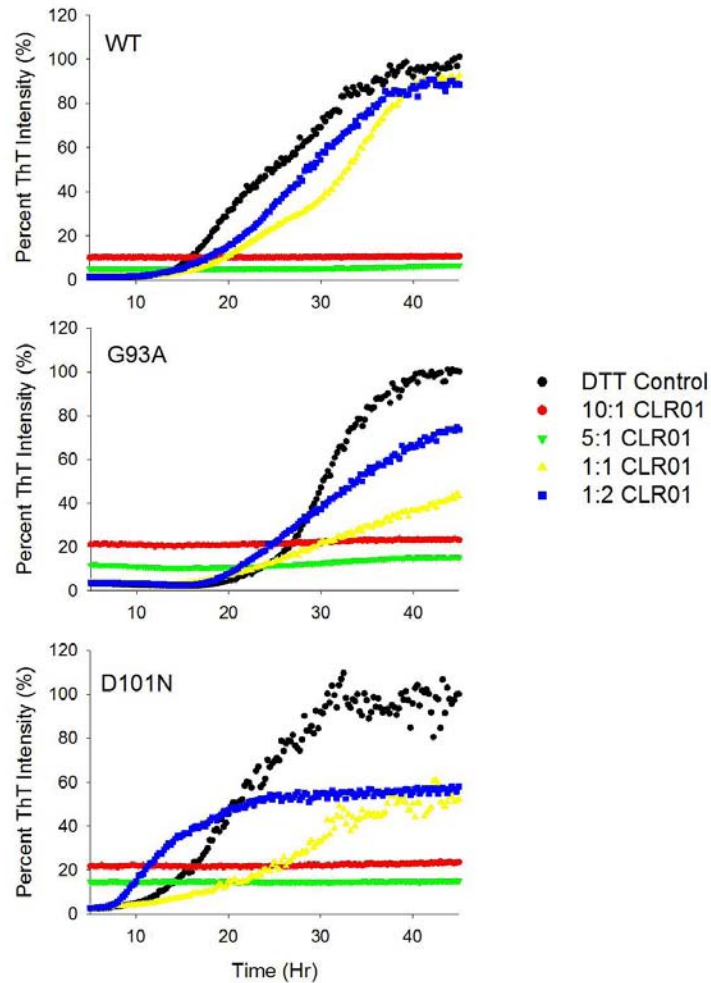
Figure 4.2. CLR01 inhibited the fibrillation of apo WT, G93A, and D101N. Thioflavin-T intensity of the CLR01-treated sample was normalized to the DTT positive control sample (No inhibitor) of the respective apo protein after forty-five hour incubation. Plotted values are average of triplicates. At 10:1 and 5:1 molar excess, CLR01 completely inhibited SOD1 fibrillation.

Characterization of Pre-fibrillar Oligomer

To ascertain the presence of SOD1 oligomers, aliquots were taken out from the 96-well plate after forty-five hours of incubation and subjected to size-exclusion chromatography (SEC) with a TSKG2000SW column. Sizing standards (Bio-rad) in combination with dimeric WT SOD1 were used to compare and estimate the size(s) of WT and mutant SOD1 proteins after treating with DTT and CLR01. Dimeric SOD1 with a rough molecular weight of about 32kD was eluted at 18.5min. In addition to dimeric SOD1, high molecular weight oligomeric SOD1 species eluting at around 16.5 min were consistently observed in WT and mutant SOD1 (G93A and D101N) reactions (Figure 3). Elution times of the standards were plotted against the log10 of the standards' known molecular weights (Figure 4). The interpolated size of the oligomers is around 87,000. Since these SOD1 oligomers are stable in the size-exclusion column, SEC-HPLC was used as a purification procedure to purify these oligomers, which we termed SOD1 prefibrillar oligomer (SPFO) to indicate these oligomers are formed before the formation of fibrils. It is important not to confuse SPFO with the general definition of prefibrillar oligomer (PFO), which describes the oligomers formed by Abeta and other amyloid proteins that can be specifically recognized by the A11 antibody since we are not implying that SPFO has the same properties and immunological structure as other PFO reported. Oligomers recognized by the A11 antibody are in general less structured than oligomers recognized by the OC antibody, which specifically recognize fibrillar oligomers and amyloid fibrils. The fundamental differences between the A11 and OC antibody rely on the different epitopes they specifically recognize along the amyloid formation pathway. The pre-fibrillar oligomers are oligomers that have yet to adapt the beta sheet enriched structure similar to mature fibrils. In theory, pre-fibrillar oligomers

have to undergo a conformational change "en bloc" to form fibrils (42). In contrary, fibrillar oligomers are thought to be the fibrillation nuclei that have immunologically similar structure with mature fibrils. Fibrillar oligomers can elongate by recruiting monomers to its end to form the resulting amyloid fibrils that are visible under electron microscopy.
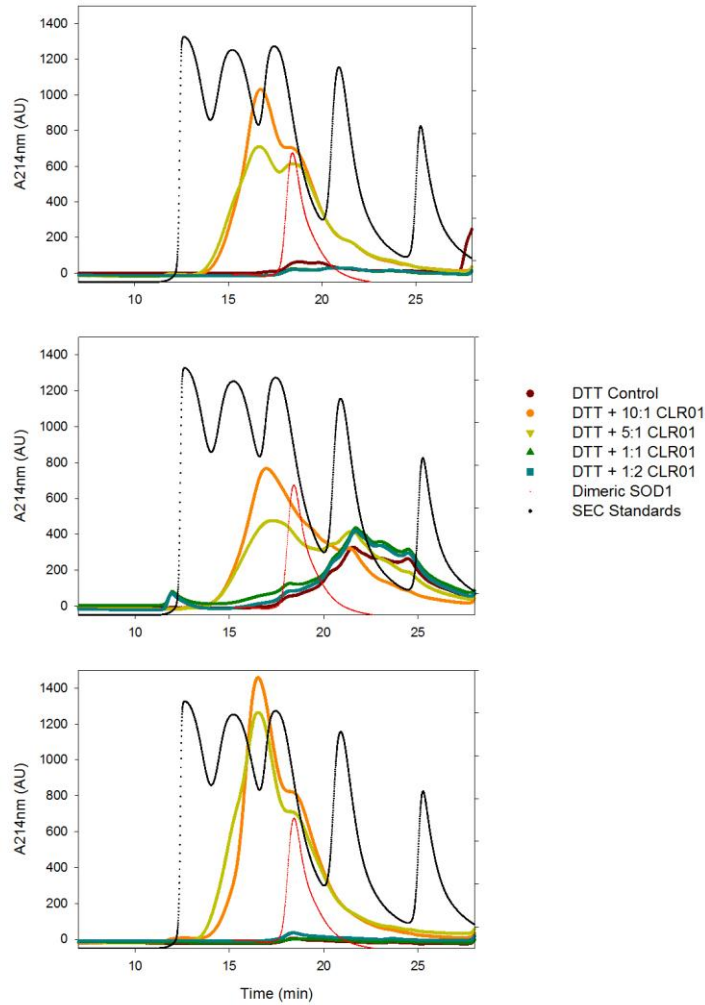
Figure 4.3. Formations of high molecular weight SOD1 prefibrillar oligomers (SPFOs) by CLR01. Top panel, WT; middle panel, G93A; bottom panel, D101N. The traces of the Bio-Rad protein standards (black) and dimeric SOD1 (red) are superimposed with the SOD1 samples treated with varying concentrations of CLR01 and control. The five molecular weight markers used are B12 (1,350), myoglobin (17,000), chicken ovalbumin (44,000), bovine γ–globulin (158,000), and thyroglobulin (670,000). Dimeric SOD1 eluted at 18.5 min. Oligomers eluted at 16.5 minute are evident for samples treated with 10:1 and 5:1 molar excess of CLR01.
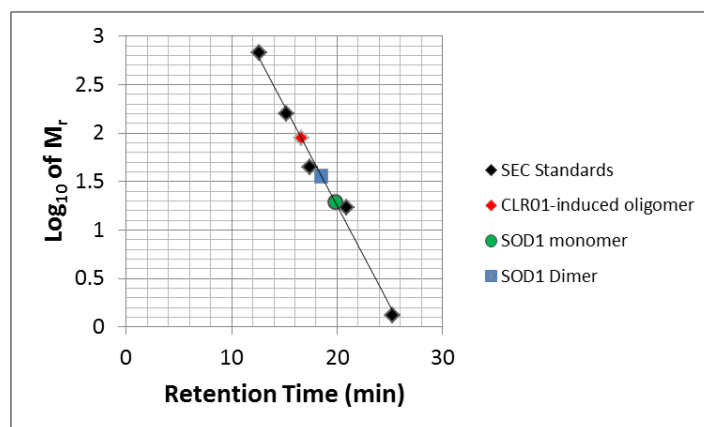
Figure 4.4. SPFOs have an estimated mass of 87,000. Observed elution times for the protein standards (Bio-Rad) (black) and dimeric SOD1 (blue) from the SEC-HPLC runs were plotted against the log10 of known molecular masses of the standards. SPFOs (red) have an interpolated molecular mass of 87,000 from this linear regression

The discovery of stable SOD1 oligomers allowed us to investigate further the properties of these oligomers. To determine the secondary structure of SPFO, circular dichroism spectroscopy (CD) was performed. As seen in Figure 5A, dimeric apo WT has a minimum and maximum at 215 nm and 230, respectively, suggesting a significant component of beta sheets. 10 fold molar excess of CLR01 has no CD absorption. Isolated SPFO has a minimum at 200 nm, suggesting that it has less beta-sheet content than apo WT SOD1 and that it contains a significant amount of random coil. However, it is lacking a maximum at 212 nm, indicating that it still retains a significant beta-sheet component. To investigate the role of the disulfide bond in the formation of SPFO, SPFO were isolated from the SEC-HPLC. Half of the oligomers were treated with 250 mM DTT for one hour at 37° C, a condition that would completely reduce and monomerize native apo WT SOD1. Both reduced and non-reduced oligomers were then injected back onto the size exclusion column. As shown in Figure 5B, a significant population of SPFO

were reduced and converted back to monomers, eluting at 20 min, suggesting that some of the SPFO were disulfide-crosslinked and were susceptible to DTT reduction. However, a sub-population of SPFO remained intact and eluted at 16.5 min. This evidence suggests that some of the SPFO are very stable and have acquired resistance to DTT reduction. To confirm the role of disulfide bond in the formation of SPFO, an SOD1 mutant with all four cysteines mutated, C6A, C57S, C111S, and C146S (NoCys SOD1), was induced to fibrillate in the presence (10:1, CLR01:SOD1) and absence of CLR01. Similar to the normal WT and mutants with normal cysteine background, NoCys fibrillation was also inhibited by CLR01 (Figure 6A). To examine whether NoCys SOD1 could form SPFO in the presence of CLR01, NoCys SOD1 and WT SOD1 were aliquoted out from the plate after forty-five hours of incubation and subjected to ultracentrifugation before running the supernatant on a native gel. While high molecular weight oligomers were consistently found in high abundance for WT SOD1, the NoCys SOD1 sample remained predominantly monomeric (Figure 6B). This observation suggests that the presence of cysteines is required for the formation of SPFO.

A

B
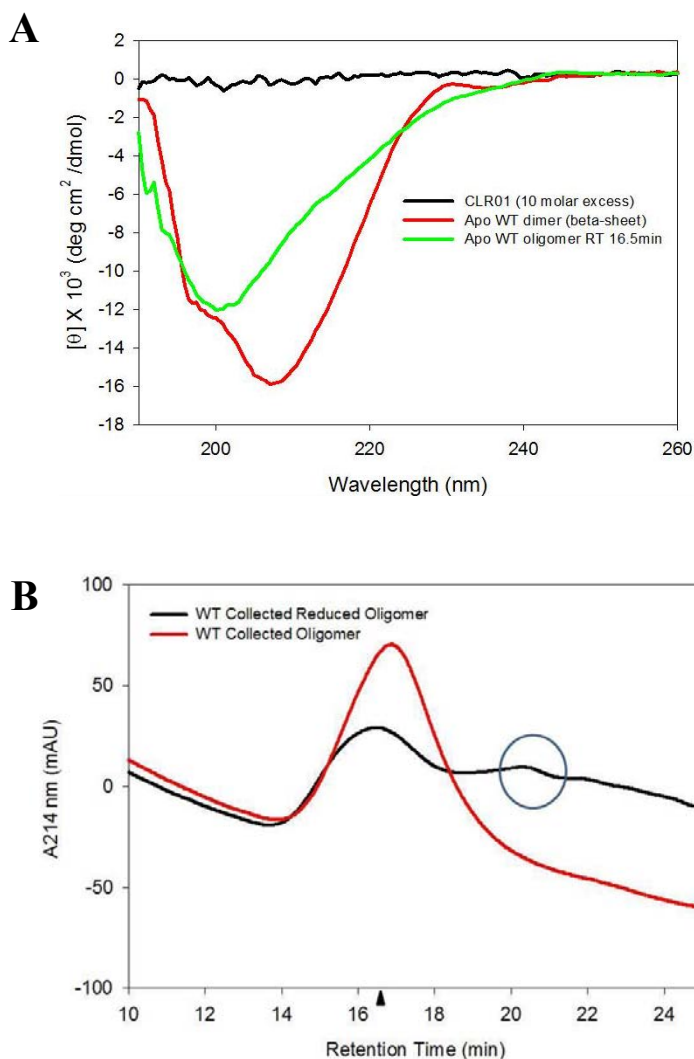
Figure 4.5. SPFOs have less beta-sheet structure than native apo WT and are partially stabilized by intermolecular disulfide bonds. (A) Circular dichroism spectroscopy (CD) of SPFOs (green) and native apo WT (red). SPFOs have a minimum at around 200nm, indicating an increase in random coil component. (B) SEC-HPLC of collected SPFOs (red) and collected, DTT-treated SPFOs (black). SPFOs are stable in SEC-HPLC but are susceptible to DTT reduction. A population of SPFOs is converted back to monomers (retention time = 20 min) after DTT reduction.
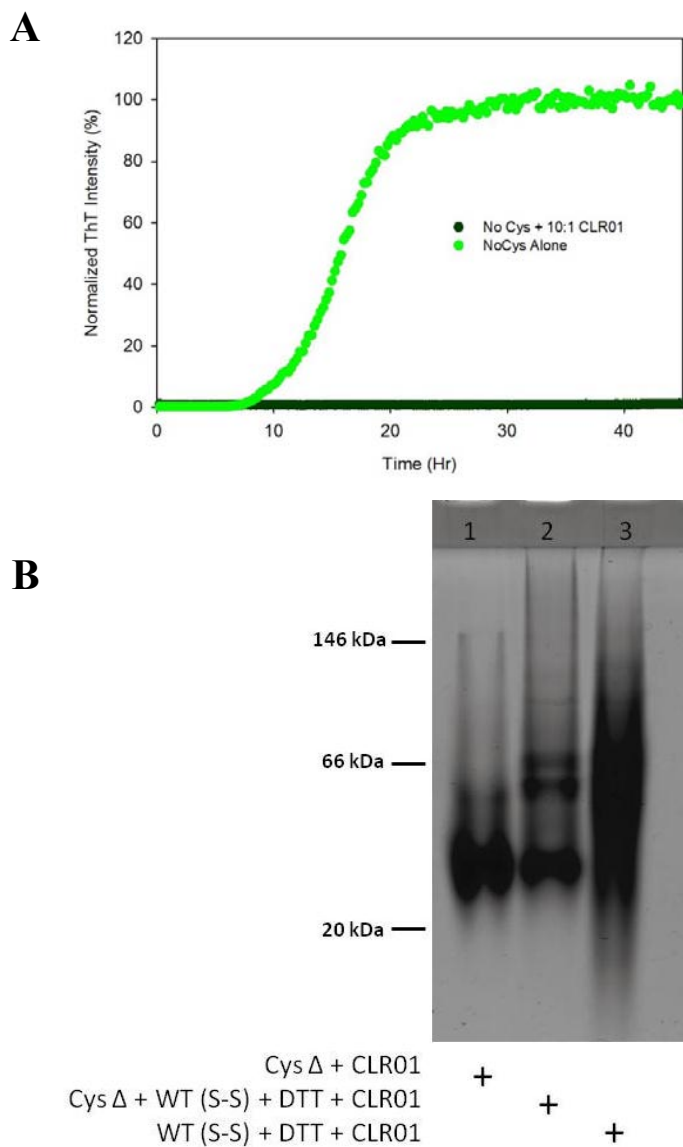
Figure 4.6. CLR01 inhibited fibrillation of NoCys SOD1(A) but did not form prefibrillar oligomers with NoCys SOD1 (B). (A) Fibril formation of NoCys SOD1 monitored by ThT fluorescence intensity. NoCys SOD1 was able to fibrillate with agitation alone. 10:1 molar excess of CLR01 completely inhibited NoCys fibrillation. (B) Oligomers bigger than the size of a tetramer were present in the WT SOD1 sample treated with CLR01 (lane 3) but absent in the NoCys sample (lane 1).

Initiation with SOD1 Pre-fibrillar oligomers (SPFOs)

Since fibril formation is known to be nucleation-dependent, we set out to determine whether the CLR01-treated SPFO could serve as a nucleus and initiate the formation of thioflavin T- positive fibrils from SOD1 dimers. Previously, Chattopadhyay et al. demonstrated that disulfide-reduced apo WT (2SH-apoWT) was sufficient to form the nuclei and able to initiate the fibrillation of disulfide-oxidized apo WT (SS-apoWT) in as low as 5% of the total volume (V/V) (43). To decrease the initiation lag time, 15% (V/V) of reduced apo WT was added instead of 5% in the following experiments (Figure 7). To prepare the SPFO as nucleating agent, SPFO were isolated from the SEC-HPLC and concentrated. 15% (V/V) of purified SOD1 SPFO were mixed with SS-apoWT. As a control, 15% (V/V) of monomeric 2SH-apoWT was mixed with SS-apoSOD1 and allowed to fibrillate alongside of the SPFO-treated sample. As shown in Figure 7. 15% of 2SH-apoWT was able to initiate fibril formation as indicated by the exponential increase in ThT signal with a lag time of ten hours. On the other hand, SPFO failed to initiate fibrillation even after forty-five hours, as indicated by the absence of increase in ThT signal.
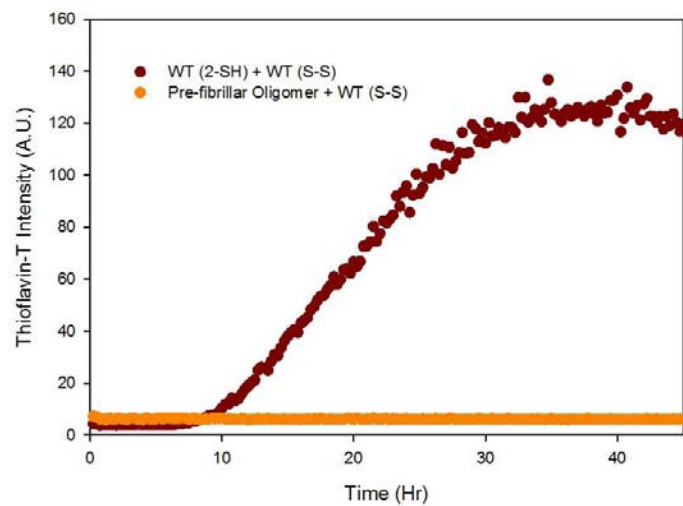
Figure 4.7. WT SPFOs did not initiate the fibrillation of WT apo disulfide-oxidized SOD1 at 15 % (V/V). 15% (V/V) WT apo disulfide-reduced SOD1 (2SH-apoSOD1) initiated fibrillation of WT apo disulfide-oxidized SOD1 (SS-apoSOD1) with a lag time less than ten hours (brown). 15% (V/V) of WT SPFOs failed to initiate fibrillation of WT SS-apoSOD1 (orange).

Dissociation of SOD1 fibrils by CLR01

To investigate whether CLR01 can dissociate pre-formed mature fibrils as reported in α-synuclein and Abeta (40, 41), pre-formed SOD1 DTT fibrils were retrieved from the 96-well plate after forty-five hours of incubation, washed and re-suspended in 10 mM potassium phosphate (KPi) with 10:1 molar excess of CLR01. Aliquots were taken out over a time course of forty days. To monitor the amount of soluble SOD1 disaggregated from the fibrils, aliquots were taken out periodically and were centrifuged at 16,000 X g for fifteen minutes to remove any remaining insoluble fibrils. The supernatants were then injected onto a size exclusion column. As demonstrated in Figure 8, large soluble oligomers eluting in the void volume (denoted as "*") and monomeric SOD1 eluting at 52 minute (denoted as "M") started to appear in the supernatant after nine days of incubation. The amount of oligomers continued to increase over time. To confirm the disaggregation, electron micrographs (EM) were taken throughout the time course, at the beginning (T=0d), middle (T=20d), and the end of the time course (T=40d). As shown in Figure 9A, at T=20d, in contrary to the abundance of long fibrils (>500 nm) seen on day 0, SOD1 fibril fragments less than 50 nm in length became the most dominant species. Small spherical oligomers with diameters as small as 7 nm were also observed. However, the disaggregation did not proceed to completion. At day 40, the amount of small SOD1 fibril fragments and oligomers were comparable to day 20. To estimate the sizes of the spherical oligomers, the diameters of twenty particles were measured by counting pixels with ImageJ. Particles were modeled as spheres with a partial specific volume of 0.74 cm³/g (see Methods). The distribution of molecular masses is shown in Figure 9B. From these measurements, the

average molecular mass of the small spherical oligomers dissociated from fibrils was calculated to be 92,000 ± 15,000 (SEM).
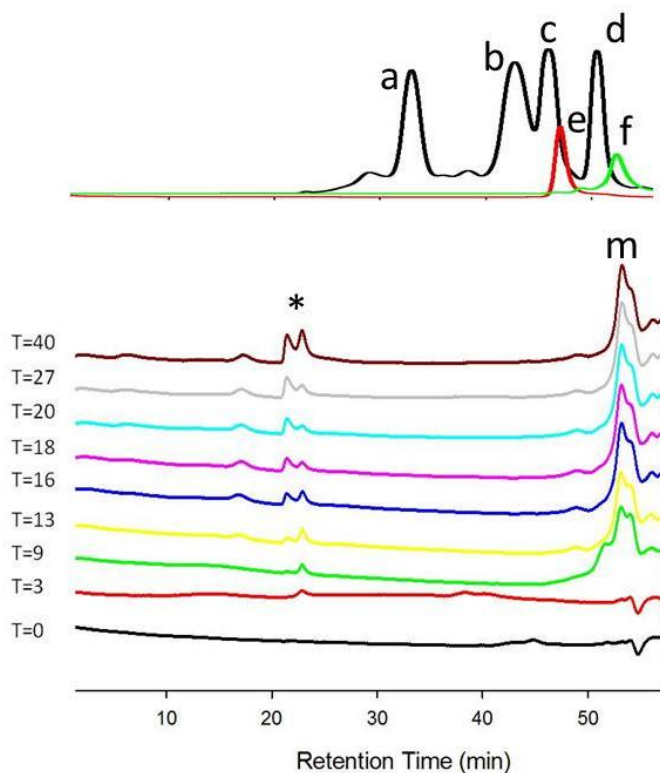
Figure 4.8. CLR01 dissociated SOD1 fibrils and released soluble oligomeric ("*") and monomeric ("m") SOD1 into the supernatant. SEC-HPLC (TSK G-4000) profiles of the supernatant of CLR01 treated fibrils from day 0 to day 40. Release of soluble SOD1 from fibrils are apparent after nine days of incubation with 10:1 molar excess CLR01. A214nm traces of SOD1 monomer (green), dimer (red), and protein standards (black) are superimposed and aligned on top as references. Molecular masses of the standards are 670,000 ("a"), 158,000 ("b"), 44,000 ("c"), and 17,000 ("d").

Figure 4.9. Dissociation of SOD1 fibrils by CLR01 monitored by TEM. (A) 10:1 molar excess of CLR01 was added to purified WT DTT fibrils at day 0. Fibril fragments and oligomers started to appear at day 21 (scale bar = 200nm). (B) Size distribution (M_r X 10^3) of twenty randomly selected small oligomers estimated from TEM with the corresponding number of SOD1 subunit listed above.
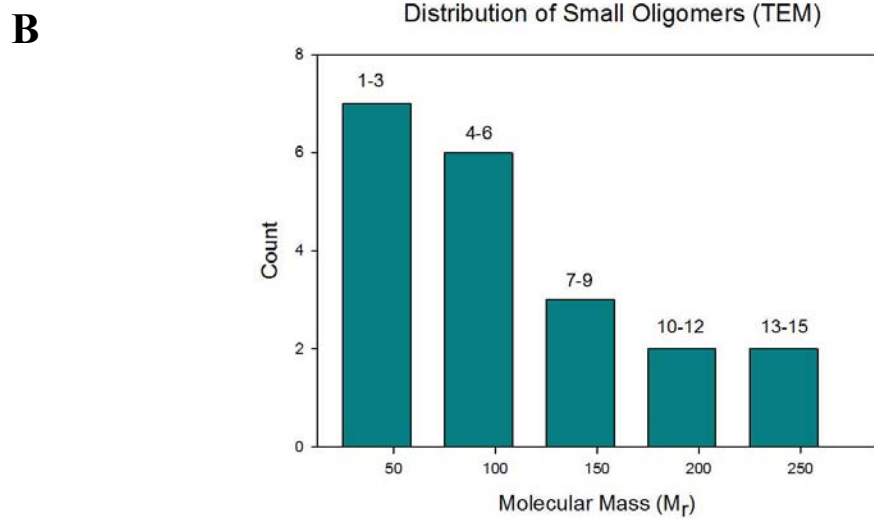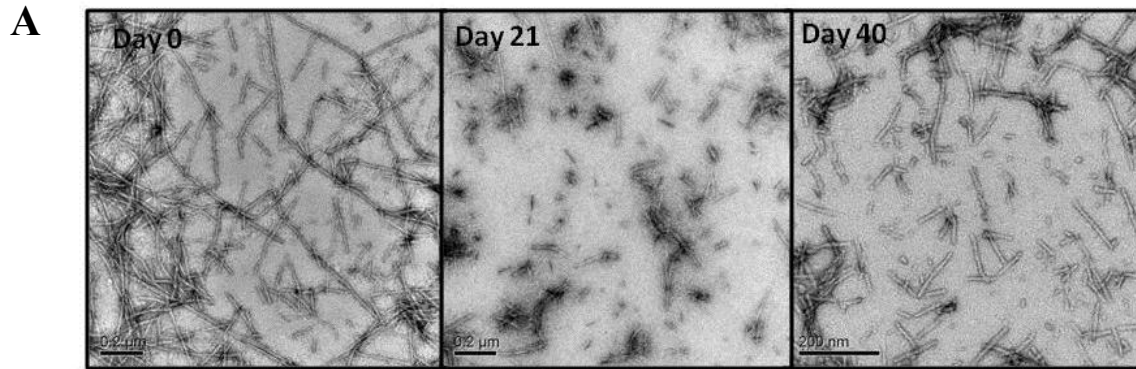
Discussion

Abnormal self-assembly of SOD1 may be pathogenic in fALS and even in some cases of sporadic ALS. Although insoluble protein aggregates containing mutant SOD1 are consistently observable in fALS patients and ALS mouse models, there is a growing realization that it is the soluble fibril precursors that are likely to be cytotoxic. However, unlike other amyloid diseases, such toxic intermediates associated with SOD1 amyloid have not been identified. In this chapter, we sought to discover, stabilize, and characterize SOD1 oligomeric species associated with the amyloid pathway through stabilization with CLR01. We show that CLR01 successfully inhibited the formation of thioflavin T-positive SOD1 fibrils. Instead of forming amyloid fibrils, soluble oligomers, which we termed, SOD1 prefibrillar oligomers (SPFOs), with an estimated molecular mass of 80,000 were observed. These oligomers are stabilized, at least partially, by inter-molecular disulfide bonds. This is evident by both reduction treatment coupled with SEC-HPLC and the inability to form oligomers by the NoCys SOD1. SPFOs were found in both WT and mutant SOD1 samples treated with CLR01.

For the first time, we have isolated and studied oligomeric SOD1 species that are associated with the amyloid pathway. Although the purified pre-fibrillar oligomers failed to initiate fibrillation of dimeric SS-apoSOD1, it is too early to conclude that these oligomers are off-pathway species. One possible explanation is that CLR01 might have a strong binding affinity to a region of SOD1 on the nucleus that is critical for the recruitment of SOD1 monomer and/or dimer, which prevents elongation to mature amyloid fibril. This region might be natively buried but become solvent exposed after its conversion to oligomers. An alternative explanation is that CLR01 might bind to monomeric and/or dimeric SOD1 and re-direct it to form oligomers

that are off-pathway from amyloid formation. Data from the circular dichroism experiments showing a shift of minimum from 215 nm to 200 nm seems to support this hypothesis. The beta-sheet content was less in the SPFOs than in the native dimeric apo SOD1, suggesting that CLR01 remodels the secondary structure of SOD1. Since beta-sheets are essential components to maintain the structural integrity of amyloid fibril, decrease in beta-sheet content in SPFOs accompanied by increased structural disorder as random coil might disfavor the conversion to amyloid fibril, driving it off the amyloid pathway. Off-pathway oligomers induced by small molecule have been reported for Abeta protein, inhibited by (-)-epi-gallocatechine gallate (EGCG) (44). These off-pathway oligomers are mostly unstructured and are non-toxic to cell culture as measured by MTT assay (5). Another example of non-toxic, unstructured oligomers was reported by Ladiwala et al (45). These unstructured Abeta oligomers (prepared at low concentration) were not recognized by the A11 antibody, suggesting that they are not pre-fibrillar oligomers. On the other hand, a large variety of toxic Abeta oligomers have also been reported. Abeta oligomers prepared by different protocols that demonstrated toxicity include the 56 kDa oligomers that causes cognitive dysfunction in transgenic mice (27), the 80 kDa Abeta1-42 fibrillar oligomers that are toxic in several cell culture systems, and 90 kDa oligomers that disrupted the calcium channel of SH-SY5Y cells (46).

Eisenberg et al. recently reported the discovery of the toxic Abeta1-42 (Abeta42) fibrillar oligomers (TABFO) that have an average molecular mass of 80,000 (47). The TABFO were made in ammonium hydroxide, which prohibited the formation of mature fibrils. However, when the solvent was exchanged to PBS, these oligomers were able to form fibrils. The average size of TABFO is similar to the SPFOs we observed (87,000). Moreover, these TABFO have similar

CD signature as the SPFO we observed. A combination of beta-sheets and random coils with negligible α-helices was observed in both TABFO and our SPFO. Similar to mature fibril, TABFO was also recognized by a fibril-specific OC antibody. The size and secondary structure similarity between TABFO and SPFO suggest that our SPFO might also be recognized by the OC antibody. TABFOs are toxic to HeLa and PC-12 cells, hence we speculate that the oligomers we observed might also carry an intrinsic toxic property.

It is interesting to point out that although the primary sequence of Abeta and islet amyloid polypeptide (IAPP) are about one quarter the size of the polypeptide chain of SOD1, the sizes of their toxic oligomers are about the same as the SPFOs (23). While a molecular mass of 80 kDa corresponds roughly to a SOD1 pentamer, it is a nonadecamer (19 subunits) for Abeta42 and henicosamer (21 subunits) for IAPP. It seems likely that there is minimum requirement in size for toxicity regardless of the protein sequence. Toxicity might begin around 80,000 and decreases as the oligomer size increases. Indeed, Kayed *et al*. compared the toxicity of low molecular weight oligomers (less than 40 kDa), high molecular weight oligomers, and amyloid fibrils. They found that oligomers larger than 40 kDa display significant toxicity while low molecular weight oligomers and fibrils are not toxic (23).

In biological systems, high molecular weight SOD1 oligomers larger than the size of trimer, were apparent in both A4V FALS patient and transgenic mice overexpressing five different SOD1 mutations (G37R, G93A, G85R, H46R/H48Q and Quad) (31). Misfolded SOD1 have also been detected in the spinal cords of sporadic ALS patients as identified by the C4F6 antibody. Unfortunately, the sizes of these misfolded species were not reported in this study. Nevertheless, high molecular weight SOD1 oligomers might be the etiological agent in ALS.

We also managed to disaggregate SOD1 fibrils into short fibrillar fragments and oligomers by the use of CLR01. Electron micrographs suggest that some of the SOD1 were converted back to hexamer and trimer, etc. However, these species were not visible in the size exclusion column. One possible explanation is that these oligomers have high propensity to aggregate; hence, as soon as CLR01 concentration was diluted in the gel filtration column, these oligomers re-aggregated. Another possibility is that the equilibrium shifted toward monomer as the concentration of SOD1 decreased in the column.

Array of soluble oligomers have also been reported for other amyloidogenic proteins such as IAPP, α-synuclein, prion, insulin, and lysozyme (19-23). While some oligomers are toxic, some are benign. In view of these considerations, it is important to study these SOD1 oligomers and their properties individually. The SPFOs and the dissociated SOD1 oligomers observed by stabilization with CLR01 might only be two out of many possible on- or off-pathway SOD1 intermediate states. To explore fully the regime of SOD1 oligomers and to pinpoint the most toxic SOD1 intermediate species, different inhibitors or varying pH and concentration of SOD1 might be utilized to stabilize other undiscovered SOD1 oligomers. The use of small molecules to modulate the toxicity of Abeta oligomers was well demonstrated by Ladiwala *et al* (48). In this study, five small molecules were selected based on its ability to convert toxic prefibrillar Abeta oligomers into non-toxic oligomers. They found that this group of aromatic small molecules was able to remodel the prefibrillar oligomers into different conformations with reduced toxicity. These non-toxic alternate conformations include smaller oligomers and fibrillar oligomers.

Since SOD1 oligomers might be the real toxic entity responsible for fALS and possibly sporadic ALS, it is uncertain whether disaggregating SOD1 fibrils would be beneficial to the cellular

environment. Future experiments should aim to isolate and stabilize the oligomers released from the dissociation experiment and further characterize the biophysical and toxicity properties of these dissociated oligomers. Since the dissociated oligomers were unstable in liquid chromatography, cross-linking agents such as glutaraldehyde, dimethyl suberimidate (DMS), dimethyl adipimidate (DMA), and Photo-Induced Crosslinking of Unmodified Proteins (PICUP) might be used to stabilize these oligomers. Any new discovered oligomers should be followed up by biophysical characterization and study in the in vivo systems for toxicity.

Materials and Methods

SOD1 Expression and Purification

WT and site-directed mutagenesis of WT were performed as described in (49, 50). WT and fALS SOD1 were purified from the EG118 strain of Saccharomyces cerevisiae following the procedures from (51), yielding SOD1 with the initial Met1 removed and Ala2 N-acetylated covalently identical to SOD1 from human sources. To convert to apo, purified SOD1 was dialyzed three times against 50 mM EDTA and 100 mM sodium acetate at pH 3.8. The protein was then dialyzed three times in 100 mM NaCl and 100 mM sodium acetate, pH 3.8, to remove SOD1-bound EDTA. After demetallation, SOD1 was dialyzed in 10 mM potassium phosphate (KPi), pH 7.0, filter-sterilized, and flash-frozen in liquid nitrogen and kept at − 20 °C until use. Inductively coupled plasma (ICP)-MS was used to quantify metal status (52). All apo-proteins contain less than 0.10 molar equivalents of copper and zinc per dimer.

In Vitro Fibrillation

To make fibrils, 50 μM of apo SOD1 was prepared in 10 mM KPi, pH 7.0, with 5 mM DTT and 40 μM of thioflavin-T (ThT) as described (43). After mixing, the solution was placed in a 96-well plate with a 1/8-in teflon ball and incubated at 37 °C with continuously shaking at 300 rpm for forty-five hours. Assembly of fibrils was monitored by fluorescence measurement at λem = 485 nm (λex =444 nm) using a Fluoroskan plate-reader (Thermo Fisher). All solutions were made with chelexed metal-free distilled deionized water (ddH2O) and filtered through a 0.22 μm filter. To inhibit SOD1 fibrillation, varying concentrations of CLR01, as stated above,

were added. All reactions were carried out in triplicate and incubated simultaneously with the control (No CLR01). 10 mM CLR01 was prepared from powder by re-suspension in ddH2O.

Size-exclusion chromatography (SEC)-HPLC

Size estimation of SPFOs. The molecular mass of SPFOs was determined by a 7.5 mm X 30 cm TSK G2000 SW column (Tosoh Bioscience, Japan) equipped with a guard column using an Agilent 1200 HPLC with a mobile phase containing 50 mM sodium chloride and 50 mM potassium phosphate at pH 6.7 at a flow rate of 0.5ml/min. SOD1 dimer, monomer, and a mixture of molecular weight markers (Bio-Rad) ranging from 1,350 to 670,000 daltons were used as sizing standards. Retention times were monitored by absorbance at A280nm. CLR01 treated samples were aliquoted from the 96-well plate after forty-five hours incubation. To isolate the soluble fraction before loading onto the SEC column, samples were centrifuged at 16,000 g for 15 min.

To monitor the release of soluble oligomers from dissociation, a 7.5 mm X 60 cm TSK G4000SW column (Tosoh Bioscience, Japan) with a flow rate of 0.5ml/min 50 mM sodium chloride and 50 mM potassium phosphate was used.

Initiating Fibril Formation

SPFOs eluting at 16.5min were collected from SEC-HPLC and concentrated with a YM-10 Microcon (Millipore). Since CLR01 also absorbs at 280 nm, Bradford assay (Bio-Rad) was used to determine SPFO concentration. For the positive control, apo WT SOD1 was previously reduced by 10 mM TCEP overnight at room temperature. To ensure complete reduction, disulfide-reduced monomeric apo WT was then purified and collected from the SEC-HPLC as

above. 15% (V/V) of both SPFO and disulfide-reduced monomeric SOD1 were then mixed with disulfide-oxidized dimeric SOD1 and incubated with continuous agitation in a 96-well plate at 37° C for forty-five hours as above.

Estimating Molecular Mass from Size-Exclusion Chromatography

Observed retention times (min) from SEC for SOD1 monomer (16,000 Da), dimer (32,000 Da) and five molecular mass markers (Bio-Rad), vitamin B12 (1,350 Da), myoglobin (17,000 Da), ovalbumin (44,000 Da), bovine γ-globulin (158,000 Da), and thyroglobulin (670,000 Da), was used to plot against the known log10 molecular mass to construct a first order linear regression best-fit line. Molecular mass of the SPFO was estimated by interpolating from the best fit line with the observed retention time of 16.5 min.

Circular Dichroism Spectroscopy

A JASCO J-715 spectrometer equipped with a JASCO PTC-348 temperature controller was used to acquire the circular dichroism spectra. Far UV spectra from 260 nm to 195 nm were collected at room temperature in a 0.1 cm path-length quartz cells. CLR01 treated SPFO were collected from SEC-HPLC, exchanged to 10 mM KPi (pH 7.0) and concentrated with a YM-10 Microcon (Millipore). 10 fold molar excess of CLR01 in KPi buffer was measured as blank.

Fibril Dissociation

Mature SOD1 fibrils formed by DTT reduction were retrieved from the 96-well plate. To purify fibrils from soluble contaminants, fibril samples were subjected to centrifugation at 16,000 X g for 15 min. Fibrils were then washed with 10mM KPi (pH 7.0), centrifuged, and re-suspended in 10mM KPi buffer. 10:1 molar excess of CLR01 was added to the fibrils. The

dissociation experiments were performed in a 2-ml glass vial with continuous agitation at 250 rpm at 37 °C. After sample was placed inside the vial, capped with a plastic cap containing a PTFE septum, the vial was purged with nitrogen gas by through a syringe. Aliquots were taken out periodically using a Hamilton gas-tight syringe through the septum.

Native PAGE

Samples were mixed in 1:1 by volume with the native sample buffer (Bio-Rad). Samples were then separated on a 10% acrylamide gel followed by staining with Coomassie Brilliant Blue, visualized by AlphaImager.

Electron Microscopy (EM)

10 μl of samples were deposited on the glow-discharged formvar-coated copper grid (Ted Pella, Inc) and allowed to absorb for one minute before blotted dry with filter paper. Samples were then washed twice with 10 μl ddH2O for twenty seconds. To achieve negative staining, samples were stained with 1% uranyl acetate for six seconds (2X) then forty-five seconds (1X) and blotted dry. Stained grids were kept in a grid box inside a desiccator before imaging.

Estimating Molecular Mass from EM

Twenty randomly selected small spherical particles were selected and the diameter of each particle was measured using ImageJ by counting pixels. The volume of each particle was estimated as a sphere with a partial specific volume of 0.73 ml/g.

References

1.   Lahiri DK & Maloney B (2010) Exp Neurol 225, 51-54.

2.   Aarsland D, Londos E, & Ballard C (2009) Int Psychogeriatr 21, 216-219.

3.   Hope J, Reekie LJ, Hunter N, Multhaup G, Beyreuther K, White H, Scott AC, Stack MJ, Dawson M, & Wells GA (1988) Nature 336, 390-392.

4.   Ratjen F & Doring G (2003) Lancet 361, 681-689.

5.   Wu JW, Breydo L, Isas JM, Lee J, Kuznetsov YG, Langen R, & Glabe C J (2010) Biol Chem 285, 6071-6079.

6.   Walsh DM, Klyubin I, Fadeeva JV, Cullen WK, Anwyl R, Wolfe MS, Rowan MJ, & Selkoe DJ (2002) Nature 416, 535-539.

7.   Bemporad F & Chiti F (2012) Chem Biol. 19, 315-327.

8.   Kuo YM, Emmerling MR, Vigo-Pelfrey C, Kasunic TC, Kirkpatrick JB, Murdoch GH, Ball MJ, & Roher AE (1996) J Biol Chem 271, 4077-4081.

9.   McLean CA, Cherny RA, Fraser FW, Fuller SJ, Smith MJ, Beyreuther K, Bush AI, & Masters CL (1999) Ann Neurol 46, 860-866.

10.   Lue LF, Kuo YM, Roher AE, Brachova L, Shen Y, Sue L, Beach T, Kurth JH, Rydel RE, & Rogers J (1999) Am J Pathol 155, 853-862.

11.   Eakin DK & Hertzog C (2006) J Gerontol B Psychol Sci Soc Sci 61, P340-347.

12.   Olofsson A, Ippel JH, Wijmenga SS, Lundgren E, & Ohman A (2004) J Biol Chem 279, 5699-5707.

13.   Quintas A, Vaz DC, Cardoso I, Saraiva MJ, & Brito RM (2001) J Biol Chem 276, 27207-27213.

14.   Lee J, Culyba EK, Powers ET, & Kelly JW (2011) Nat Chem Biol 7, 602-609.

15.   Petty SA & Decatur SM (2005) J Am Chem Soc 127, 13488-13489.

16.   Wei L, Jiang P, Xu W, Li H, Zhang H, Yan L, Chan-Park MB, Liu XW, Tang K, Mu Y, et al. (2011) J Biol Chem 286, 6291-6300.

17.   Thakur AK, Jayaraman M, Mishra R, Thakur M, Chellgren VM, Byeon IJ, Anjum DH, Kodali R, Creamer TP, Conway JF, et al. (2009) Nat Struct Mol Biol 16, 380-389.

18.   Bader R, Bamford R, Zurdo J, Luisi BF, & Dobson CM (2006) J Mol Biol 356, 189-208.

19. Gosal WS, Morten IJ, Hewitt EW, Smith DA, Thomson NH, Radford SE (2005) J Mol Biol 351, 850-864.

20. Mastrangelo IA, Ahmed M, Sato T, Liu W, Wang C, Hough P, Smith SO (2006) J Mol Biol 358, 106-119.

21. Pountney DL, Voelcker NH, Gai WP (2005) Neurotoxicity research 7, 59-67.

22. Calamai M, Chiti F, Dobson CM (2005) Biophysical journal 89, 4201-4210.

23. Kayed R, Head E, Thompson JL, McIntire TM, Milton SC, Cotman CW, Glabe CG (2003) Science (New York, N.Y 300, 486-489.

24. Lambert MP, Viola KL, Chromy BA, Chang L, Morgan TE, Yu J, Venton DL, Krafft GA, Finch CE, Klein WL (2001) Journal of neurochemistry 79, 595-605.

25. Winner B, Jappelli R, Maji SK, Desplats PA, Boyer L, Aigner S, Hetzer C, Loher T, Vilar M, Campioni S, et al. (2011) Proc Natl Acad Sci U S A 108, 4194-4199.

26. Morgan D, Diamond DM, Gottschall PE, Ugen KE, Dickey C, Hardy J, Duff K, Jantzen P, DiCarlo G, Wilcock D, et al. (2000) Nature 408, 982-985.

27. Lesne S, Koh MT, Kotilinek L, Kayed R, Glabe CG, Yang A, Gallagher M, Ashe KH (2006) Nature 440, 352-357.

28. Shankar GM, Li S, Mehta TH, Garcia-Munoz A, Shepardson NE, Smith I, Brett FM, Farrell MA, Rowan MJ, Lemere CA, et al. (2008) Nature medicine 14, 837-842.

29. Campioni S, Mannini B, Zampagni M, Pensalfini A, Parrini C, Evangelisti E, Relini A, Stefani M, Dobson CM, Cecchi C, et al. (2010) Nat Chem Biol 6, 140-147.

30. Rosen DR, Bowling AC, Patterson D, Usdin TB, Sapp P, Mezey E, McKenna-Yasek D, O'Regan J, Rahmani Z, Ferrante RJ, et al. (1994) Human molecular genetics 3, 981-987.

31. Wang J, Slunt H, Gonzales V, Fromholt D, Coonfield M, Copeland NG, Jenkins NA, & Borchelt DR (2003) Human molecular genetics 12, 2753-2764.

32. Cudkowicz ME, McKenna-Yasek D, Sapp PE, Chin W, Geller B, Hayden DL, Schoenfeld DA, Hosler BA, Horvitz HR, & Brown RH (1997) Ann Neurol 41, 210-221.

33. Chia R, Tattum MH, Jones S, Collinge J, Fisher EM, Jackson GS (2010) PloS one 5, e10627.

34. Williams AD, Sega M, Chen M, Kheterpal I, Geva M, Berthelier V, Kaleta DT, Cook KD, & Wetzel R (2005) Proc Natl Acad Sci U S A 102, 7115-7120.

35. Bulic B, Pickhardt M, Schmidt B, Mandelkow EM, Waldmann H, Mandelkow E (2009) Angew Chem Int Ed Engl 48, 1740-1752.

36. Amijee H, Scopes DI (2009) J Alzheimers Dis 17, 33-47.

37.   Stains CI, Mondal K, Ghosh I (2007) ChemMedChem 2, 1674-1692.

38.   Kodali R, Wetzel R (2007) Curr Opin Struct Biol 17, 48-57.

39.   Fokkens M, Schrader T, & Klarner FG (2005) J Am Chem Soc 127, 14415-14421.

40.   Prabhudesai S, Sinha S, Attar A, Kotagiri A, Fitzmaurice AG, Lakshmanan R, Ivanova MI, Loo JA, Klarner FG, Schrader T, et al. (2012) Neurotherapeutics 9, 464-476.

41.   Sinha S, Lopes DH, Du Z, Pang ES, Shanmugam A, Lomakin A, Talbiersky P, Tennstaedt A, McDaniel K, Bakshi R, et al. (2011) J Am Chem Soc 133, 16958-16969.

42.   Glabe CG (2008) J Biol Chem 283, 29639-29643.

43.   Chattopadhyay M, Durazo A, Sohn SH, Strong CD, Gralla EB, Whitelegge JP, & Valentine JS (2008) Proc Natl Acad Sci U S A 105, 18663-18668.

44.   Ehrnhoefer DE, Bieschke J, Boeddrich A, Herbst M, Masino L, Lurz R, Engemann S, Pastore A, & Wanker EE (2008) Nat Struct Mol Biol 15, 558-566.

45.   Ladiwala AR, Litt J, Kane RS, Aucoin DS, Smith SO, Ranjan S, Davis J, Van Nostrand WE, & Tessier PM (2012) J Biol Chem 287, 24765-24773.

46.   Demuro A, Mina E, Kayed R, Milton SC, Parker I, & Glabe CG (2005) J Biol Chem 280, 17294-17300.

47.   Stroud JC, Liu C, Teng PK, & Eisenberg D (2012) Proc Natl Acad Sci U S A 109, 7717-7722.

48.   Ladiwala AR, Dordick JS, & Tessier PM J (2011) Biol Chem 286, 3209-3218.

49.   Hough MA, Grossmann JG, Antonyuk SV, Strange RW, Doucette PA, Rodriguez JA, Whitson LJ, Hart PJ, Hayward LJ, Valentine JS, et al. (2004) Proc Natl Acad Sci U S A 101, 5976-5981.

50.   Wiedau-Pazos M, Goto JJ, Rabizadeh S, Gralla EB, Roe JA, Lee MK, Valentine JS, & Bredesen DE (1996) Science 271, 515-518.

51.   Doucette PA, Whitson LJ, Cao X, Schirf V, Demeler B, Valentine JS, Hansen JC, & Hart PJ (2004) J Biol Chem 279, 54558-54566.

52.   Shaw BF, Lelie HL, Durazo A, Nersissian AM, Xu G, Chan PK, Gralla EB, Tiwari A, Hayward LJ, Borchelt DR, et al. (2008) J Biol Chem 283, 8340-8350.